Order Number 9510734

Photocatalytic behavior of tungsten hexacarbonyl, and ruthenium dodecacarbonyl supported on porous Vycor glass

Xu, Shuping, Ph.D.

City University of New York, 1994

U·M·I

300 N. Zeeb Rd.
Ann Arbor, MI 48106

PHOTOCATALYTIC BEHAVIOR OF TUNGSTEN HEXACARBONYL, AND RUTHENIUM DODECACARBONYL SUPPORTED ON POROUS VYCOR GLASS

by

Shuping Xu

A dissertation submitted to the Graduate Faculty in Chemistry in partial fulfillment of the requirements for the degree of Doctor of Philosophy, The City University of New York.

1994

This manuscript has been read and accepted for the Graduate Faculty in Chemistry in satisfaction of the dissertation requirement for the degree of Doctor of Philosophy.

8/30/94
Date

Chair of Examining Committee

8/30/94
Date

Executive Officer

Supervisory Committee

The City University of New York

ABSTRACT

PHOTOCATALYTIC BEHAVIOR OF TUNGSTEN HEXACARBONYL, AND RUTHENIUM DODECACARBONYL SUPPORTED ON POROUS VYCOR GLASS

by

Shuping Xu

Adviser: Professor Harry D. Gafney

UV photolysis ($\lambda_{ex} \leq 310$ nm) of $W(CO)_6$ physisorbed onto Corning's code 7930 porous Vycor glass in vacuo leads to CO evolution followed by CH_4 evolution. Although photoinduced CH_4 evolution initially occurs with concurrent oxidation of the metal, photoactivation leads to a catalytic system where excitation of the resultant metal oxide continues CH_4 evolution. Isotope labeling experiments confirm that these photoactivated hybrid systems are capable of promoting the hydrogenation of an external carbon source, i.e., $^{13}CO_2$. Stoichiometry and deuterium labeling experiments indicate that the metal oxide catalyzes the reaction, $CO_2 + 2H_2O$ ---------> $CH_4 + 2O_2$, in which water acts as the source of hydrogen and the reducing equivalents. The relative rates of methane evolution suggest that methanation occurs at a site originally occupied by a carbonaceous impurity.

Diffuse reflectance FTIR and emission spectra indicate that both tetrahedral and octahedral tungsten oxide species are present on the PVG surface. Selective emission quenching and rate data suggest that the tetra-

hedral tungsten oxide species selectively photocalyzes CH_4 formation, while the octahedral tungsten oxide species photocatalyzes CO evolution.

UV photolysis of $Ru_3(CO)_{12}$ physisorbed onto PVG leads to oxidative addition of a surface silanol group across an Ru-Ru band and formation of the surface grafted species $(\mu\text{-H})Ru_3(CO)_{10}(\mu\text{-OSi})$. The latter species is bound to the glass via electron deficient bonds and exposure to an alkene results in immediate reaction. UV photolysis of the 1- pentene adduct leads to cis- and trans-2-pentene, where the trans-cis ratio increases from 1.5 ± 0.2 to 2.5 ± 0.1 during photolysis, but remains significantly smaller than the thermodynamic ratio. Deuterating the oxidative addition product yields deuterated olefines, and the product distribution suggests an excited state similar to a pi-allyl complex. The photogenerated grafted complex shows a high selectivity for olefin isomerization with no evidence for hydrogenation even in the presence of H_2.

ACKNOWLEDGEMENTS

I would like to express my appreciation to the members of the thesis committee, especially my adviser Dr. Harry D. Gafney, for their time and kind assistance in the preparation of this thesis.

I am very grateful to Dr. David C. Locke for his kind assistance in GC-MS analysis, to Dr. Thomas C. Strekas for his assistance in ESR analysis. I would like to thank Mr. Ottmar Safferling for his services in repair and construction of the special glassware used in my research, thank the staff of the Chemistry Department for their multiple assistance.

To my wife and best friend Zhong-shi, I would like to thank you for being patient and helping me through the difficult time.

To my parents, I would like to thank you for helping me complete the advanced education.

TABLE OF CONTENTS

ABSTRACT iii

ACKNOWLEDGEMENTS v

TABLE OF CONTENTS vi

LIST OF TABLES viii

LIST OF FIGURES x

CHAPTER 1. INTRODUCTION

1.1. INTRODUCTION 1

1.2. CATALYTIC REACTIONS OF CARBON DIOXIDE WITH HYDROGEN 2

1.3. HOMOGENEOUS PHOTOCATALYTIC REDUCTION OF CO_2 10

1.4. HETEROGENEOUS PHOTOCATALYTIC REDUCTION OF CO_2 14

1.5. HYBRID CATALYSTS 17

1.5.1. THERMAL ACTIVATION OF SUPPORTED GROUP VIB HEXACARBONYLS 19

1.5.2. PHOTOACTIVATION OF SUPPORTED GROUP VIB CARBONYLS 22

1.5.3. PHOTOACTIVATION OF SUPPORTED $Ru_3(CO)_{12}$ 27

1.6. POROUS VYCOR GLASS AND SOL-GEL-GLASS 31

CHAPTER 2. EXPERIMENTAL

2.1. MATERIAL 34

2.2. IMPREGNATION PROCEDURES 39

2.3. PHOTOCHEMICAL PROCEDURES 43

2.4. PHYSICAL MEASUREMENTS 46

CHAPTER 3. RESULTS

3.1. MORPHOLOGIES AND SURFACES OF POROUS VYCOR AND SOL-GEL GLASSES 59

3.2. PHOTOINDUCED METHANATION OF CO_2 WITH $W(CO)_6$(ADS) AND WO_3(ADS) 66

3.2.1. DISTRIBUTION OF ADSORBED $W(CO)_6$ AND WO_3 66

3.2.2. SPECTRAL PROPERTIES OF ADSORBED $W(CO)_6$ AND WO_3. 67

3.2.3. PHOTOINDUCED METHANATION OF CO_2 80

3.2.4. PHOTOLUMINESCENCE STUDIES OF WO_3(ADS) 110

3.3. PHOTOCATALYZED ISOMERIZATION OF 1-PENTENE 125

3.3.1 PHOTOLYSIS OF $Ru_3(CO)_{12}$(ADS) 125

3.3.2. PHOTOCATALYZED ISOMERIZATION OF 1-PENTENE 128

CHAPTER 4. DISCUSSION

4.1. PHOTOINDUCED METHANATION OF CO_2 141

4.2. PHOTOINDUCED ISOMERIZATION OF 1-PENTENE 156

REFERENCES 162

LIST OF TABLES

I. Composition of silica xerogels 36

II. Parameters of gas chromatograph 51

III. Fractional surface coverage of $W(CO)_6$ and WO_3 on PVG 68

IV. UV-Visible and IR absorption of $W(CO)_6$ and $Ru_3(CO)_{12}$ 70

V. Changes of intensity of free silanol band (3744 cm^{-1}) in the spectra of PVG impregnated with WO_3 79

VI. Rates of CO and CH_4 evolution during 254-nm photolysis of PVG impregnated with $W(CO)_6$ or WO_3 82

VII. Quantum yield data 90

VIII. Photocatalytic activity of WO_3/PVG catalysts for the methanation of CO_2 during periodic evacuation and recharging with 20 torr $^{13}CO_2$ 92

IX. Peak height of N_2 and O_2 obtained during 254 nm photolysis of PVG samples containing $W(CO)_6$ or WO_3 94

X. Theoretical and experimental yield of O_2 obtained during 254 nm photolysis of PVG samples containing $W(CO)_6$ or WO_3 95

XI. Effect of H_2 on the rates of CO and CH_4 evolution 97

XII. Assignment of IR bands for adsorbed CO_2 in the range of 1000 cm^{-1} to 1800 cm^{-1} 100

XIII. Effects of NH3 on the rates of CO and CH_4 evolution 105

XIV. Effect of sample preparation on the rates of CO and CH_4 evolution 106

XV. Effect of excitation energy on the intensity of emission bands at 298 K for a powdered WO_3/PVG sample 115

XVI. Stern-Volmer constant for powdered WO_3/PVG sample at 298 K 122

XVII. Fractional surface coverage of $Ru_3(CO)_{12}$ on PVG 127

XVIII. Assignment of pentene fragments in GC-MS spectra 137

LIST OF FIGURES

Figure 1. Oxidative addition of $Ru_3(CO)_{12}$ on PVG 30

Figure 2. DRIFT spectrum of calcined PVG at 298 K in vacuo ($P \leq 10^{-3}$ torr) .. 37

Figure 3. DRIFT spectrum of deuterated PVG 38

Figure 4. Sublimation apparatus 41

Figure 5. Calibration curve of $Ru_3(CO)_{12}$ adsorbed on Plate PVG 42

Figure 6. Photolysis cell 44

Figure 7a. Toepler pump apparatus 48

Figure 7b. Connection of gas sampling loop to gas chromatograph system .. 49

Figure 8. Calibration curve of H_2, CH_4 and CO 50

Figure 9. Chromatogram of methanation products 52

Figure 10. Calibration curve of 1-pentene, cis- and trans-2-penten..... 54

Figure 11. Chromatogram of gaseous products in 1- pentene isomerization. 55

Figure 12. Catalytic reactor system 56

Figure 13. FTIR high vacuum chamber and diffuse reflectance attachment. 57

Figure 14. Thermal gravimetric analysis of PVG 60

Figure 15. DRIFT spectrum of uncalcined PVG at 298 K 61

Figure 16. DRIFT spectrum of calcined sol-gel 63

Figure 17. Scanning electron micrograph of calcined PVG 64

Figure 18. Scanning electron micrograph of calcined sol-gel 65

Figure 19. Electronic spectrum of 4.0×10^{-6} mol of $W(CO)_6$ /g of PVG 71

Figure 20. Electronic spectrum of $W(CO)_6$ in hexane, 1.2×10^{-5} M 72

Figure 21. DRIFT spectrum of 1.2×10^{-5} mol of $W(CO)_6$ /g of PVG 73

Figure 22. Electronic spectra of WO_3 aqueous solutions 74

Figure 23. Electronic spectra of WO_3 (ads) 75

Figure 24. DRIFT spectrum of 1.5 x 10^{-5} mol of WO_3 /g of PVG 77

Figure 25. Intensity of the 3744 cm^{-1} free silanol band as a function of WO_3(ads) loading 78

Figure 26. Spectral changes during 254 nm photolysis of 4.2 x 10^{-6} mol of $W(CO)_6$(ads)/g of PVG in vacuo..... 81

Figure 27a. GC-MS spectrum of gaseous products generated from 254 nm photolysis of a sample contained 2.8 x 10^{-6} mol of $W(CO)_6$ (ads) under 2.0 x 10^{-4} mol $^{13}CO_2$ in 8.6 x 10^4 sec 84

Figure 27b. GC-MS spectrum of gaseous products generated from 254 nm photolysis of a sample contained 2.8 x 10^{-6} mol of $W(CO)_6$ (ads) under 2.0 x 10^{-4} mol $^{13}CO_2$ in 8.8 x 10^5 sec 85

Figure 28. Yields of $^{13}CH_4$ and ^{13}CO during 254 nm photolysis of 2.8 x 10^{-6} mol of $W(CO)_6$(ads) in 2.0 x 10^{-4} mol of $^{13}CO_2$ 86

Figure 29. Yields of CH_4 and CO during 254 nm photolysis of 2.8 x 10^{-6} mol of $W(CO)_6$(ads) in vacuo 87

Figure 30. UV spectrum of (a) 2.7 x 10^{-6} mol of WO_3/g of PVG, (b) the final photoproduct of 1.9 x10^{-6} mol $W(CO)_6$/g of PVG..... 89

Figure 31. DRIFT spectrum of PVG containing 1.9 x 10^{-6} mol of WO_3/g exposed to 25 torr of CO_2..... 98

Figure 32. DRIFT spectra of NH_3 adsorbed on PVG contained 1.7 x 10^{-5} mol of WO_3 103

Figure 33. DRIFT spectra changes during 254 nm photolysis of 1.5 x 10^{-5} mol of WO_3(ads)/g of PVG after exposed to 20 torr CO_2 107

Figure 34. DRIFT spectrum of sol-gel contained 3.9 x 10^{-6} mol of WO_3 after 2 hours photolysis with 254 nm light in vacuo 109

Figure 35. Photoluminescence spectrum of powdered WO_3/PVG (4.6 x 10^{-5} mol/g) and its excitation spectra at 298 K 111

Figure 36. Effect of temperature on intensity and position of phosphorescence spectra of powdered WO_3/PVG sample (5.3 x 10^{-5} mol/g) 113

Figure 37. Effect of excitation energy on the intensity of phosphorescence spectrum of powdered WO_3/PVG sample 114

Figure 38. Change in the emission spectrum of powdered WO_3/PVG sample (4.6 x 10^{-5} mol/g) as a function of O_2 pressure at 298 K 117

Figure 39. Change in the emission spectrum of powdered WO_3/PVG sample (4.6 x 10^{-5} mol/g) as a function of CO_2 pressure at 298 K 118

Figure 40. Change in the emission spectrum of powdered WO_3/PVG sample (4.6 x 10^{-5} mol/g) as a function of NH_3 pressure at 298 K 119

Figure 41. Stern-Volmer plots for powdered WO_3/PVG sample (4.6 x 10^{-5} mol/g) at 298 K 121

Figure 42a. Emission spectra of powder WO_3/PVG samples with different W contents at 298 K 123

Figure 42b. Emission intensity with W content 124

Figure 43. Photoluminescence spectrum of pure CaWO4 powder..... 126

Figure 44. Electronic spectra of $Ru_3(CO)_{12}$ on PVG (7.0×10^{-7} mol/g) 129

Figure 45. DRIFT spectra of $Ru_3(CO)_{12}$ on PVG (4.5×10^{-5} mol /g) 130

Figure 46. Electronic spectra of (a) physisorbed $Ru_3(CO)_{12}$ on PVG (7.0×10^{-7} mol/g), (b) (μ-H)$Ru_3(CO)_{10}$(μ-OSi), (c) (μ-H)$Ru_3(CO)_{10}$(μ-OSi) under 400 torr of 1-pentene..... 131

Figure 47. DRIFT spectra of (a) (μ-H)$Ru_3(CO)_{10}$(μ-OSi), and (b) (μ-H)$Ru_3(CO)_{10}$(μ-OSi) under 400 torr of 1-pentene..... 132

Figure 48. Profile of (a) cis-2-pentene , and (b) trans-2-pentene during 254 nm photolysis of (μ-H)$Ru_3(CO)_{10}$(μ-OSi) under (c) 400 torr of 1- pentene..... 135

Figure 49. GC-MS spectrum of gaseous products generated from 254-nm photolysis of 400 torr of 1-pentene with (μ-D)$Ru_3(CO)_{10}$(μ-OSi)... 136

Figure 50. Yields of 2-pentenes during 254 nm photolysis of 1.2×10^{-6} mol of $Ru_3(CO)_{12}$ physisorbed onto PVG under 400 torr 1-pentene..... 139

Figure 51. DRIFT spectra of (a) (μ-H)$Ru_3(CO)_{10}$(μ-OSi), and (b) (μ-H)$Ru_3(CO)_{10}$(μ-OSi) under 500 torr of CH_2CH_2 140

Chapter 1. INTRODUCTION

1.1. Introduction

The 1973 oil crisis stimulated efforts and searches for alternative energy sources. Photochemists took up the challenge in earnest in the mid-1970s. Many proposals appeared regarding generating chemical fuels from readily available raw materials. The production of dihydrogen from the photosplitting of water, hydrogenation of carbon monoxide and carbon dioxide are three examples. Although the initial impetus has declined, research on photochemical energy conversion, storage, and related reactions based on photoelectrochemical cells and photocatalytical systems continues in universities and industrial laboratories throughout the would.

In addition to searching for new energy resources, the global climate change has received much attention in recent years. An authoritative scientific assessment by the United Nations-sponsored Intergovernmental Panel on Climate Change (IPCC), a group of several hundred scientists from 25 countries, predicted in the 1990's that the Earth's average temperature would increase about 0.3 °C per decade, warming roughly 3 °C by 2100, unless action was taken to reduce emissions of greenhouse gases into the atmosphere. The gases of major concern are carbon dioxide, methane, chlorofluorocarbons (CFCs), and nitrous oxide. Most research has focused on carbon dioxide, by far the largest single contributor to the greenhouse effect. The major source of carbon dioxide is the burning of fossil fuels, the primary energy supply of the industrialized world. However, to reduce carbon dioxide emission with available technologies, such as energy conservation and fuel

switching, will be extremely costly.[1] An attractive strategy, from the economic and environmental points of view, is to develop new chemical processes that efficiently convert carbon dioxide to chemical fuels. Transition metal systems are good candidates for a catalyst in the activation and fixation of the molecule. The efforts currently made are intended to find out the correct reaction conditions and catalysts to accomplish the synthesis with high yields and good selectivity.

1.2. Catalytic Reactions of Carbon Dioxide with Hydrogen

The reduction of carbon dioxide by hydrogen yields, depending on the catalyst and the reaction conditions, formaldehyde, methanol or methane. The Sabatier reaction:

$$CO_2 + 4H_2 \text{ ----------> } CH_4 + 2H_2O \qquad \Delta G^\circ = -27 \text{ kcal mol}^{-1} \quad (1.1)$$

is an important catalytic process of wide industrial and academic interest. It is applied to synthesis gas conversion and the treatment of waste streams.[2-5] Methane is one of the most important carbon resources of the world, serving as an energy vector as well as a feedstock for higher-value chemicals.[6-8] Intensive investigations during the past decade have therefore been aimed at improving the activity and selectivity of methanation catalysts.

Heterogeneous catalysts of nickel, ruthenium and rhodium have proved to be the best for the Sabatier process. The kinetics and mechanism of

CO_2 hydrogenation on nickel catalysts has been investigated by Weatherbee and Bartholomew.[9] These investigators measured rate of CO_2 hydrogenation on Ni/SiO_2 as a function of H_2 and CO_2 partial pressures at 500-600 K, 140 kPa total pressure, and a gas hourly space velocity (GHSV, mL of gas per mL of catalyst per hour) at 30,000- 90,000 h^{-1}. The data show that the rate of CO_2 hydrogenation is moderately dependent on CO_2 and H_2 concentration at low partial pressures, but essentially concentration independent at higher partial pressures. Reaction orders and the true activation energy are quite temperature dependent indicating a complex Langmuir - Hinshelwood mechanism involving dissociative adsorption of CO_2 to CO and atomic oxygen. The dissociative adsorption is followed by hydrogenation of CO to methane via a carbon intermediate.

The effect of the silica and titania on the supported nickel catalysts was examined by Spinicci and Tofanari using temperature-programmed reduction and temperature-programmed desorption method.[10] The two supports exhibit different levels of NiO reduction after the reducing pretreatments. The smaller surface area and absence of acidic centers in Ni/TiO_2 catalysts result in a less carbon dioxide adsorption, and higher levels of NiO reduction compared to that on Ni/SiO_2 catalysts. The greater amounts of Ni and smaller amounts of carbon dioxide adsorbed on the surface of Ni/TiO_2 catalysts are offset by the larger amount of hydrogen adsorbed on the metallic nickel which evidently fosters carbon dioxide hydrogenation because of a favorable hydrogen to carbon dioxide ratio.

Ruthenium catalysts were first used in the Sabatier reaction by Lunde and Kester.[11] They examined the reaction at 1 atm using a 0.5 % ruthenium supported on alumina as a catalyst. The experiment was performed in a 4.15 cm^3 isothermal reactor with 0 to 85 % conversion of the inlet feed gases at feed flow ratio (H_2 to CO_2) of 1.9 to 3.9, and temperatures of 400 to 680 °F. Since the high activity of the catalyst in the CO_2 methanation, many studies of carbon dioxide hydrogenation on ruthenium catalysts have followed this initial report.[12-17]

Gupta and coworkers investigated the mechanism of CO and CO_2 methanation over a Ru/molecular sieve (13 X) catalyst.[12] The chromatographic analysis and ESR results indicate that CO disproportionation occurs on the catalyst to give "active" carbon and CO_2. The active carbon thus formed reacts with H_2 to give CH_4. Unlike CO, CO_2 does not directly decompose on the catalyst, but when H_2 is passed over the adsorbed CO_2, carbon is formed and subsequently reduced by H_2 to give CH_4. The ESR signal of carbon is reduced on subsequent H_2 injection initially, but a low intensity ESR signal persists even after continuous passage of H_2 for hours, and at reaction temperatures above 470 K, the carbon signal is not reduced on subsequent passage of H_2. The authors suggest that the carbon atoms, formed on disproportionation of CO, or reduction of CO_2 are initially reactive and converted with time and temperature to an inactive form. Also, the fact that deposited carbon does not react with preadsorbed H_2 suggests that CH_4 is formed by the reaction of the active form of carbon directly with the

H_2 in the gas phase.

Zagli and Falconer studied the adsorption and methanation of carbon dioxide on a ruthenium-silica catalyst using temperature-programmed desorption (TPD) and temperature-programmed reaction (TPR).[13] The results show that CO_2 adsorption increases significantly as the temperature increases from 298 to 435 K. Heating in a hydrogen flow (TPR) following CO_2 adsorption produces both CH_4 and H_2O. Methanation of adsorbed CO and of adsorbed CO_2 in flowing hydrogen yields a single CH_4 peak with the same peak temperature of 459 K for both adsorbates. Based on these results, the authors claim that adsorption onto supported ruthenium activates CO_2, and some of the CO_2 dissociates to carbon monoxide and oxygen. Upon exposure to hydrogen at room temperature, the oxygen reacts to form water, and carbon monoxide follows the mechanism of carbon monoxide methanation.

Prairie and coworkers studied the low-temperature (T<200 °C) methanation of CO_2 over Ru on TiO_2 supports and on Al_2O_3 using diffuse-reflectance Fourier transform (DRIFT) spectroscopy.[18] With a 3.8 % Ru/TiO_2 catalyst, the reaction exhibits an activation energy ,Ea, of 19 kcal/mol and is essentially independent of CO_2 concentration. At 110 °C, 40 % of the available metal sites are occupied by CO (θco = 0.4), a known methanation intermediate. In contrast to Ru/TiO_2, Ru/Al_2O_3, despite having the same Ea and θco = 0.2, is 15 times less active. No dependence of methanation activity on the rate of CO adsorption, designated CO_a, or on θco indicate heterogeneity in the active sites and CO_a hydrogenation proceeds only on a small number

of highly active sites since CO dissociation is known to be structure-sensitive.[18a] The high Ru dispersion on TiO_2 is believed to contribute to the enhanced activity over this support. Adsorbed CO_2 and H_2 react, possibly at the metal-support interface, to form CO_a via rapid equilibration of the reverse water-gas shift reaction. The intense band at 2051 cm^{-1} observed on a Ru/TiO_2 catalyst with 10 mol% CO_2/40 mol% H_2 at 110 °C has been assigned to a linearly bound CO on Ru. [18b] The CO(ads) hydrogenation step is proposed as a rate-controlling step.

Solymosi and coworkers investigated the synthesis of methane from CO_2 and H_2 on supported Rh catalysts.[19] The hydrogenation of CO_2 on Rh/Al_2O_3 occurs at a measurable rate above 443 K, yielding exclusively methane, and the hydrogenation of CO_2 occurs much faster than that of CO. The support exerts a marked influence on the specific activity of Rh. The most effective support is TiO_2 and the least effective one is SiO_2. IR spectroscopy reveals that linearly bonded CO and adsorbed formate species are present on the catalyst surface during the reaction. When the $H_2 + CO_2$ +He inlet feed gases flow is replaced with He and then with a H_2 + He stream, the formation of CH_4 is observed for the next 10-20 minutes. IR spectroscopic measurements reveal that in the case of the Rh/SiO_2 sample all of the adsorbed CO is removed in 2-3 minutes. Therefore, the investigators assumed that the observed CH_4 evolution is exclusively due to the hydrogenation of surface carbon formed in the H_2 + CO_2 reaction. It is proposed that the important steps in CH_4 formation are the dissociation of CO_2 promoted by

adsorbed hydrogen, the subsequent dissociation of CO into reactive surface carbon, and hydrogenation of latter.

The rate of CO_2 methanation increases as the metal dispersion increases, that is, as the particle size decreases. Ichikawa, for example, reported that the turnover frequency for CO_2 methanation on highly dispersed rhodium (Rh/SiO_2), prepared by cation exchange, was about fifty times that on a low dispersed Rh/SiO_2 catalyst, and comparable to a highly dispersed Rh/TiO_2 catalyst.[20] Henderson and Worley also reported that all catalysts having 0.5 % Rh loading were more highly dispersed than the catalysts with 10 % Rh loading.[21]

Somorjai and coworkers studied the kinetics of CO_2 hydrogenation on a Rh foil promoted by titania overlayers.[22] Submonolayer deposits of titania on a Rh foil were found to increase the rate of CO_2 hydrogenation. The primary product, methane, exhibits a maximum rate at a TiO_x coverage of 0.5 monolayer (ML), which is a factor of 15 higher than that over the clean Rh surface. The methanation of CO_2 is proposed to start with the dissociation of CO_2 into $CO_{(a)}$ and $O_{(a)}$, and then proceed through steps which are identical to those for the hydrogenation of CO, i.e.,

$$2H_{(a)} + CO_{(a)} \text{-------} > H_2CO_{(a)}$$
$$H_2(CO)_{(a)} \text{-------} > CH_{2(a)} + O_{(a)}$$
$$CH_{2(a)} + H_{(a)} \text{-------} > CH_{3(a)}$$
$$CH_{3(a)} + H_{(a)} \text{-------} > CH_{4(a)}$$

The increase in the rate of CO_2 hydrogenation in the presence of titania is attributed to an interaction between the adsorbed CO, released by CO_2 dissociation, and Ti^{3+} ions located at the edge of TiO_x islands covering the surface.

Hydrocarbons, mostly within the C-number range C_2-C_{18}, are generally produced by the Fischer-Tropsch process using the synthesis gas, CO/H_2. Recently, Fischer-Tropsch syntheses have been achieved with CO_2/H_2 mixtures. [23-29] One interesting aim is the synthesis of lower alkanes and alkenes from carbon dioxide. Barrault and co-workers reported that C_2 to C_5 alkanes and alkenes are formed by using iron catalysts, doped with copper.[30] Pijolat achieved similar results using Fe/Al_2O_3 catalysts.[31] Fujimoto and Shikada combined a copper-zinc methanol synthesis catalyst with a high silica NaY zeolite to study the direct synthesis of hydrocarbons from carbon dioxide and hydrogen. The efficiency of conversion of CO_2 is low, but C_2-C_5 hydrocarbons are obtained.[32] Kuei and Lee investigated direct synthesis of aromatics from carbon dioxide and hydrogen using hybrid catalysts composed of iron catalysts and HZSM-5 zeolite.[33] Carbon dioxide is first converted to CO, followed by the hydrogenation of CO to hydrocarbons on iron catalyst, and finally the hydrocarbons are converted to aromatics in HZSM-5. Fujiwara and Souma reported that combinations of Cu-Zn-Cr oxides and zeolites are effective for the conversion of carbon dioxide into C_2 and higher hydrocarbons.[34]

Methanol synthesis from CO_2 and H_2 has also received considerable attention in recent years. It has been shown that CuO/ZnO-based catalysts are highly effective for this reaction.[35-41] Tanabe and coworkers investigated the support effect of zinc oxide catalyst on synthesis of methanol from CO_2 and H_2.[42] The ZnO/ZrO_2 catalyst shows high activity and selectivity for methanol formation. Millar and coworkers studied the interaction of CO_2 and H_2 on reduced and oxidized silica-supported copper catalysts.[43a] At room temperature, carbon dioxide initially dissociates to produce carbon monoxide and surface oxygen on the surface of the reduced catalyst. Further carbon dioxide adsorption interacts with the surface oxygen to produce a symmetric carbonate species. Co-adsorption of H_2 and CO_2 (1:1, at 1 atm) on a reduced copper catalyst results in dissociation of H_2 producing adsorbed hydrogen atoms and symmetric carbonate species. Heating these adsorbates to 388 K causes them to react producing a surface formate species, the dominant intermediate of methanol synthesis. Fujita and coworkers reported that two types of formate species, HCOO-Cu, HCOO-Zn, and zinc methoxide, CH_3O-Zn, are formed in the reaction of CO_2 and H_2 over a Cu/ZnO catalyst.[43b] CH_3OH is produced by hydrolysis of CH_3O-Zn in the course of the methanol synthesis, that is, CH_3O-Zn reacts with H_2O formed via the reverse water gas shift reaction. Dubois and coworkers reported that a combination of a CH_3OH synthesis catalyst (Cu-ZnO-Al_2O_3) with a solid acid, such as a Y-zeolite, SiO_2, or Al_2O_3, promotes CH_3OCH_3 formation, which creates a strong driving force for CO_2 conversion.[44]

Although significant progress has been made in catalytic hydrogenation of CO_2, elevated temperatures (T > 300 °C) and pressures (P > 1 atm) are still required for the reactions to proceed at significant rates and yields. As a result, recent work has been directed toward the development of light induced CO_2 hydrogenation processes.

1.3. Homogeneous Photocatalytic Reduction of CO_2

The photoreduction of CO_2 using homogeneous catalysts can be achieved in several ways. Transition metal complexes and colloidal semiconductors have been employed as catalysts, and organic solvents or water used as electron sources.

The first photochemical system for carbon dioxide reduction in homogeneous conditions consisted of $[Ru(bipy)_3]^{2+}$ (bipy = 2,2 bipyridine) and $[Co(bipy)_3]^{2+}$ or a Co^{2+} species in organic solvents with added tertiary amines.[45] The products of the reaction are CO and H_2. The maximum quantum yield and the CO/H_2 ratio obtained depended on the amount of free ligand (2,2'-bipyridine) present in the medium and the nature of the tertiary amine, ethylamine or hydroxylated amines, which is used as an electron donor.

Spreer has reported a system affording a good CO/H_2 ratio composed of $[Ru(bipy)_3]^{2+}$ and $[Ni(cyclam)]^{2+}$ (cyclam = 1, 4, 8, 11- tetraazacyclotetradecane) complexes in aqueous solution with an ascorbate buffer as

electron donors.[46] The dependence of CO/H_2 ratio on the pH of the medium was studied and the best CO/H_2 ratio was observed at pH=6.

Tanaka and coworkers studied a photochemical system with $[Ru(bipy)_3]^{2+}$ and $[Ru(bipy)_2(CO)_2]^{2+}$ dissolved in TEOA/DMF (1:4 v/v) (TEOA= triethanolamine, DMF= dimethylformamide) mixture saturated with CO_2.[47] This system catalyzes a selective CO_2 reduction to formate with maximum quantum yield of 14 %.

Calvin and coworkers investigated the photochemical reduction of CO_2 using nickel tetraazamacrocycles in an ascorbate-buffered solution at room temperature under 1 atm of CO_2.[48] $Ru(bpy)_3^{2+}$ is used as a photosensitizer, and it is found that the Ni(II) macrocycles, $[Ni\ (14\text{-}aneN_4)]^{2+}$ and $[Ni\ (12\text{-}aneN_4)]^{2+}$ ($14\text{-}aneN_4$ = 1, 4, 8, 11-tetraazacyclo-tetradecane, $12\text{-}aneN_4$ = 1, 4, 7, 10-tetraazacyclododecane), reduce CO_2 to CO with similar quantum yields. In addition, $[Ni(12\text{-}aneN_4]^{2+}$ produces formate as well as carbon monoxide. The difference in product distribution is explained by the different structures and properties of the two nickel complexes. The $[Ni\ (14\text{-}aneN_4]^{2+}$ is a low- spin square-planar complex, while $[Ni(12\text{-}aneN_4]^{2+}$ is six-coordinated with two cis water molecules.

Kimura and coworkers synthesized a bifunctional supramolecular complex $Ru(phen)_2(phen\text{-}cyclam\text{-}Ni)(ClO_4)$ (phen-cyclam = 1 - (1 , 10 -

phenanthrolin-5-ylmethyl)-1, 4, 8, 11-tetraazacyclotetradecane) for the catalytic photoreduction of carbon dioxide.[49] Irradiation of the complex in a CO_2-saturated ascorbate buffer solution (pH 4.0) at 25 °C results in a CO/H_2 ratio of 2.5.

The photochemical conversion of carbon dioxide has been also achieved by using tungsten carbonyl complexes, $[W_2(CO)_{10}]^{2-}$.[50] Irradiation of a CO_2 saturated CH_3CN solution of $Na_2W_2(CO)_{10}$ and PPh_3 with visible light ($\lambda > 420$ nm) produces a white precipitate containing $NaHCO_2$, Na_2CO_3 and $NaHCO_3$. The proposed mechanism considers the reactive species as a 19 electron metal complex, $[W(CO)_5PR_3]^-$, which is obtained by irradiation of the dimer $W_2(CO)_{10}^{2-}$ in the presence of PPh_3, and the residual water in the system is the source of hydrogen for the formate. The dimer exhibits adsorptions at 347 nm and 390 nm that are assigned to the σ ---> σ^* and $d\pi$ ---> σ^* transitions, respectively.[51] Therefore, irradiation with light of $\geq$ 420 nm, which initiates CO_2 reduction, results in excitation of the low energy tail of the $d\pi$ ----> σ^* transition. This photochemical conversion is reminiscent of the so called "disproportionation" of carbon dioxide

$$2CO_2 + 2e^- \text{--------} > CO + CO_3^{2-}$$

promoted by several metal system.[52]

Colloidal semiconductors combine a number of desirable properties such as high extinction coefficients, fast carrier diffusion to the interface and

suitable positioning of valence and conduction bands to achieve high efficiencies in light energy conversion processes. As a result, these systems currently receive enormous scientific attention. For example, Yanagida and coworkers reported that colloidal CdS microcrystallites prepared from $Cd(ClO_4)_2$ and H_2S in N , N - dimethylformamide catalyzed a selective photoreduction of CO_2 to CO with apparent quantum yield, Φ= 0.098 (400 nm), using triethylamine as a sacrificial electron donor.[53] Aliwi used a new type of organometallic complex semiconductor: hydroxo-oxobis (8-quinolyloxo) vanadium(V) as a photocatalyst for the reduction of CO_2 to formic acid and formaldehyde in aqueous medium.[54] In this case, it is found that the reduction rate is enhanced by the presence of a methyl viologen - ethylenediaminetetraacelate, MV^{2+} - EDTA, electron relay system.

As described above, most efforts to effect the photoreduction of CO_2 in homogeneous solution photoreactions leads to formation of carbon monoxide or formate as the carbon-containing products. Willner and coworkers explored the photoreduction of CO_2 to methane and higher hydrocarbons in aqueous solution by using visible light and Ru or Os colloids as catalysts.[55] One system is composed of tris(bipyridine)Ru(II) ($Ru(bpy)_3^{2+}$) as photosensitizer, triethanolamine (TEOA) as the electron donor, and one of the following bipyridinium charge relays: N, N'- dimethyl-2, 2'- bipyridinium, N, N'- trimethylene-2, 2'- bipyridinium, N, N'- tetramethylene-2, 2'- bipyridinium, or N,N'-bis-(3-sulfonatopropyl)-3,3'-dimethyl-4,4'bipyridinium. Illumination of these systems under CO_2 in the presence of Ru or Os colloids

leads to the formation of methane, ethylene and H_2. The second system is composed of Ru(II) tris(bipyrazine) as sensitizer, TEOA as electron donor, and Ru colloids. Illumination of this system in an aqueous solution under CO_2 leads to the formation of methane, ethylene and ethane, but in this case, H_2 evolution did not occur. The authors examined the H_2 evolution process in the presence and absence of bipyrazine, and conclude that H_2 evolution is inhibited by the bipyrazine ligand. They also examined reduction of CO_2 by hydrogen in an aqueous bicarbonate solution (pH 7.8) under a gaseous atmosphere of H_2 (0.75 atm) and CO_2 (0.75 atm) in the dark. In the presence of the Pt colloid, either Ru or Os colloids and N, N'- dimethyl-2, 2'-bipyridinium as the charge relay, photolyses yield methane and ethylene. When the charge relay is excluded from the system, no reduction of CO_2 occurs. The need for the electron relay implies that the methanation process occurred through an electron-transfer mechanism. Therefore, they emphasized that photo-reduction of CO_2 occurs via electron transfer followed by protonation steps rather than by a hydrogenation mechanism.

A problem which is immediately evident in homogeneous solution is that back electron transfer is often more rapid than forward electron transfer. To circumvent this energy-wasting back reaction, researchers have directed their attention to organized assemblies and heterogeneous phase processes.

1.4. Heterogeneous Photocatalytic Reduction of CO_2

Most primary heterogeneous photocatalysts are semiconductors. Semiconductors are particularly useful for such applications because of a

favorable combination of electronic structure, light absorption properties, charge transport characteristics, and excited-state lifetimes. Although the semiconductor photocatalyst functions in a manner similar to the molecular photocatalyst, it possesses several properties characteristic of the solid:

1. The semiconductor photocatalyst functions as a pool of electrons or holes, which is advantageous in multielectron transfer reactions.
2. Efficient charge separation occurs at the interface between the semiconductor and a liquid or gas, owing to the electric field in the space charge layer of the semiconductor.
3. The catalytic effect of the semiconductor surface can be utilized and modified by the deposition of a photoredox catalyst.

As early as 1979, Inoue and coworkers have carried out a systematic study of a variety of semiconductor powders in aqueous suspensions.[56] Product yields of formaldehyde and methanol decrease in the following order of semiconductor particulates: SiC > CdS > GaP > ZnO > TiO_2 > WO_3. Estimated quantum yields for SiC as the photocatalyst, with respect to the number of incident photons, are 0.0005 for HCHO and 0.0045 for CH_3OH.

Further studies on the photoassisted reductions of CO_2 in semiconductor particulate system have been reported.[57-62] Dzhabiev and coworkers studied the photocatalytic reduction of CO_2 in aqueous CdS, SiC, TiO_2 and $SrTiO_3$ suspensions with supported catalytic additions of Pt, Rh, Ru, Ag and Cu.[63] In the absence of the specially added electron donors, the CO_2

photoreduction is observed on the TiO_2 and $SrTiO_3$ suspensions only, while those with CdS and SiC are inactive. The ratio of the reaction products (CO, C, CH_4) is dependent on the specific metal-catalyst on the semiconductor surface. Hirano and coworkers obtained methanol and formaldehyde from the photocatalyzed reduction of CO_2 in a TiO_2 powder suspended solution mixed with copper powder.[64]

Only a few literature reports have described the photocatalytic reduction of CO_2 on gas-solid systems. Thampi and coworkers found a heterogeneous catalytic system for the photoassisted reduction of atmospheric CO_2 with sunlight.[65] The catalyst exhibiting the highest efficiency for CO_2 methanation consists of ca. 75 % RuO_x ($x \leq 2$) and 25 % Ru, as shown by X-ray photoelectron spectroscopy (XPS). CO_2 is selectively converted to CH_4 over highly dispersed Ru/RuO_x mixture loaded on TiO_2, and the reaction rate is sharply enhanced through photo-excitation of the supported materials. The authors proposed that a key role in the methanation of CO_2 on Ru was played by a surface carbidic bond to Ru, i.e., Ru-C. However, Melsheimer and coworkers question this postulation since no evidence for Ru-C species as carbides is found in their experiment with the same catalysts.[66] The selective conversion of CO_2 to CH_4 is found to be strongly dependent on temperature. Therefore, the authors concluded that the photoenhancement of the conversion was a thermal effect under their testing conditions.

Lichtin and coworkers investigated the photoassisted reduction of CO_2 by H_2 over a series of metal oxides, i.e., α-Fe_2O_3, Zn-Fe-oxide, Pt-La-Ni-oxide,

Co-Mo-Al-oxide, Co-Mo-Ti-oxide and Pt-$SrTiO_3$, in the presence and absence of water vapor.[67] In the absence of water vapor, CO is the major product formed over all the catalysts, while CH_4 is the principal minor product. In the presence of water vapor, formic acid, CH_3OH and traces of CH_2O are observed besides CO and CH_4.

Ogura and coworkers studied a dark catalytic reduction of CO_2 over photo-pretreated NiO/ksgr catalyst.[68] A NiO/ksgr (kieselguhr) catalyst is pre-irradiated with a 15 W low-pressure mercury lamp (185 and 245 nm) in hydrogen atmosphere and subjected to flowing CO_2 in the dark. CH_4 is preferentially formed with small amount of C_2H_6 and C_3H_8. The authors proposed that the reduction of CO_2 was performed by chemisorbed hydrogen atoms which were produced during the pre-irradiation of the catalyst in H_2.

Ogura and coworkers also studied the visible-light-assisted decomposition of H_2O and photomethanation of CO_2 over CeO_2-TiO_2 catalyst.[69] A 500 W xenon lamp served as the light source, and the light was passed through a Toshiba UV-37 filter, which cut out wavelengths shorter than 370 nm. Under these conditions, i.e., visible light irradiation, H_2O is stoichiometrically decomposed to H_2 and O_2, and CH_4 is produced from the methanation of CO_2 by the generated H_2.

1.5. Hybrid Catalysts

As described in the preceding sections, transition metal complexes play

an important role in photocatalysis. An important attribute of transition metal complexes originates from their ability to provide sensitizers capable of using sunlight, i.e. visible and near UV light. To examine their potential as new catalysts, a particularly attractive approach is to use transition metal carbonyls that possess a number of advantages as catalytic species. For example, the metal carbonyl are commercially available, or readily synthesized. Their structure and bonding are well characterized, and many form cluster compounds so that reactions requiring multiple metal sites might be accomplished. And lastly, since CO is a gas, it can be exploited as a renewable and readily available ligand.

It is generally accepted that photocatalysis by transition metal carbonyls involves photoinduced decarbonylation to yield a coordinately unsaturated species.[70] In fluid solution, the coordinately unsaturated intermediate is highly reactive and it is difficult to characterize this species or an active complex derived from it. Also, additional difficulties in homogeneous catalysis arise from the separation of the reaction mixture. An attractive alternative is to develop "heterogeneized" homogeneous catalysts, i.e., hybrid catalysts, where the catalytically active form of a metal carbonyl is bound to solid surfaces. A hybrid catalyst retains many of the properties of a homogeneous species, such as control of the catalyst on a molecular level, higher activity and deeper mechanistic understanding, while enjoying the additional advantages of a heterogeneous system, such as easy catalyst-reactant separation and catalyst stability.

The support used to hybridize a transition metal complex must be inert

to the reaction mixture, withstand the reaction conditions, and possess a large surface area. However, commonly used supports, such as inorganic oxides, graphite and organic polymers, do not necessarily behave as inert supports. These substrates may act as acids or bases, adsorbents, photosensitizers or quenchers, and restrictive environments for size - specific reactions. In addition, many supports are opaque which in photocatalysis reduces the efficiency of optical excitation. Thus, the catalyst, the adsorbent, and the interaction between the two can enhance or reduce photoabsorption, reaction rates and selectivities.

In spite of a large effort during the past decade, photocatalysis by hybrid catalysts has, to a significant extent, progressed slowly. This is due to the fact that it is difficult to control the photochemistry on solid surface since surface reactions are affected by a number of factors, such as adsorption, desorption, diffusion and nucleation. Nevertheless, significant advances in the development of analytical instruments and techniques to probe surfaces and adsorbed species has led to an increased interest in the photoactivation of hybrid system.

1. 5. 1. Thermal Activation of Supported Group VIB Hexacarbonyls

The thermal activation of supported metal carbonyls has been examined for preparing well characterized catalytically active species on solid surfaces.[71,72] Howe reported that $Cr(CO)_6$ supported on alumina would undergo complete decarbonylation in vacuo above 283 °K to form dispersed

metallic particles.[73] The decarbonylation is established by IR spectroscopy and by the observation that treatment with CO (6.6 x 10^3 N/m^2) at 318 °K partially restores the $Cr(CO)_6$ bands. Subsequent work by Brenner and Hucul using a temperature programmed decomposition technique, TPDE, demonstrates that in the presence of flowing helium, temperatures in excess of 573 °K are required to achieve complete decarbonylation.[74] The TPDE profile illustrates two distinct regions of decarbonylation, the first occurs between 50 - 200 °C and the second between 200 - 500 °C. CO evolution at the latter temperatures is accompanied by hydrogen evolution, derived from surface hydroxyl groups. The hydrogen evolution suggests that the originally zerovalent metal has been oxidized.

Alternatively, when $Cr(CO)_6$ is bound to silica somewhat different results are obtained. Temperature programmed decomposition of $Cr(CO)_6/SiO_2$ in flowing helium establishes that all the carbonyl ligands are lost in rapid succession over a narrow temperature range.[75] Similar to the results obtained on alumina, hydrogen evolution accompanied by metal oxidation occurs during the decarbonylation. At 873 °K, the number of equivalents of hydrogen evolved establishes that chromium is at a +4 oxidation state. EPR studies indicate that $Cr(CO)_6/Al_2O_3$ catalysts activated at 473 °K and then exposed to oxygen generate Cr^{5+} ions in square - pyramidal and tetrahedral coordination.[76]

Howe and coworkers report that thermal activation of immobilized

$Mo(CO)_6$ catalysts involves complex decomposition,[77] where the extent of decarbonylation is a function of the basicity and/or hydroxylation of the support. In general, supports that did not readily stabilize subcarbonyl species by coordination to the vacated sites induce rapid decarbonylation of the adsorbed complex.

Using IR spectroscopy, Howe established that when $Mo(CO)_6$ is exposed to SiO_2 or Al_2O_3, the carbonyl is physisorbed onto the solid surface.[73] However, the physisorbed $Mo(CO)_6$ is not stable in vacuo at a temperature as low as -10 °C and immediately loses CO to form $Mo(CO)_5$(ads). The latter then decomposes further to give a stable subcarbonyl species of unknown stoichiometry. Upon exposure to CO ($< 1.33 \times 10^4$ N/m^2), however, this stable carbonyl species, $Mo(CO)_x$, can be reversibly carbonylated to $Mo(CO)_5$(ads) and at higher CO pressures ($>6.67 \times 10^4$ N/m^2) $Mo(CO)_6$(ads) slowly reappears. Identical results are obtained with both $W(CO)_6$ and $Cr(CO)_6$ on alumina and silica.

Although Howe concluded that the decarbonylation of the Group VIB hexacarbonyls was complete and reversible, subsequent work by Brenner and coworkers establishes that following partial decarbonylation on a fully hydroxylated support, additional CO could no longer recarbonylate the metal.[75] The authors investigated the possibility of oxidized species forming during the TPDE of Group VIB hexacarbonyls bound to γ - alumina and silica.[75,78] At higher temperature (200-500 °C), decarbonylation is

accompanied by hydrogen evolution. It is proposed that the evolved hydrogen originates from H^+ in the surface hydroxyl groups of the alumina and is reduced to hydrogen gas, accompanied by an equivalent amount of transition - metal oxidation.

$W(CO)_6$ bound to inorganic support has received less attention than its molybdenum analog. Early studies of the the $W(CO)_6/Al_2O_3$ system suggested that no stable subcarbonyl species is formed during thermal activation up to -10 °C.[73] However, Brenner and Hucul have demonstrated that $W(CO)_3$(ads) is formed at 408 °K in the TPDE systems.[79] A temperature of 673 °K is required to produce complete decarbonylation, and W^{6+} is formed on highly hydroxylated supports whereas W^0 is formed on highly dehydroxylated supports. This behavior is similar to that of the corresponding $Mo(CO)_6/Al_2O_3$ systems,[80] and silica-supported $W(CO)_6$ also resembles $Mo(CO)_6/SiO_2$.[75]

Studies of supported VIB carbonyls used as catalysts for olefin metathesis,[81] olefin hydrogenation[75], and polymerization[82] have been reported. The active form of the catalysts is not the original hexacarbonyl, but a subcarbonyl species of unknown stoichiometry.

1. 5. 2. Photoactivation of Supported Group VIB Carbonyls

Nevertheless, there are some disadvantages in thermal activation of metal carbonyls on a surface. It is difficult to control the reactions of the carbonyls to form desired catalytical species by thermal activation. Oxidation of the metal carbonyl by hydroxyl groups on the solid surface is possible, and aggregation of the species formed by thermal decomposition of metal carbonyl may lead to larger metal clusters.

Photoactivation of metal carbonyls might be a way to resolve some of the above disadvantages. Light is a more controllable energy source than heat. A monochromatic irradiation could selectively induce a specific photochemical reaction to form an active species for catalysis. Moreover, the d^6 metal hexacarbonyls are extremely photosensitive with respect to dissociative loss of CO. The decomplexation of CO in the excited state has been estimated to be 10^{16} times greater than that same reaction in the ground state.[83] However, the opacity of many traditional oxide support materials have limited the application of photochemical methods to prepare catalytically active species on solid surface. The opaque nature of these supports drastically reduces the efficiency of any photochemical process due to a nearly complete loss of useful light by scattering, reflection or absorption. Therefore, only a few literature reports have described the use of the photochemistry of metal carbonyls on a solid surface to prepare catalyst.

Almond and coworkers have reported that prolonged photolysis of $M(CO)_6$ (M = Cr, Mo, W) trapped in O_2-doped Ar matrices generated free CO and CO_2 together with CrO_2 and MO_3 (M = Mo and W).[84]

Germer and Ho investigated the irradiation of $Mo(CO)_6$ on Rh (100) surface with IR laser absorption methods.[85] The results suggest that at least two, but not all, of the CO ligands are removed from each physisorbed $Mo(CO)_6$ molecule.

Wada and coworkers reported that UV photoactivation of $Mo(CO)_6$ and $W(CO)_6$ adsorbed on solid supports, such as porous Vycor glass and NaY zeolite, results in a catalytical species for propene metathesis.[86] Once activated, the catalysts remain active after the light irradiation is ceased, suggesting that the catalytically active species is formed by the irradiation. Formation of a subcarbonyl molybdenum is observed by UV spectroscopy after the $Mo(CO)_6$/PVG catalyst is irradiated under UV light. The authors proposed that the subcarbonyl is stabilized by the interaction with the solid surface and acts as the active sites or its precursor for the metathesis.

The photochemical behavior of the group VI B hexacarbonyls adsorbed onto porous Vycor glass have been studied in this laboratory.[87] The electronic spectra of the adsorbed complexes closely resemble spectra of the complexes in n-hexane.[88-89] In the 500 - 260 nm region, spectra of $Cr(CO)_6$(ads), $Mo(CO)_6$(ads), and $W(CO)_6$(ads) show intense bands centered at 280, 286, and 287 nm, respectively. DRIFT spectra of $Cr(CO)_6$(ads), $Mo(CO)_6$(ads), and $W(CO)_6$(ads) show intense bands centered at 1999, 2005, and 1986 cm^{-1}, respectively. With the exception of some broadening, particularly of the lower energy shoulders, these spectra also resemble the spectra of the complexes in

n-hexane.[88] The absence of decomposition products, such as CO or H_2, during adsorption as well as the similarity of spectra of the adsorbed complexes with fluid-solution spectra establish that the complexes physisorb onto PVG as distinct molecular entities without disruption or significant distortion of their primary coordination spheres.

However, excitation with 350 nm light causes an immediate decline in the UV absorption characteristic of each hexacarbonyl and a concurrent growth of bands in the 240-250 and 400-450 nm regions. While an isosbestic point is maintained, GC analysis of the reactor cell contents after 350 nm photolysis in vacuo yields 1.0 ± 0.1 mol of CO/mol of $M(CO)_6$ reacted. The reaction stoichiometry and the similarity of the photoproduct spectra with those of the corresponding pentacarbonyls generated in low-temperature matrices,[90,91] and the recovery of ≥ 96% of the hexacarbonyl on exposure to CO (1 atm) establish the primary photochemical event to be

$$M(CO)_6(ads) \text{ ---------> } M(CO)_5(ads) + CO \qquad (1.2)$$

where $M(CO)_5$(ads) denotes a pentacarbonyl with the vacated coordination site occupied by an oxygen atom from either a silanol group or chemisorbed water.

The primary photochemical reaction is independent of the excitation wavelength, whereas the secondary photochemistry exhibits a marked dependence on excitation wavelength. Prolonged excitation with 350 nm light causes only CO evolution, while continued photolysis of a $W(CO)_6$(ads)/ PVG

sample in vacuo with 310 nm light causes CO, H_2, and CH_4 evolution. Similar results are obtained with 254 nm excitation except that the initial spectral changes indicative of $M(CO)_5$(ads) formation are not as well resolved. With both excitation wavelengths, CO_2 is also detected, but in trace amounts corresponding to ≤ 10% of the amount of CH_4 evolved.

The absence of CH_4 evolution during the initial photochemical reaction precludes the primary photoproduct species as the active reagent. During 254 nm photolysis, extrapolations of the initial rates of methane evolution reveal a short induction period preceding H_2 and CH_4 evolution. CO evolution continues during initial stages of the reaction, but eventually CH_4 becomes the dominant gaseous photoproduct. GC analyses and spectroscopic data yield an average stoichiometry of $W(CO)_4$ at the onset of CH_4 evolution.

H_2 evolution suggests metal oxidation, and stoichiometric measurements show that oxidation of the metal initially occurs in a 1 : 1 ratio with the moles of CH_4 evolved. However, the continued CH_4 evolution after complete oxidation of the complex indicates that the agglomerated metal oxide is photocatalytic on the surface.

A 310 or 254 nm photolysis of the complexes adsorbed onto deuteriated PVG leads to the evolution of deuteriated methanes. Mass spectral analyses of the surrounding gas phase reveal CH_4, CH_3D, and small amounts of CH_2D_2. The results suggest that the silanol group and/or chemisorbed water is the hydrogen source in the photoreaction. However, C^{13} labeling confirms that

CH_4 does not derive from the coordinated CO. Isotope labeling experiments with $W(^{13}CO)_6$ establish that in all cases ≤ 1% of the label occurs in the evolved CH_4. Since CH_4 evolution occurs from samples that had been calcined at 650 °C for at least 72 hours, CH_4 does not derive from an adsorbed hydrocarbon. Elemental analysis of calcined PVG indicates trace amounts, ≤ 1%, of C that is thought to be a C_1 oxide in the glass matrix.[92] Therefore, the CH_4 evolution is attributed to a metal promoted reduction of a C_1 oxide present in the glass matrix.

Two questions arose from these previous studies that became the focus of this doctoral dissertation. If the carbon source is a C_1 oxide in the glass matrix, is this hybrid system capable of photocatalyzing the hydrogenation of an external carbon source, specifically CO_2? And if it does, what is the nature of the active center(s) that promotes the hydrogenation of a C_1 oxide?

1. 5. 3. Photoactivation of supported $Ru_3(CO)_{12}$

$Ru_3(CO)_{12}$ has been used as a catalyst or catalyst precursor for a number of transformations. The effectiveness of $Ru_3(CO)_{12}$ as a catalyst for the carbonylation of acetylene has been described as early as 1968.[93] Kuznetsov and coworkers report that $Ru_3(CO)_{12}$ physisorbs onto alumina and silica with the metal framework intact, and the adsorbed complex thermally decomposes to mononuclear species.[94] Basset and coworkers assign a set of IR absorptions that appear during thermal activation of $Ru_3(CO)_{12}$ on silica gel under

vacuum to an oxidative addition of a silanol group.[95] The grafted cluster, $HRu_3(CO)_{10}(OSi)$, is postulated to decompose at ≥ 100 °C to form aggregated metal particles covered with CO and oxidized Ru (II) carbonyl species. Simpson and Whyman have shown that thermal decomposition of $Ru_3(CO)_{12}$ under H_2 on high surface supports yields 15 - 20 Å dia. metal particles that exhibit enhanced activity and selectivity in the hydrogenolysis of straight chain hydrocarbons to methane.[96] Doi and Yano studied the photochemistry of $Ru_3(CO)_{12}$ supported on silica.[97] The adsorbed $Ru_3(CO)_{12}$ exhibits a new absorption at 330 nm, and UV photolysis of the adsorbed complex leads to a monomeric species, which they postulate to be $Ru(CO)_4/SiO_2$.

The photochemical reactions of $Ru_3(CO)_{12}$ adsorbed onto PVG have been studied in this laboratory.[98] Regardless of the impregnation method, the UV-visible spectrum and DRIFT spectrum of the adsorbed trimer closely resembles spectra of the trimer in fluid solution. GC analysis of the surrounding vapor phase after subliming the complex onto PVG gives no indication of CO, CO_2, or H_2 evolution. The similarity with solution spectra and the absence of the evolution of possible decomposition products establishes that $Ru_3(CO)_{12}$ physisorbs onto PVG without disruption or significant distortion of the complex.

The photochemistry of $Ru_3(CO)_{12}$ (ads), however, differs from that in fluid solution. The dominant photochemical reaction of $Ru_3(CO)_{12}$ in fluid

solution is fragmentation,[99-101] whereas scavenging experiments with CO (1 atm) or P(t-Bu)$_3$ (0.25 atm) indicate that the quantum yield of formation of monomeric products is $\leq 10^{-5}$ on PVG.[98] Instead, photolysis of $Ru_3(CO)_{12}$(ads) with light of $\leq$ 310 nm leads to the evolution of 1.8 $\pm$ 0.2 mol of CO/mol of $Ru_3(CO)_{12}$ (ads) reacted. Electronic spectra show that concurrent with a decline in absorbance at 395 nm, an absorbance develops at 330 nm with isosbestic points maintained at 295 and 365 nm through $\geq$ 80% reaction. UV spectra are consistent with quantitative formation of an oxidative addition product.[94-95,97] The DRIFT spectrum of the photoproduct, composed of a weak band at 2109 cm^{-1}, intense bands at 2078 and 2069 cm^{-1}, and a broad band at 2034 cm^{-1} with shoulders at 2017 and 1999 cm^{-1}, confirms the formation of $HRu_3(CO)_{10}(OSi)$.[98] Thus, UV photolysis of $Ru_3(CO)_{12}$(ads) leads to oxidative addition of a surface silanol group across an Ru-Ru bond and formation of the surface grafted species (Figure 1). Oxygen, which anchors the complex to the support, acts as a three electron donor and hydrogen binds to the metal cluster with a two electron, three center bond.[102] Although stable for weeks in vacuo, the grafted complex remains highly reactive. This suggests that this grafted complex might exhibit catalytical properties. A second aspect of this thesis was to examine the possible catalytic activity of the grafted photoproduct on Corning code 7930 porous Vycor glass.

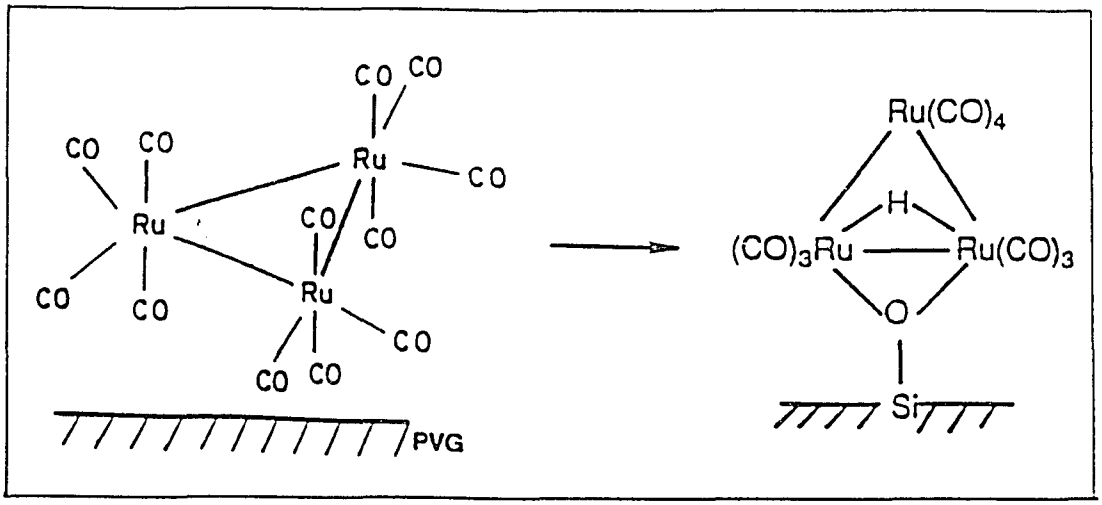

Figure 1. Oxidative addition of $Ru_3(CO)_{12}$ on PVG

1. 6. Porous Vycor Glass and Sol-Gel-Glass

As pointed out by Jackson and Thrusheim, the principal difficulty in quantitating the photochemical behavior of an adsorbed complex is the opacity of the support.[103] Highly scattering supports such as high surface area silicas or alumina, limit the use of absorption spectroscopy and encumber the measurement of quantum efficiencies. To circumvent this difficulty, we make use of Corning's code 7930 porous Vycor glass (PVG) and porous glasses prepared by sol-gel techniques.

Corning's code 7930 PVG is made from sodium borosilicate glass. When the borosilicate melt is cooled below its phase-transition temperature, the silica phase separates from the boron oxide-alkali oxide phase, and acid leaching of the latter phase yields a random, three dimensional network of interconnected pores throughout the glass. Pore size and surface area are determined by the extent of phase separation in the melt and acid leaching. Pore sizes ranging from 20 to 2500 Å are currently available, but larger pore sizes, generally > 100 Å in diameter, reduce optical transparency. The glass used in our experiments has an average pore diameter of 100 ± 10 Å and a surface area of 183 ± 15 m^2/g.[104] Its void space is about 30%.[106] The composition, by weight, of the final porous material is 96% SiO_2, 2.6 ± 0.1% B_2O_3, and ≤ 1% Na_2O and Al_2O_3. [105] PVG has a strong adsorption capacity and can be readily impregnated with a variety of complexes that can serve as precursors to catalytical species.

PVG is stable up to temperatures of ca. 1000°C. Like other silicas, its surface is essentially hydroxylic.[107] DRIFT spectra of the calcined glass reveal a surface composed of free, 3744cm^{-1}, and associated, 3655 cm^{-1}, silanol groups.[108-109] The number of silanol groups depends on the sample's thermal history, but studies of a variety of hydroxylated silicas yield silanol numbers of 4-7 per 100 Å^2 with the highest density within the pores.[110-111] Trace amounts of chemisorbed water are also present in calcined (650 °C) samples.[87] PVG is often likened to silica gel, but the two materials are not chemically equivalent. In addition to the silanol groups, which function as weak Brønsted acids, PVG also possesses B_2O_3 Lewis acid sites. As a result of its method of manufacture, i.e., acid leaching, these sites are dispersed on surfaces throughout the glass matrix. X-ray photoelectron spectroscopic (XPS) analyses indicate that the amount of B present in the first 50 Å of the samples used in our experiments is 2.6 ± 0.1%.[104]

Sol-gel glass is a porous pure silica glass made by hydrolysis-polymerization of silicon alkoxides via a sol-gel-glass route. Using this process, a solution of silicon alkoxides, water, alcohol and a catalyst react to form a gel, which is then dried to form a porous hydrated glass. The glasses prepared by these sol-gel procedures are microporous, transparent materials.[112] One of the most attractive feature of porous silica glass is its ability to incorporate organic molecules during gelation. Susa and coworkers report that residual organic compounds remain in the silica gel up to 700 °C.[113] The

sol-gel glass used in our experiments is made from mixtures of tetramethylorthosilicate (TMOS)-methanol-water. Ammonia is used as a catalyst. As found by Susa and coworkers, after calcination in a muffle furnace at 650 °C, the sol-gel glass retains some Si-OCH_3 and silanol groups on the surface.

This thesis reports the studies of catalytical behavior of tungsten and ruthenium carbonyls supported on PVG. Attention is focused on the CO_2 methanation on $W(CO)_6$/PVG, WO_3/PVG as well as WO_3/sol-gel catalysts, and 1-pentene isomerization on $Ru_3(CO)_{12}$/PVG catalysts.

Chapter 2. EXPERIMENTAL

2. 1. Materials

$Ru_3(CO)_{12}$ (Pressure Chemical), $W(CO)_6$ (Pressure Chemical), and WO_3 (Pfaltz & Bauer, 99.75%) were used without further purification since UV-visible and IR spectra of the complexes agreed with published spectra.[114-120] HPLC grade 1-pentene (Matheson Coleman & Bell) and hexane (Aldrich) were used as received since GC analysis showed no detectable impurities. D_2O (Norell, 99%) was used as received. All gases were from the Linde Corporation and were used as received since the purity levels of each exceeded 99%.

Code 7930 porous Vycor glass containing 100 ± 10 Å diameter cavities and $1.2 \pm 0.3 \times 10^{18}$ pores/g was obtained from the Corning Glass Works. The glass was obtained as polished 25 mm x 25 mm x 2 mm plates. All glass samples were first extracted with 50% acetone and 50% distilled water in a Soxhlet extractor for 24 hours then with distilled water for 24 hours. The extracted glass was dried under reduced pressure ($P \leq 400$ torr) at 50 °C, and calcined in air at 600 °C for ≥ 72 hours. The calcined samples were stored at 600 °C until needed. At which point, a sample was transferred while hot to a vacuum desiccator and cooled to room temperature, 22 ± 1°C, under vacuum ($P \leq 10^{-3}$ torr).

Sol-gel glass was prepared by mixing tetramethylorthosilicate (TMOS),

methanol and water (Table I). The TMOS, water and methanol were mixed for about 10 minutes, then a catalyst, ammonia, was added to facilitate the polymerization process. After adding the catalyst, the solution was poured onto mercury surface. Casting the gel on mercury minimizes the stresses that arise between the glass container and the gel during drying. This minimizes cracking during gelation and drying, and has added advantage of yielding an optically flat surface. The sample containers were covered with polyethylene film and maintained at 60 °C for 2 hours. The gels were then cooled to room temperature (23 °C) and allowed to dry for 2-3 weeks. After drying at room temperature, the gels were removed from mercury and heated to 60 °C under vacuo ($P \leq 1.0 \times 10^{-3}$) for 12 hours, and then calcined at 600 °C for ≥ 72 hours.

For diffuse reflectance FTIR (DRIFT) and photoluminscence measurements, cleaned pieces of PVG were crushed and sieved to ≤ 200 mesh (≤ 0.074 mm) powder. The powder was calcined at 600 °C for 24 hours, and then cooled and stored in a vacuum desiccator.

Deuteriation was accomplished by refluxing either powdered or plate samples of calcined PVG in 30 mL of D_2O (Norell, 99 %) at 100 °C. After refluxing for 24 hours, the solution was replaced by fresh D_2O, and the samples refluxed for an additional 24 hours. The deuterium exchanged samples were then dried under vacuum ($P \leq 10^{-3}$ torr) at 60 °C, and the extent of deuterium exchange was calculated from the decrease in the intensity of the 3744 cm^{-1} band corresponding to the silanol group. As illustrated in Figure 2, the intensity (log Io/I) of the 3744 cm^{-1} band in the spectrum of a

Table I. Composition of Silica Xerogels

Sample	TMOS (mL)	CH_3OH (mL)	H_2O (mL)	NH_4OH (mL)[a]
1	6.0	4.0	3.0	1.0
2	6.0	10.0	3.0	1.0
3	6.0	15.0	3.0	1.0
4	6.0	20.0	3.0	1.0
5	6.0	25.0	3.0	1.0
6	6.0	35.0	3.0	1.0

[a] 15 M NH_4OH

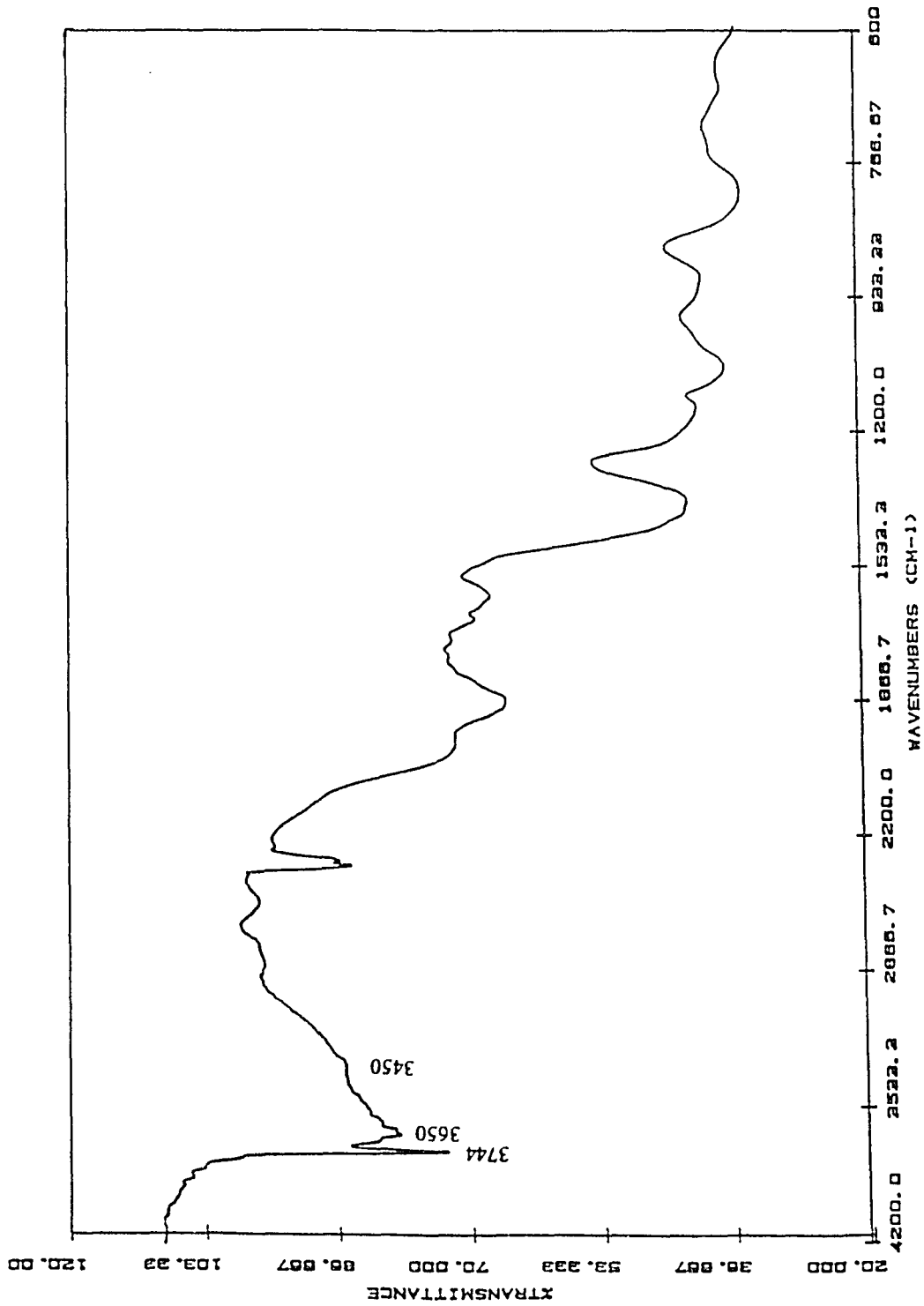

Figure 2. DRIFT spectrum of calcined PVG at 298 K in vacuo ($P \leq 10^{-3}$ torr)

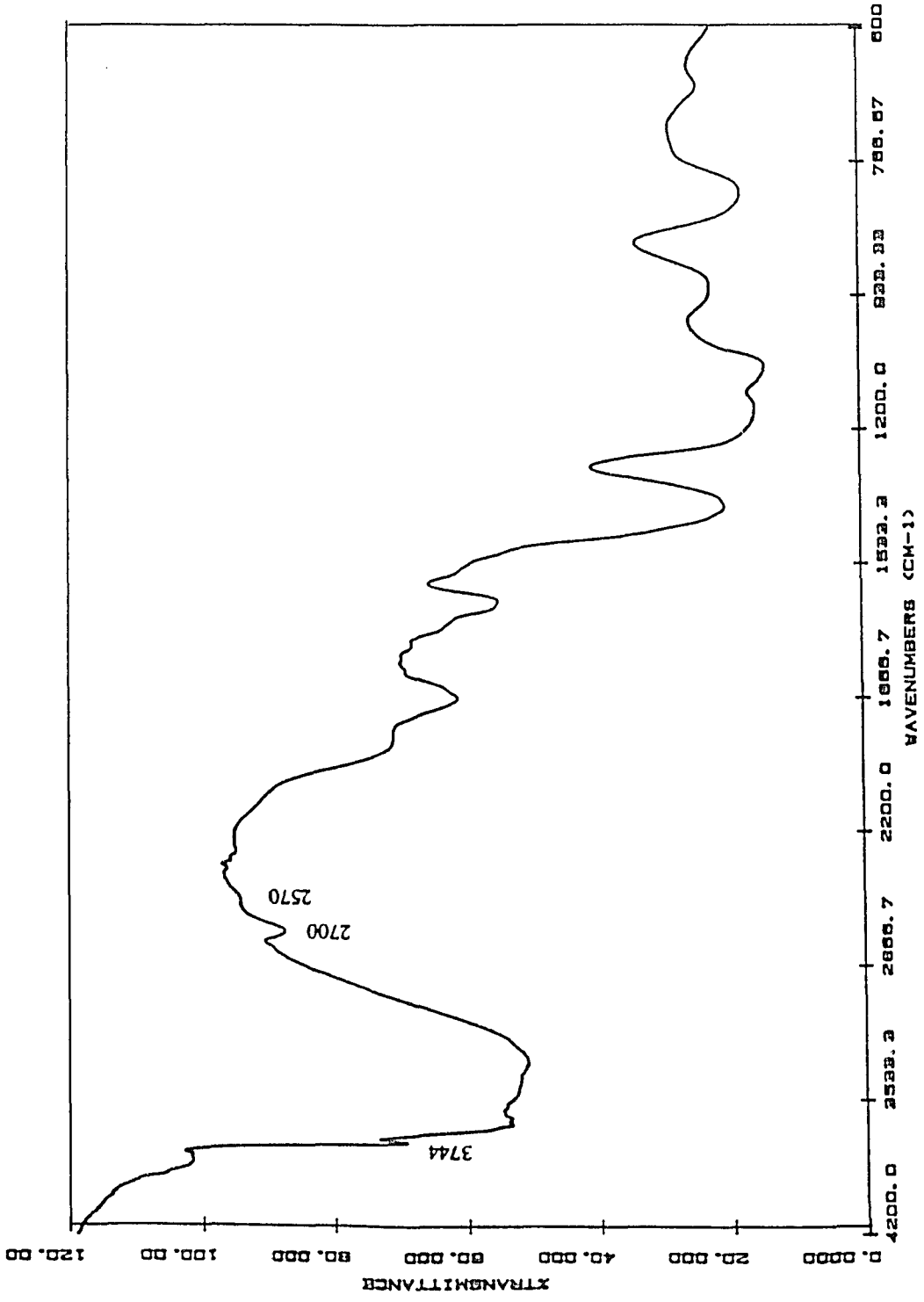

Figure 3. DRIFT spectrum of deuterated PVG

calcined PVG is 0.172, whereas the intensity of the 3744 cm^{-1} band of a deuteriated PVG decreases to 0.155 (Figure 3), the decrease corresponds to 10% deuterium exchange. The extent of deuteriation in the glass prepared by above method is in the range of 10-15% of the spectroscopically detectable silanol groups.

2. 2. Impregnation Procedures

Plate samples of calcined PVG were impregnated with $W(CO)_6$ or $Ru_3(CO)_{12}$ by the liquid phase equilibrium adsorption technique using a hexane solution of the compound. Impregnation with WO_3 was accomplished by adsorbing a slightly alkaline (pH 8), aqueous solution of the oxide. Typically, one to three cleaned PVG samples were weighed and mounted upright in an Eastman Kodak Chromagram Developing Jar containing 50 mL of the adsorbate solution. The concentration was generally 10^{-3} in the tungsten compounds and 10^{-4} in $Ru_3(CO)_{12}$. The impregnating times ranged from 12 to 48 hours, and in all cases, the impregnation was carried out in the absence of light and the solvents incorporated during impregnation were removed under vacuum at room temperature.

To determine the amount of the compound adsorbed onto the PVG sample, the absorbances of the solution were recorded before and after impregnation. The moles of compound adsorbed, n_{ads}, was calculated from the relation:

$$n_{ads} = (1 - OD_f/OD_i) \times n_i \qquad (2.1)$$

where OD is the optical density at the monitoring wavelength. The subscripts i and f denote the initial and final values, and n_i is the number of moles of adsorbate in the solution prior to impregnation.

The moles of $W(CO)_6$ and WO_3 adsorbed onto the glass were calculated from the absorbance change at 287 nm and 220 nm respectively, while the moles of $Ru_3(CO)_{12}$ adsorbed was calculated from the absorbance change at 395 nm. The samples prepared in these experiments contained 10^{-6} to 10^{-5} moles of W/gm of glass, either in the form of $W(CO)_6$ or WO_3. Ruthenium loadings ranged from 10^{-7} to 10^{-6} moles of $Ru_3(CO)_{12}$/gm of the glass.

The powdered WO_3/PVG samples were prepared by the conventional impregnation procedures. An appropriate volume of aqueous WO_3 solution, usually 1-3 mL for 1 g of PVG, was added to the support. The mixture was allowed to stand for ca. 10 hours in a partially covered beaker in the hood at 298 K to remove the solvent, and then dried overnight at 383 K. The dried samples were calcined in a muffle furnace at 823 K for ≥ 24 hours before being used. The amount of WO_3 loaded was calculated from the concentration and volume of the solution used.

Highly loaded $Ru_3(CO)_{12}$/PVG samples, i.e., containing ≥ 10^{-6} mol of $Ru_3(CO)_{12}$ per gram of glass, were prepared by sublimation techniques. Both plate and powdered samples of PVG were suspended above the solid complex in the sublimation apparatus shown in Figure 4. The chamber was evacuated, and the complex sublimed onto the support under vacuum at 50 °C. The

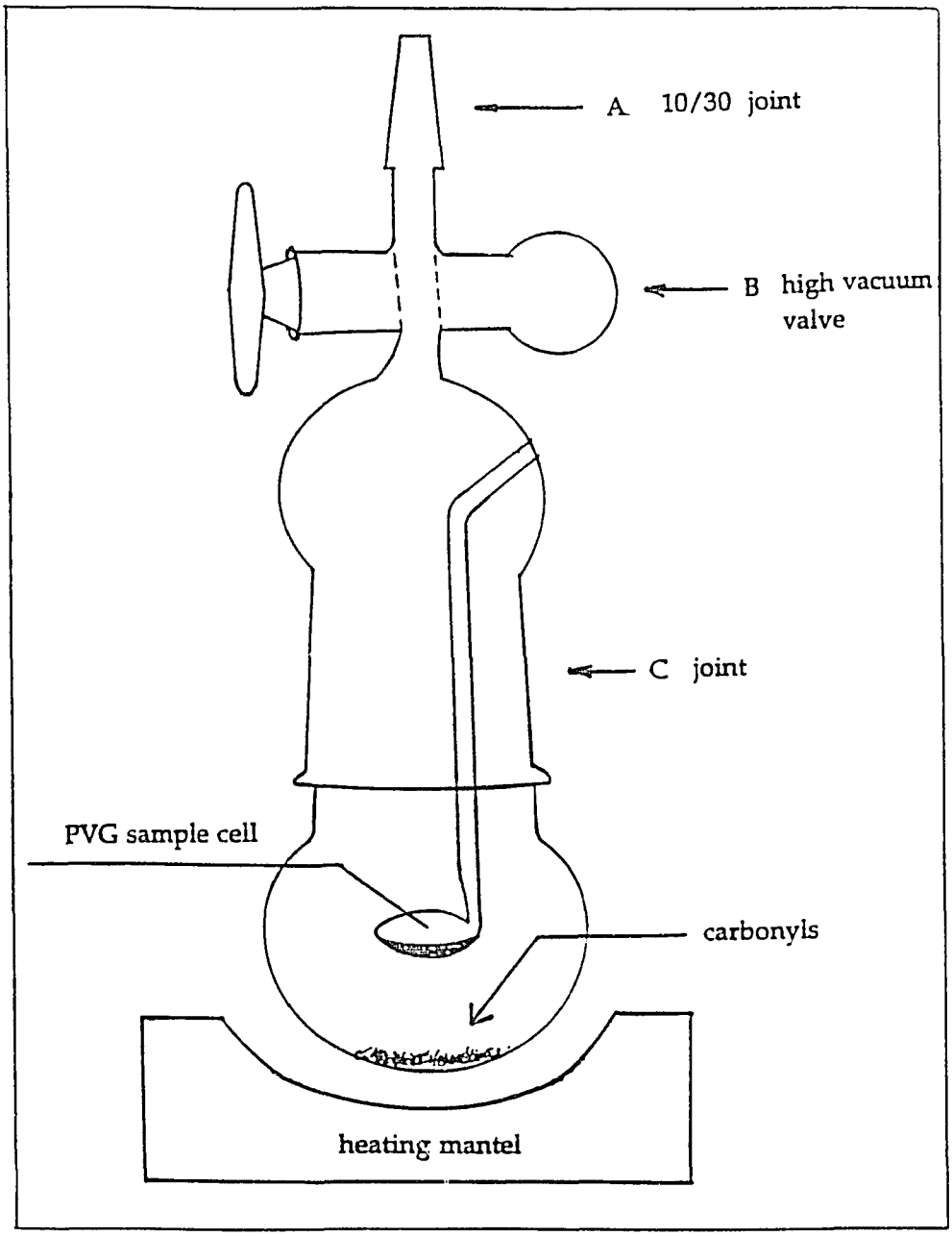

Figure 4. Sublimation apparatus

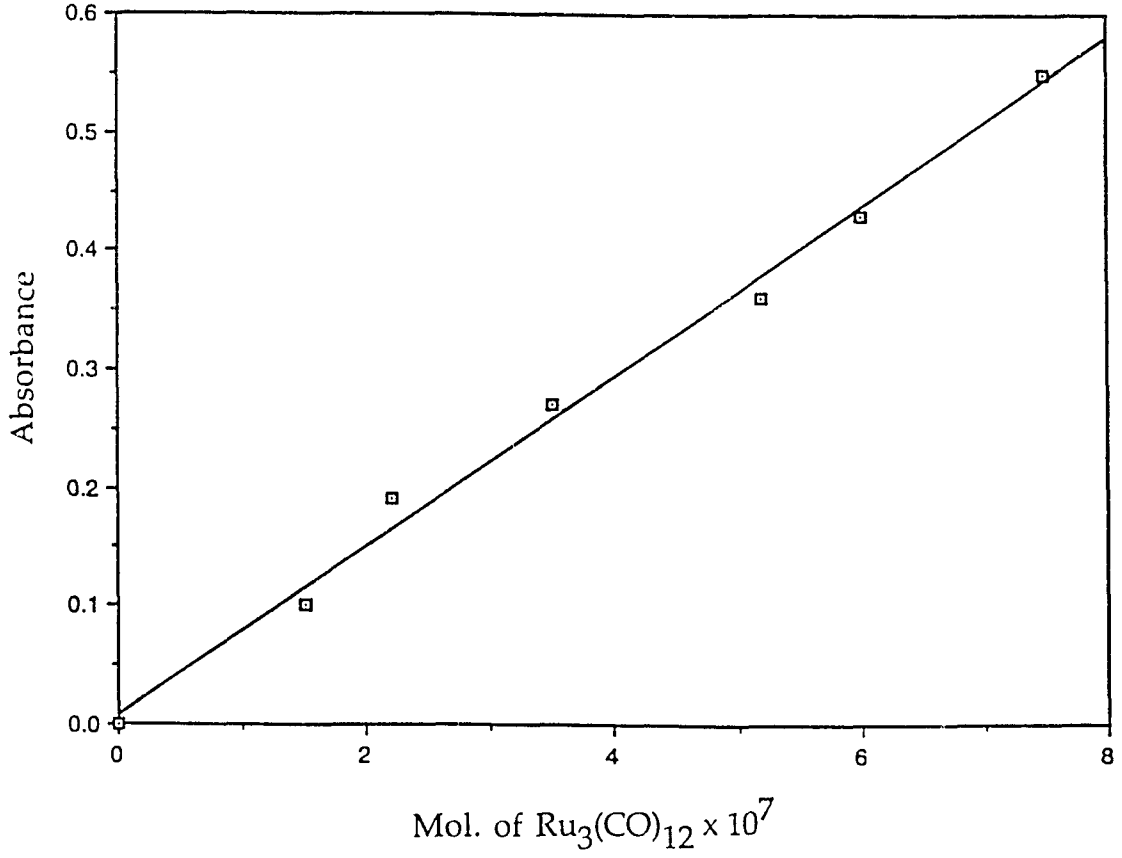

Figure 5. Calibration curve of $Ru_3(CO)_{12}$ adsorbed on Plate PVG
The absorbance is measured at 395 nm, and the moles of adsorbed $Ru_3(CO)_{12}$ is calculated from equation 2.1

moles of $Ru_3(CO)_{12}$ adsorbed was determined by comparing the optical density of the impregnated sample to that of samples containing known $Ru_3(CO)_{12}$ loadings. The calibration curve of $Ru_3(CO)_{12}$(ads) is illustrated in Figure 5.

2. 3. Photochemical Procedures.

An impregnated PVG sample was rigidly mounted with a Teflon holder in a 5 cm x 2.5 cm x 1 cm quartz cell equipped with a 5.5 cm diameter O-ring joint. The cell was attached to a Pyrex top which has two side arms with high vacuum valves for the admission and withdrawal of gas samples. The entire cell apparatus, illustrated in Figure 6, was then attached through the 10/30 joint to a vacuum line equipped with an oil diffusion pump isolated from the line by a trap at 77 K for evacuation and transfer of gases. Unless otherwise specified, the cell and enclosed sample were evacuated to a pressure of $\leq 10^{-5}$ torr prior to irradiation.

For the methanation reaction, a sample impregnated with either $W(CO)_6$ or WO_3 was irradiated either under vacuum ($P \leq 10^{-5}$ torr) or a $^{13}CO_2$ atmosphere in the rectangular quartz cells. In studies of the photoinduced isomerization of 1-pentene, $(\mu\text{-H})Ru_3(CO)_{10}(\mu\text{-OSi})$ was generated in situ by irradiation of $Ru_3(CO)_{12}$/PVG under vacuum ($P \leq 10^{-5}$ torr). Formation of the oxidative addition product was monitored by the increase in absorbance of the characteristic 330 nm absorption.[98] The cell was

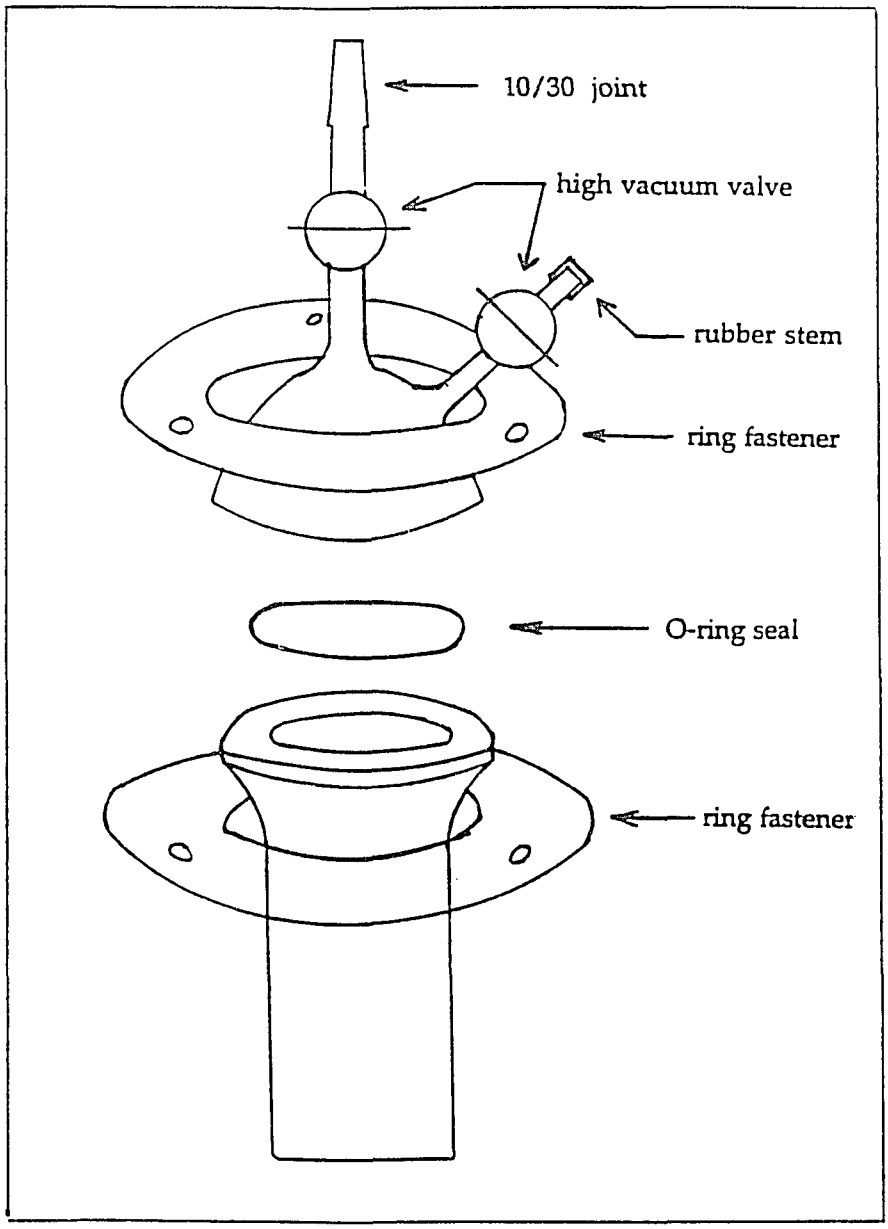

Figure 6. Photolysis cell

then evacuated to remove the evolved CO, and exposed to 400 torr of 1-pentene (3.45×10^{-3} moles). The isomerization was induced by continued irradiation.

All samples were irradiated in a Rayonet Reactor (Southern New England Ultraviolet Corp.) equipped with either 254, 310, or 350 nm bulbs. Incident intensities, were determined by ferrioxolate actinometry.[121] The fraction of the incident light absorbed by potassium ferrioxalate, $1 - (I/I_o) = 1 - 10^{-A}$ (A denotes absorbance at the specific excitation wavelength), was measured experimentally. The number of moles of ferrous formed, $n_{Fe^{2+}}$, in a measured irradiation time t, was determined by reacting the Fe^{2+} with 1, 10-phenanthroline and measuring the absorbance of the resulting complex at 510 nm. The quantum yields of Fe^{2+} formation, $\phi_{Fe^{2+}}$, were taken from the literature, and the incident intensities in the photolysis cell were calculated from equation 2.2.

$$I_o = n_{Fe^{2+}} / [\phi_{Fe^{2+}} S t (1-10^{-A})] \qquad (2.2)$$

where S is the area of $K_3Fe(C_2O_4)_3$ in the photolysis cell. Consequently, the units of Io in these experiments are einsteins cm^{-2} sec^{-1}. The incident intensities were typically on the order of 10^{-9} Einstiens cm^{-2} sec^{-1}. Quantum yields of formation of photoproducts were calculated from equation 2.3.

$$\phi = R/Ia \qquad (2.3)$$

where R is the average rate of photoproduct formation, and Ia is the average number of einsteins absorbed per unit volume and time in fluid solution. For supported catalysts, unit surface area was used instead of unit volume, and the light absorbed was calculated from equation 2.4.

$$Ia = Io\, S' (1 - 10^{-A}) \qquad (2.4)$$

where Io is calculated from equation 2.2, S' is the area of a sample, and A is determined from the absorption spectrum for a particular excitation wavelength.

2. 4 Physical Measurements.

UV-visible spectra of the impregnated samples were recorded relative to calcined blank PVG on an AVIV 14 DS spectrophotometer. Diffuse reflectance FTIR (DRIFT) spectra of the powder samples, diluted with KBr (1:10), were recorded on a Nicolet 5/20 DX FTIR equipped with an intensified source, MCTB detector maintained at 77 K, and a Harrick's diffuse reflectance accessory. The instrument gain was set to the limiting value of 8 and 500 scans were selected for each spectrum. All spectra were ratioed against a background of blank PVG diluted with KBr (1:10).

Emission spectra of WO_3 were recorded on a Perkin-Elmer Hitachi MPF-2A emission spectrophotometer equipped with a red-sensitive

Hamamatsu R818 photomultiplier tube. To measure the emission from WO_3 on the PVG, the spectrometer cell holder was adapted to rigidly hold the rectangular cell and the PVG sample within at an angle of 50° relative to the exciting light. The emission was monitored at an angle of 90° to the excitation, or 40° to the front face of the sample. The excitation wavelength was set at 270 nm, and emission wavelengths were set at 410 and 460 nm.

In all experiments, electronic spectra were recorded periodically during photolysis, and correlated with periodic GC analyses of the gas phase in the photolysis cell. The gaseous photoproducts in the methanation reaction were collected by expanding the gas in the photolysis cell into a Toepler pump and then transferring the gas to the sample loop (Figure 7). Generally, three cycles were needed to quantitatively transfer the gas to the loop. The loop was then closed off and connected to a Gow-Mac 69-100 gas chromatograph equipped with a rhenium-tungsten thermal conductivity detector. A 6' x 1/4" diameter stainless steel column packed with activated 5 Å molecular sieve (80/100 mesh, Supelco) was used for analysis of H_2, CH_4 and CO. CP grade He was used as a carrier gas (35 mL/min), the thermal conductivity detector was maintained at room temperature, and the detector current was set at 200 mA. The detector response was displayed on a Shimadzu R-111 recorder and calibrated with CP grade H_2, CH_4 and CO. The calibration plots, constructed by plotting peak height versus the moles of pure gas injected, are illustrated in Figure 8. Retention times and slopes of calibration curve for above gases are summarized in Table II. A typical chromatogram of gaseous products is displayed in Figure 9.

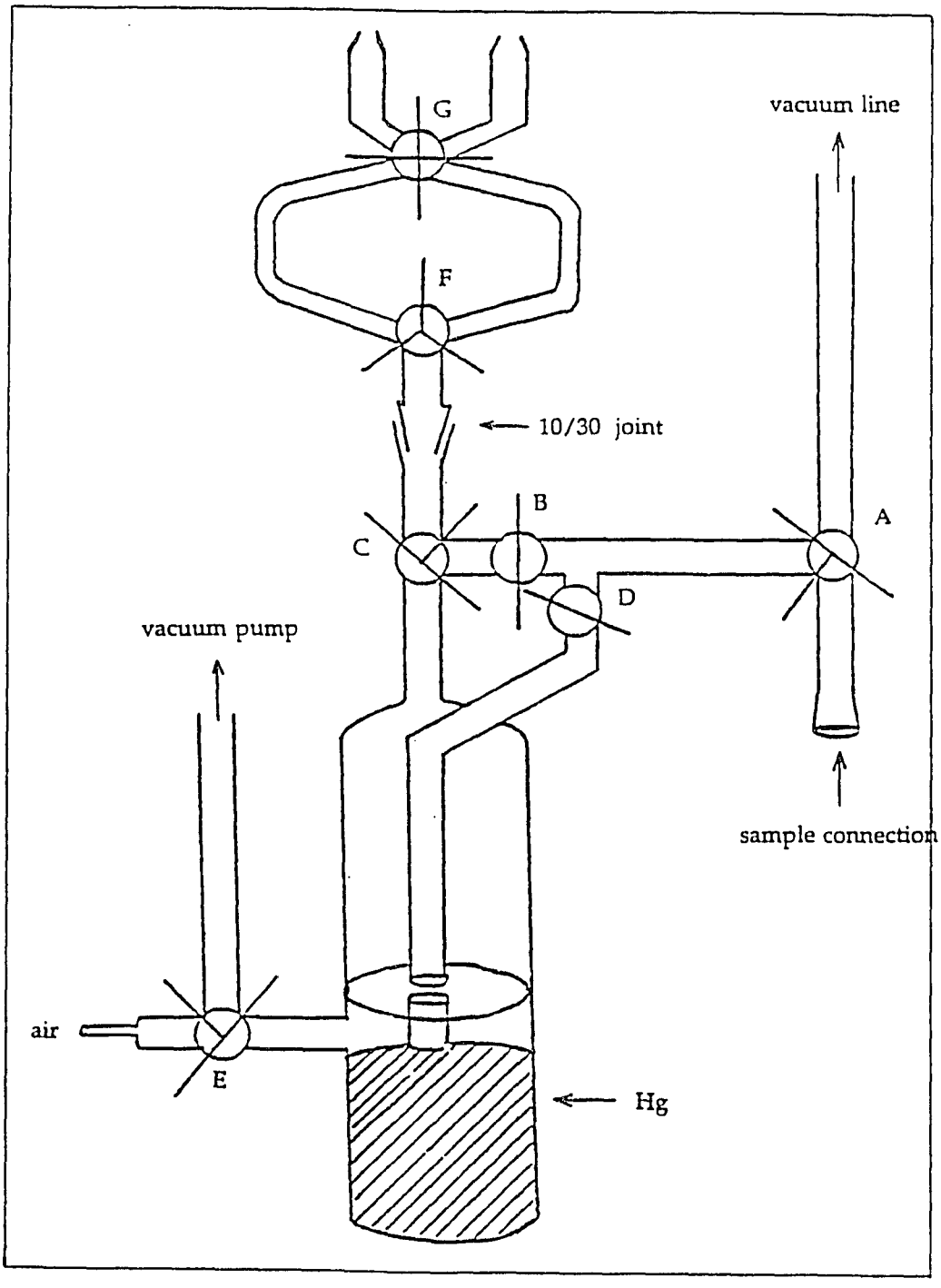

Figure 7a. Toepler pump apparatus

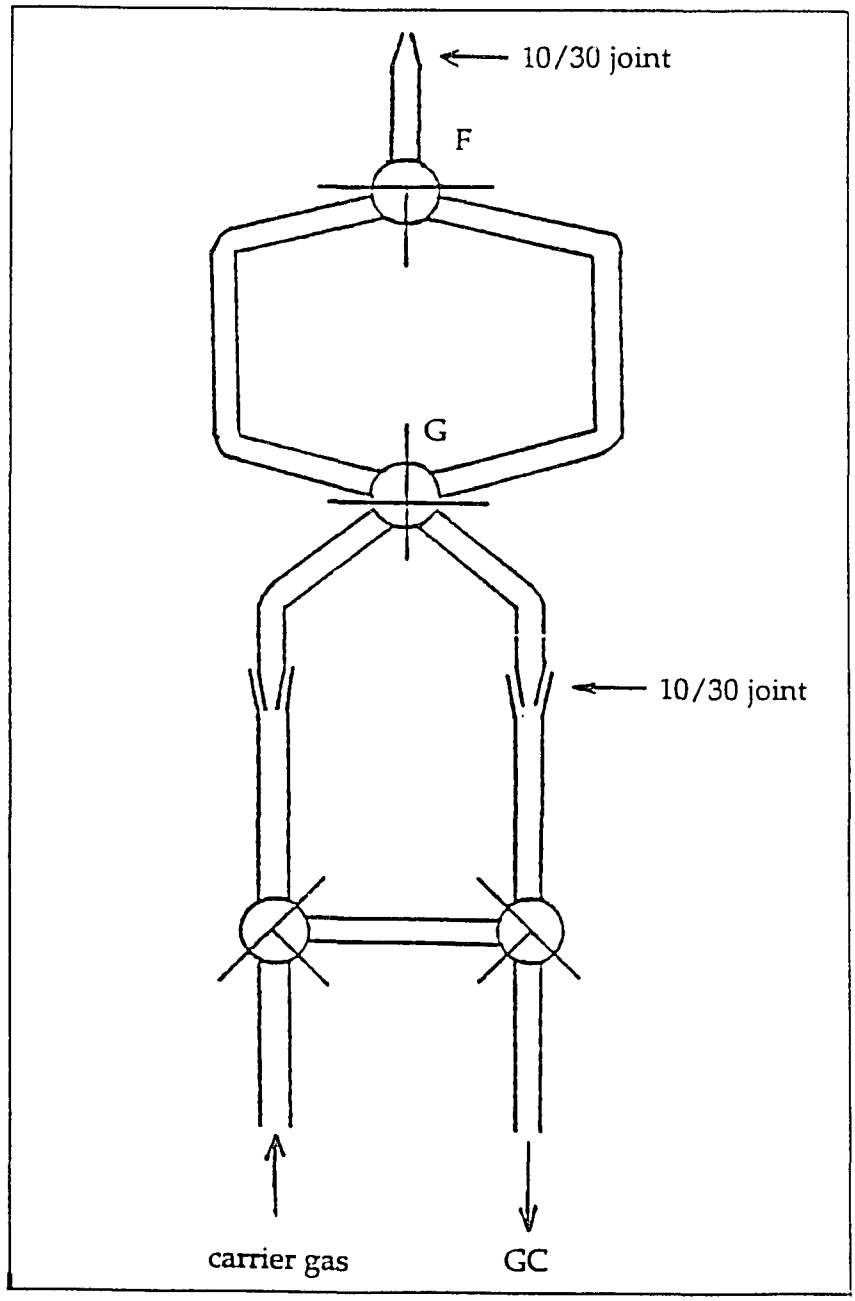

Figure 7b. Connection of gas sampling loop to gas chromatograph system

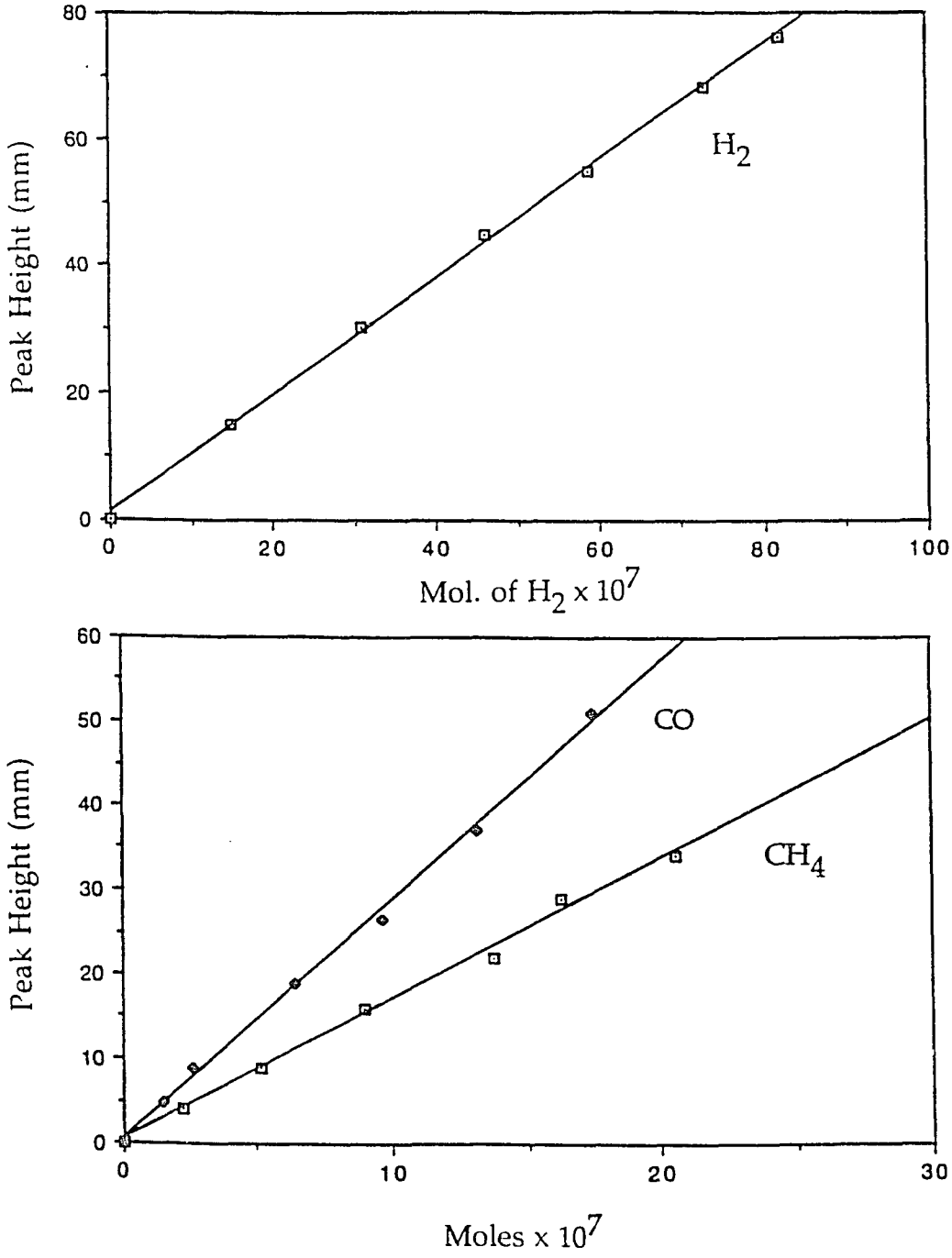

Figure 8. Calibration curve of H_2, CH_4 and CO

carrier gas: He at 35 mL/min, detector: TCD at 200 mA

attenuation: 2

Table II. Parameters of Gas Chromatograph

Compound	Retention Times	Calibration Slope (cm/mole)
H_2	1.7 minutes	9.21×10^6
O_2	3.3 minutes	5.26×10^6
N_2	5.3 minutes	7.16×19^6
CH_4	10.5 minutes	1.66×10^7
CO	18.5 minutes	2.82×10^7
n-pentene	13.0 minutes	2.33×10^8
cis-2-pentene	14.2 minutes	2.17×10^8
trans-2-pentene	16.4 minutes	1.76×10^8

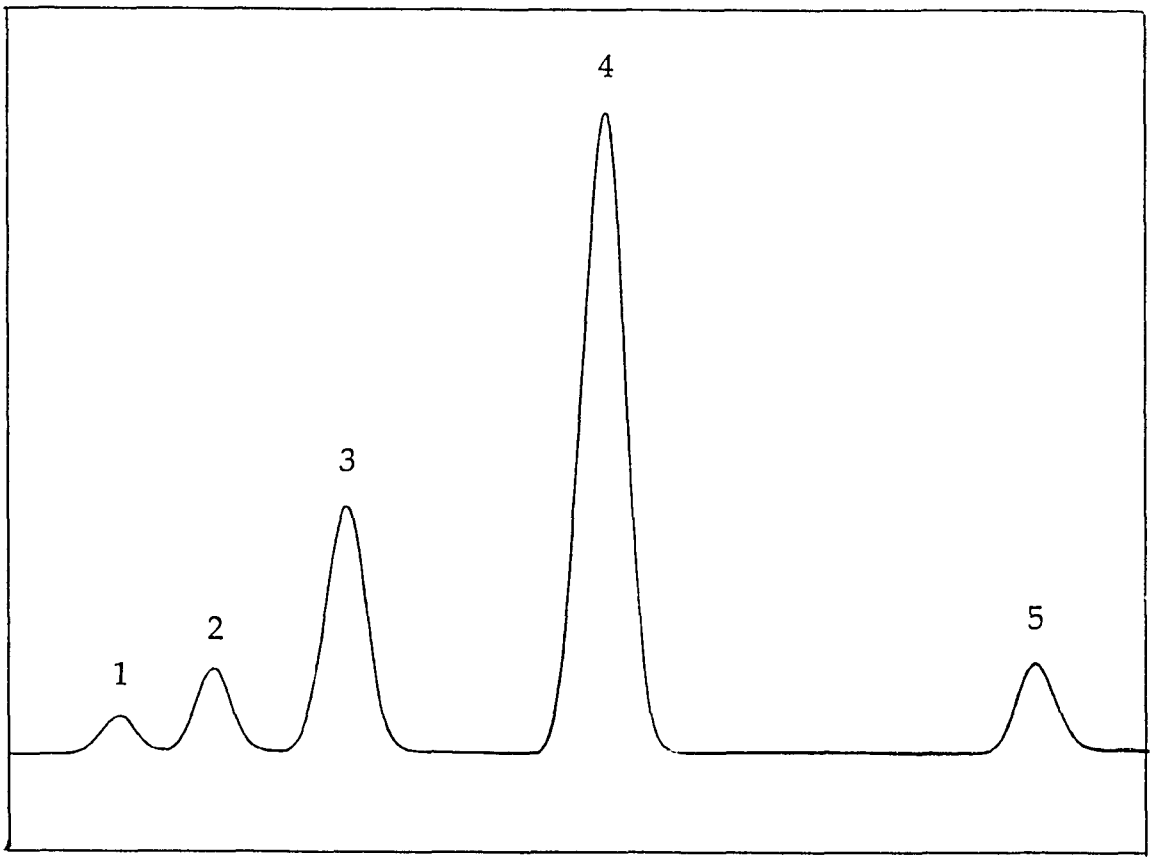

Figure 9. Chromatogram of methanation products

1=H_2, 2=O_2, 3=N_2, 4=CH_4, 5=CO

GC conditions: carrier gas = He at 35 mL/min,

detector = TCD at 200 mA.

attenuation = 2

In the photocatalyzed isomerization of 1-pentene, the gaseous products were sampled with a gas tight syringe (Hamilton, Model # 1001) through the rubber septum in the side arm of the photolysis cell, and transferred to a Varian Aerograph Series 2400 GC equipped with a 2 m x 1/8 inch diameter stainless steel column containing GP 80/100 Carbopack with 0.19% picric acid(Supelco).

To separate the olefins, the column was maintained at 50°C and N_2 was used as the carrier gas (30 mL/min). The FID detector was maintained at 100°C, and its response, recorded on a Shimadzu R-111 recorder, was calibrated by direct injection of 1-pentene and cis- and trans-2-pentene (Aldrich). The calibration plots are illustrated in Figure 10, and a typical chromatogram of the photoproducts is shown in Figure 11.

In the isotope labeling experiments, the gaseous photoproducts of methanation or isomerization were collected with a gas tight syringe (Hamilton, Model # 1001) and analyzed in a Hewlett-Packard 5988A GC/MS spectrometer.

In situ FTIR monitoring of the photoreactions was accomplished on the catalysis reactor system shown in Figure 12. A commercial high vacuum chamber (HVC) supplied by Harrick Scientific was mounted in the diffuse reflectance attachment of the Nicolet FTIR, illustrated in Figure 13. The chamber was fitted with one 10 mm diameter x 2 mm thick quartz observation/photolysis window and with two 19 mm diameter x 2 mm thick KBr or CaF_2 IR-transparent windows. Two connections allowed for the

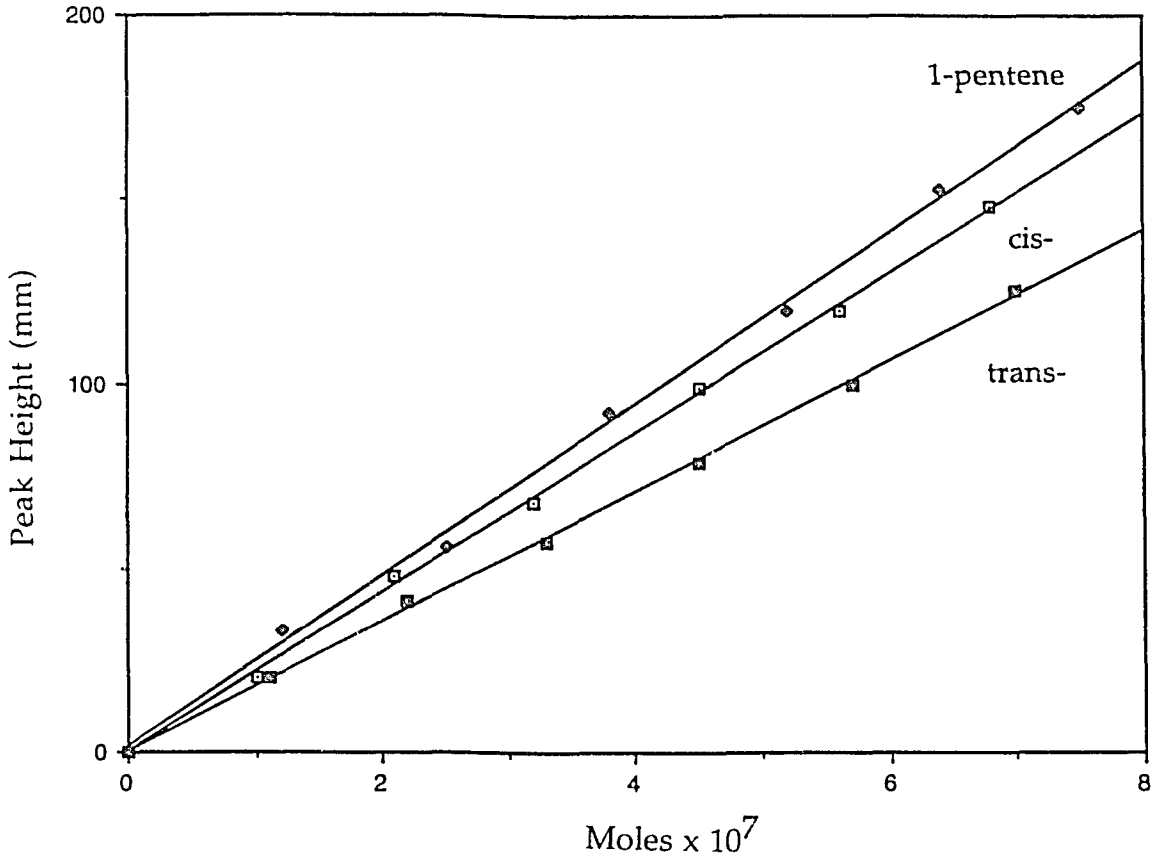

Figure 10. Calibration curve of 1-pentene (▫), cis- (▫)and trans-2-pentene (▫)

GC conditions: carrier gas = N_2 at 30 mL/min,

detector = FID at 100 °C.

attenuation = 32

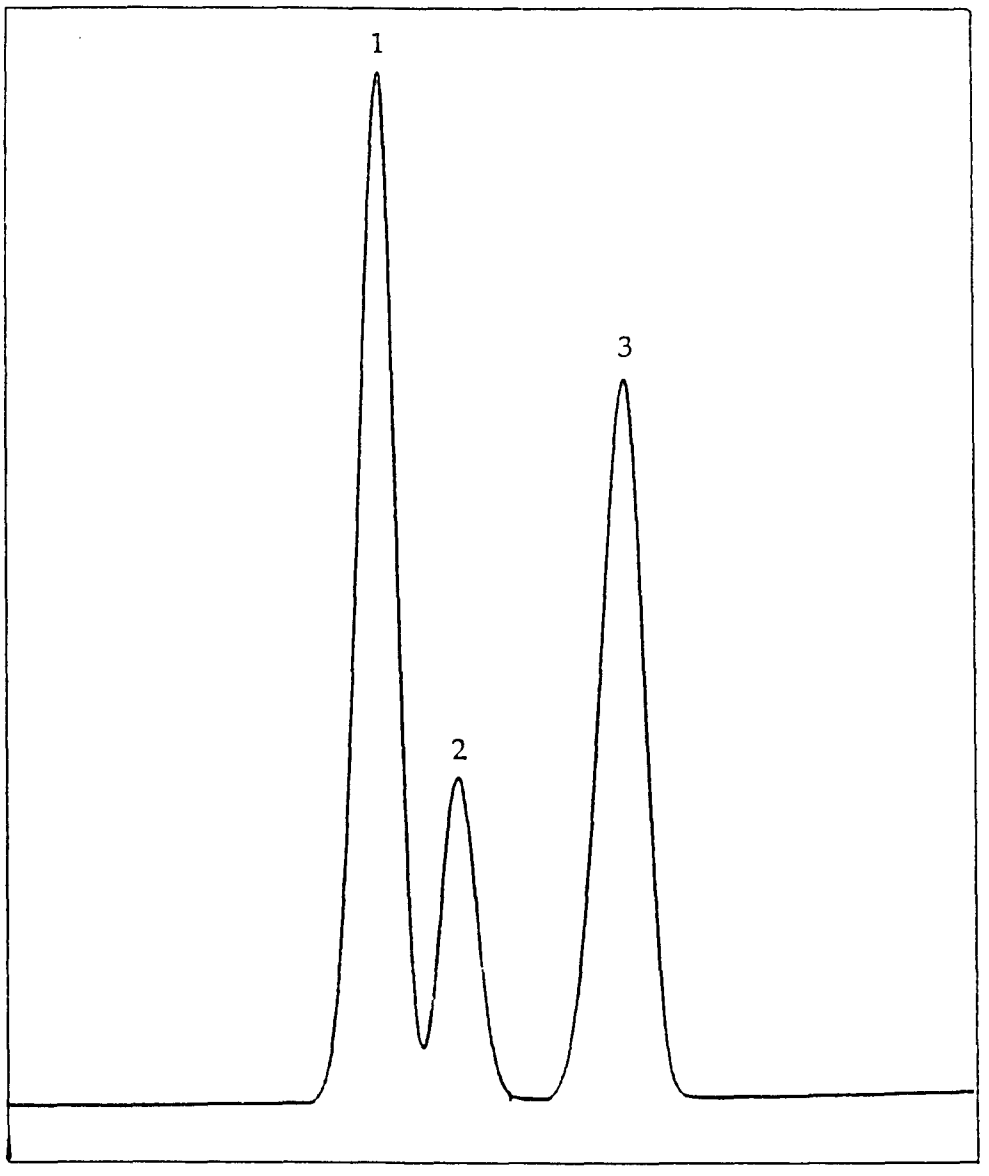

Figure 11. Chromatogram of gaseous products in 1- pentene isomerization

1 = 1-pentene, 2 = cis-2-pentene, 3 = trans-2-pentene

GC conditions: carrier gas = N_2 at 30 mL/min

detector = FID at 100 °C.

attenuation = 32

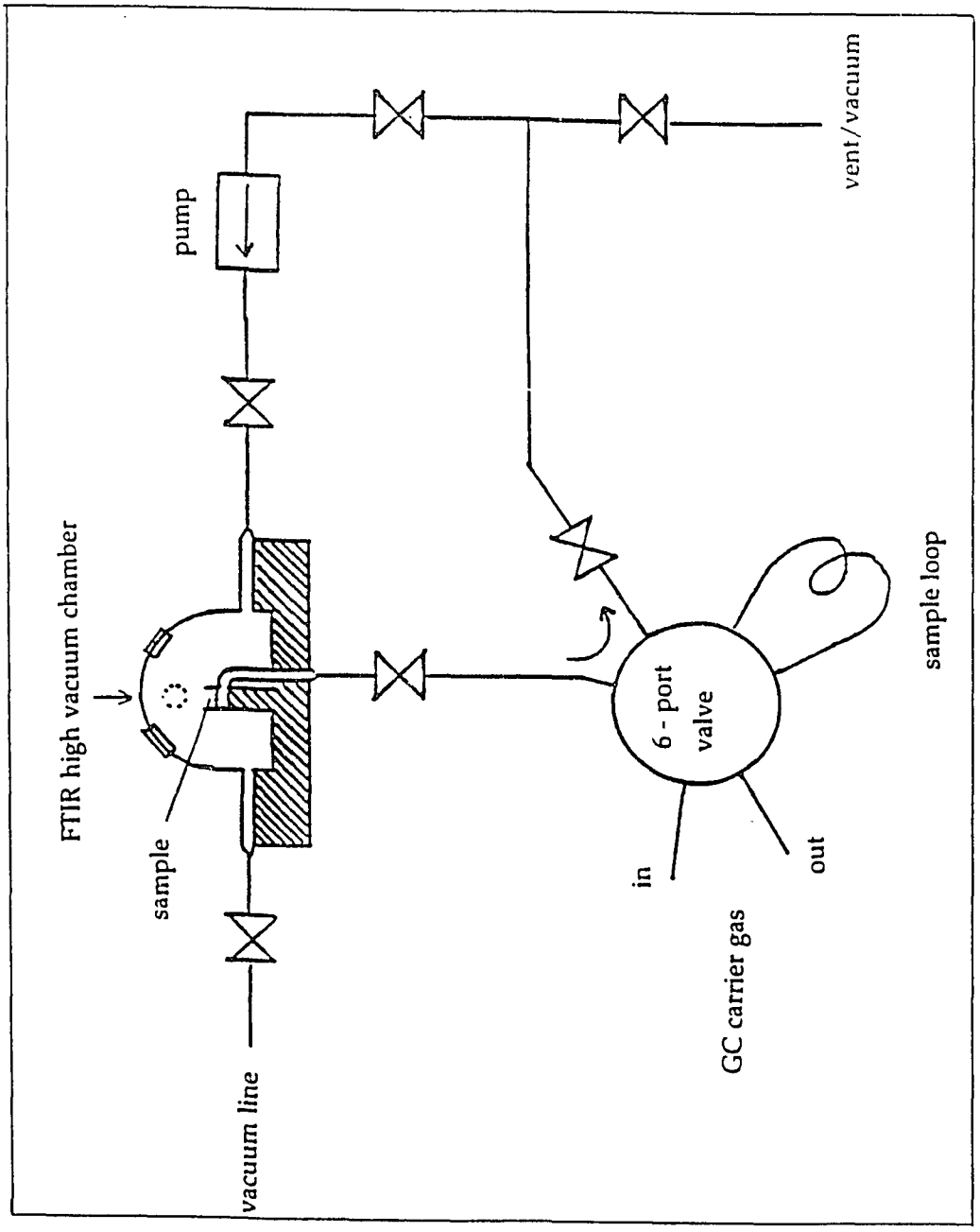

Figure 12. Catalytic reactor system

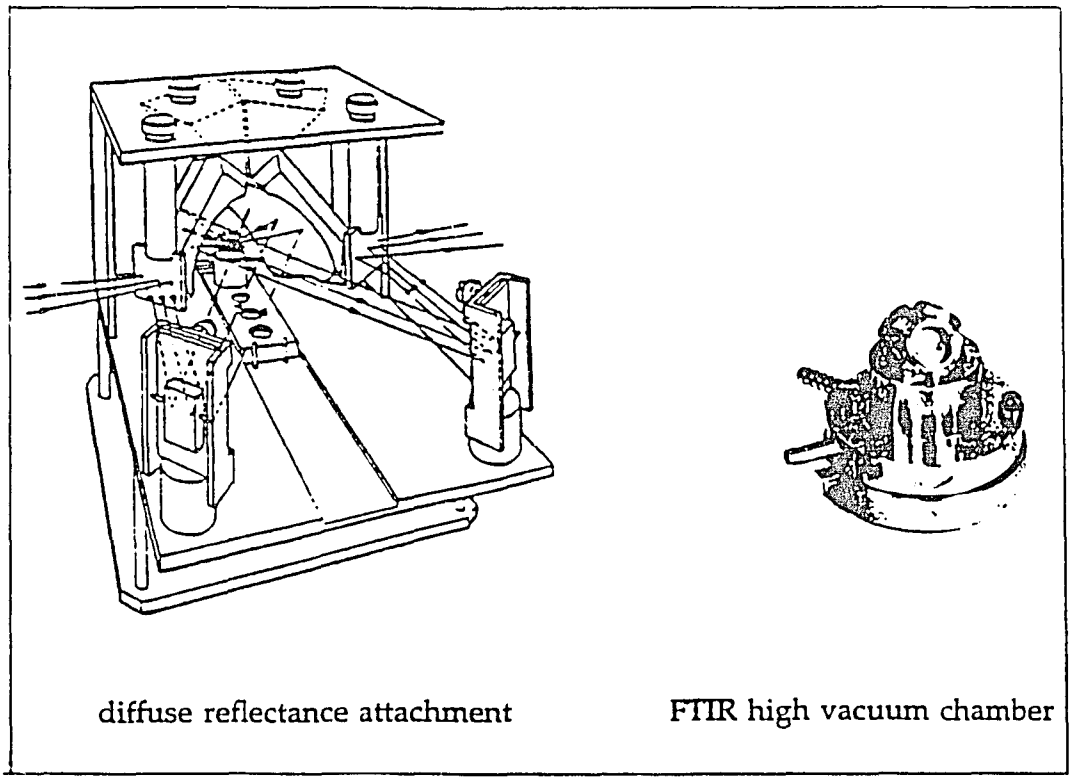

Figure 13. FTIR high vacuum chamber and diffuse reflectance attachment

addition and removal of gases. A third connection, terminating underneath the sample cup, enabled the circulation of gases through the sample. The cell could therefore be operated in a batch, pulse, or flow mode. The sample cup in the center of the cell accepted up to 300 mg of solid sample and could also be heated to 650 °C with a 7 W heater and an Omega Engineering Model 49 proportional temperature controller.

To induce a reaction, the sample was photolyzed through the quartz observation window. In this case, impregnated powder samples, diluted 1 : 10 with IR grade KBr, were irradiated in the Harrick's diffuse reflectance accessory with either 254 nm light from a pen lamp (Analamp Model 90-0001-01), or ≥ 350 nm light from a Plexiglas filtered (50% T at 351 nm) high pressure Xe lamp (SA Instruments). In the latter experiments, the excitation intensity was typically 10^{-7} Einsteins/sec-cm^2 determined by ferrioxolate actinometry. $(\mu\text{-H})Ru_3(CO)_{10}(\mu\text{-OSi})$ was generated in situ, and its formation was monitored by the growth of its characteristic 2078 cm^{-1} band.[98] CO evolved during the reaction was removed under vacuum to a final pressure of ≤ 10^{-3} torr. The sample chamber was then charged with 400 torr of 1-pentene, and the irradiation continued. Diffuse reflectance FTIR (DRIFT) spectra were recorded periodically during photolysis. The DRIFT spectra obtained were ratioed against a background of blank PVG diluted with KBr (1 : 10). The gas phase was sampled through the 6 - port valve (Figure 12), and analyzed with the Varian Aerograph 2400 GC.

Chapter 3. RESULTS

3. 1. Morphologies and Surfaces of Porous Vycor and Sol-gel Glasses

Porous Vycor glass (PVG) is a transparent, surface-hydroxylated amorphous material with a myriad of randomly dispersed 100 ± 10 Å diameter pores.[104] Thermal gravimetric analysis indicates that PVG possesses both physisorbed (bulk) and chemisorbed water. As shown in Figure 14, physisorbed water desorbs at 323 - 473 K while chemisorbed water desorbs slowly up to 1073 K.

It is well known that infrared absorption spectroscopy is very informative of the hydration state on silica surfaces.[124,158] The diffuse reflectance FTIR (DRIFT) spectrum of PVG recorded at 298 K, as shown in Figure 15, exhibits a sharp, intense band at 3744 cm^{-1} with a shoulder at 3650 cm^{-1} that have been assigned to free and hydrogen bonded silanol groups respectively.[109,122] The weak shoulder at 3702 cm^{-1} is assigned to the hydroxyl groups attached to boron (B-OH),[123] and the broad band centered at 3450 cm^{-1} indicates the presence of adsorbed water on the surface of PVG.

The DRIFT spectrum of calcined PVG recorded under vacuum ($P \leq 10^{-3}$ torr), as illustrated in Figure 2, exhibits a considerable reduction in the intensity of the 3450 cm^{-1} band, but no significant changes in the vibrational

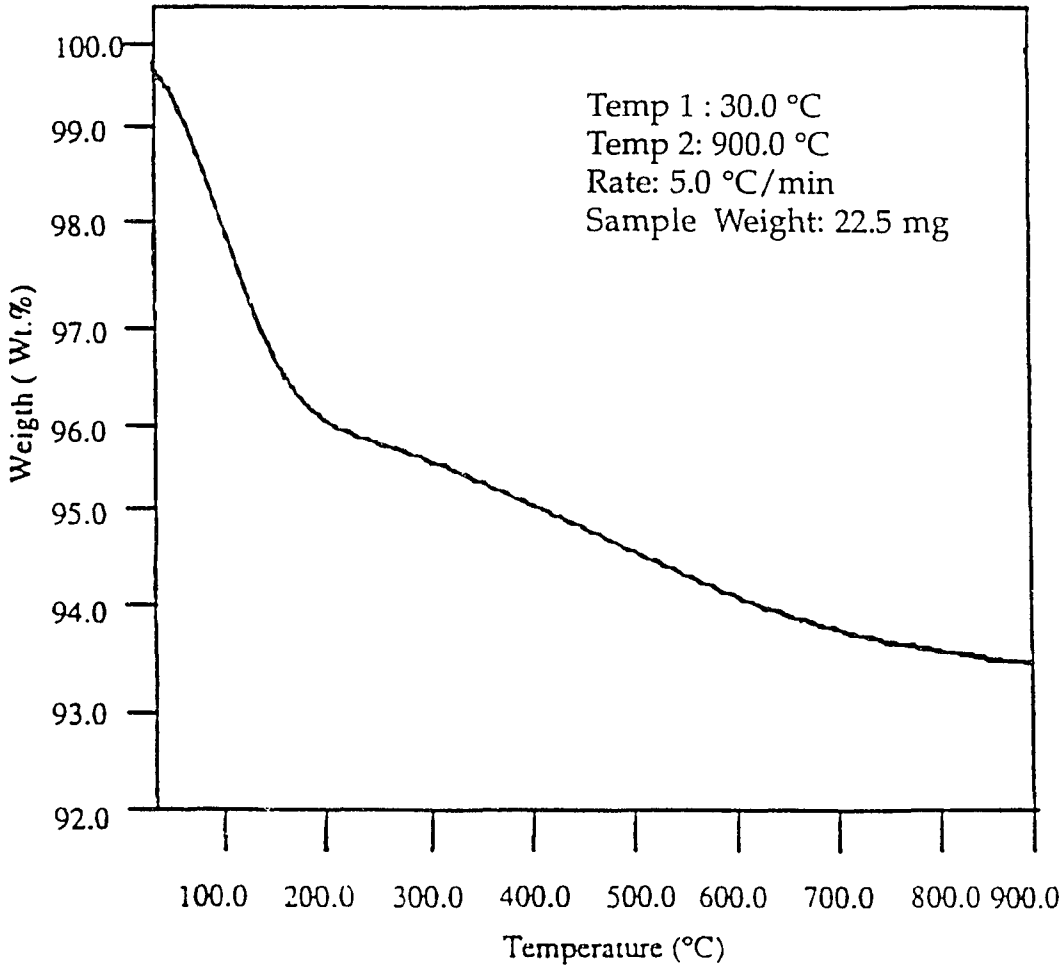

Figure 14. Thermal gravimetric analysis of PVG

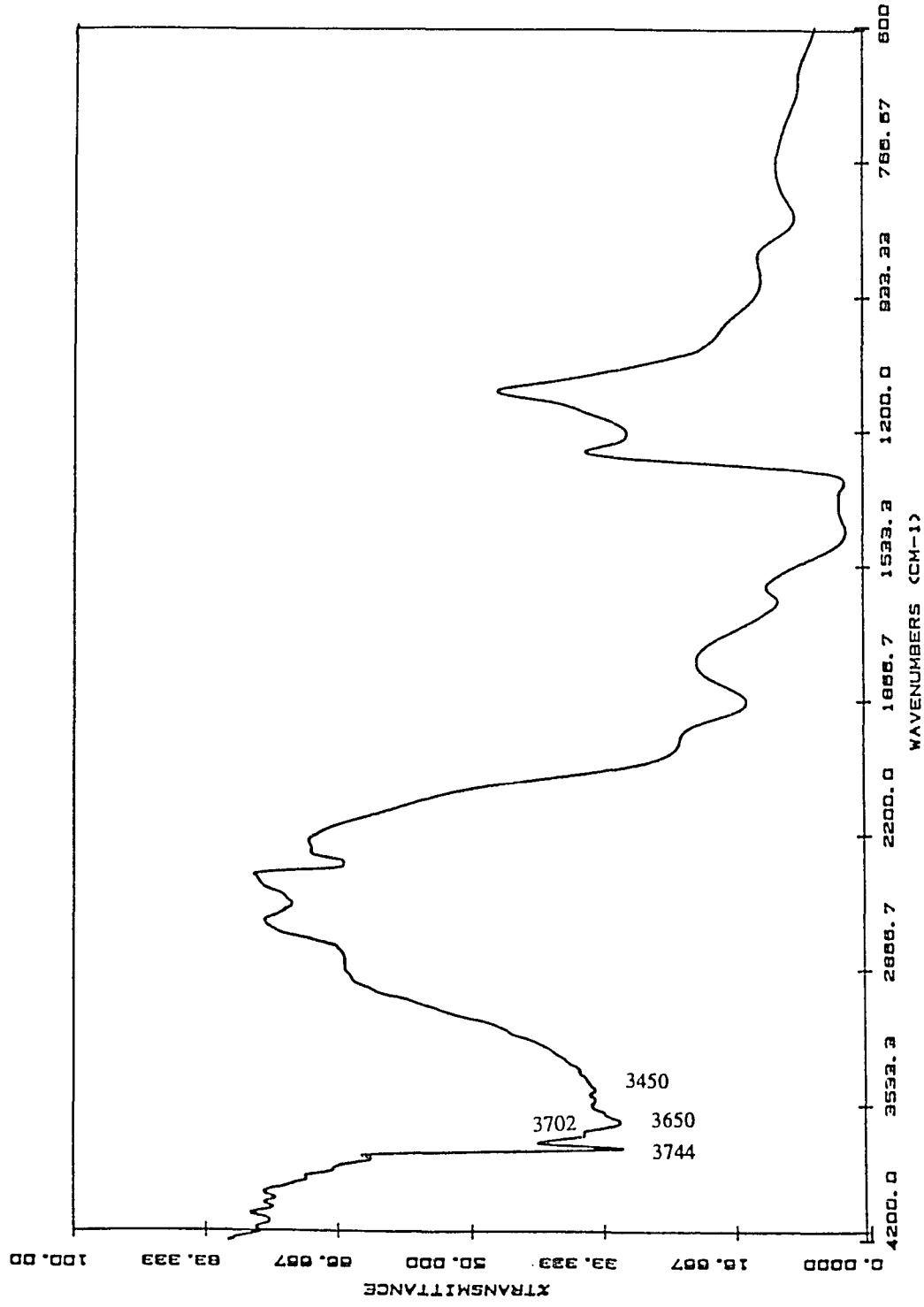

Figure 15. DRIFT spectrum of uncalcined PVG at 298 K

characteristics of free and associated silanol groups. The residual intensity of the weak, broad band at 3450 cm^{-1} for calcined PVG indicates the presence of small amounts of chemisorbed water on the surface.

Deuteration of PVG, as shown in Figure 3, reduces the intensity of 3744 cm^{-1} band and leads to an additional band at 2700 cm^{-1} with a shoulder at 2570 cm^{-1} that are assigned to the deuterated analogous of the free and associated silanols, respectively. [98]

After drying and calcination, the principal IR absorptions of base catalyzed sol-gel glass (TMOS/CH_3OH/H_2O xerogel) resemble those of PVG. As illustrated in Figure 16, the DRIFT spectrum of calcined sol-gel exhibits a sharp, intense band at 3744 cm^{-1} with a shoulder at 3650 cm^{-1}, and a broad band at 3450 cm^{-1}. In addition to the hydroxyl vibrations, however, bands indicative of C-H vibrations, ca. 2900 cm^{-1}, appear in the sol-gel spectrum. The bands at 2944, and 2967 cm^{-1} are consistent with the methyl C-H symmetric and asymmetric stretching vibrations of methoxy groups ($SiOCH_3$) that form via the reaction between methanol and surface hydroxyl groups.[124,159] Therefore, the DRIFT spectrum demonstrates that small amounts of methoxy groups remain on the surface even though the sol-gel has been calcined at 600 °C for 24 hours.

Scanning electron microscope (SEM) analyses of calcined PVG or sol-

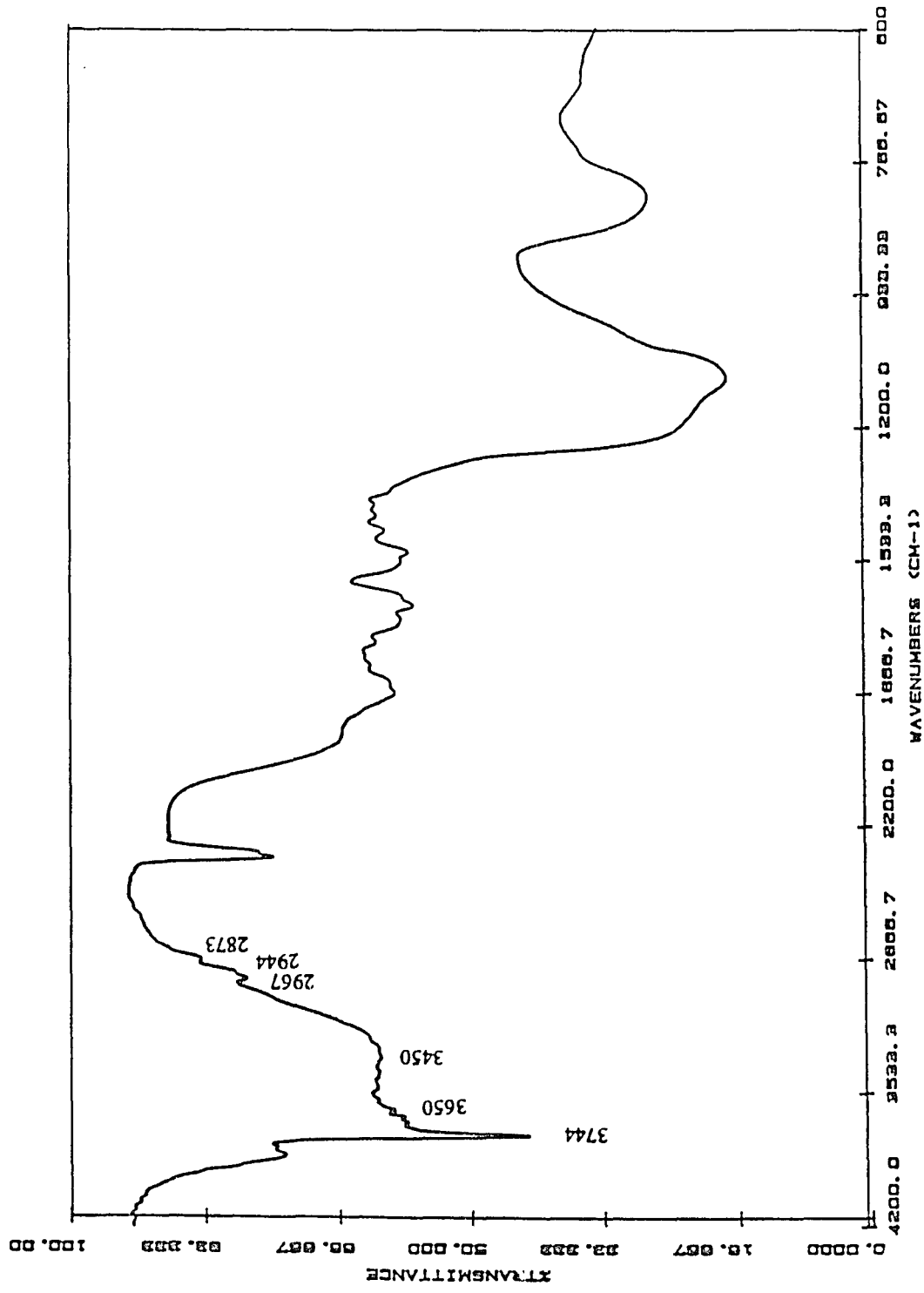

Figure 16. DRIFT spectrum of calcined sol-gel

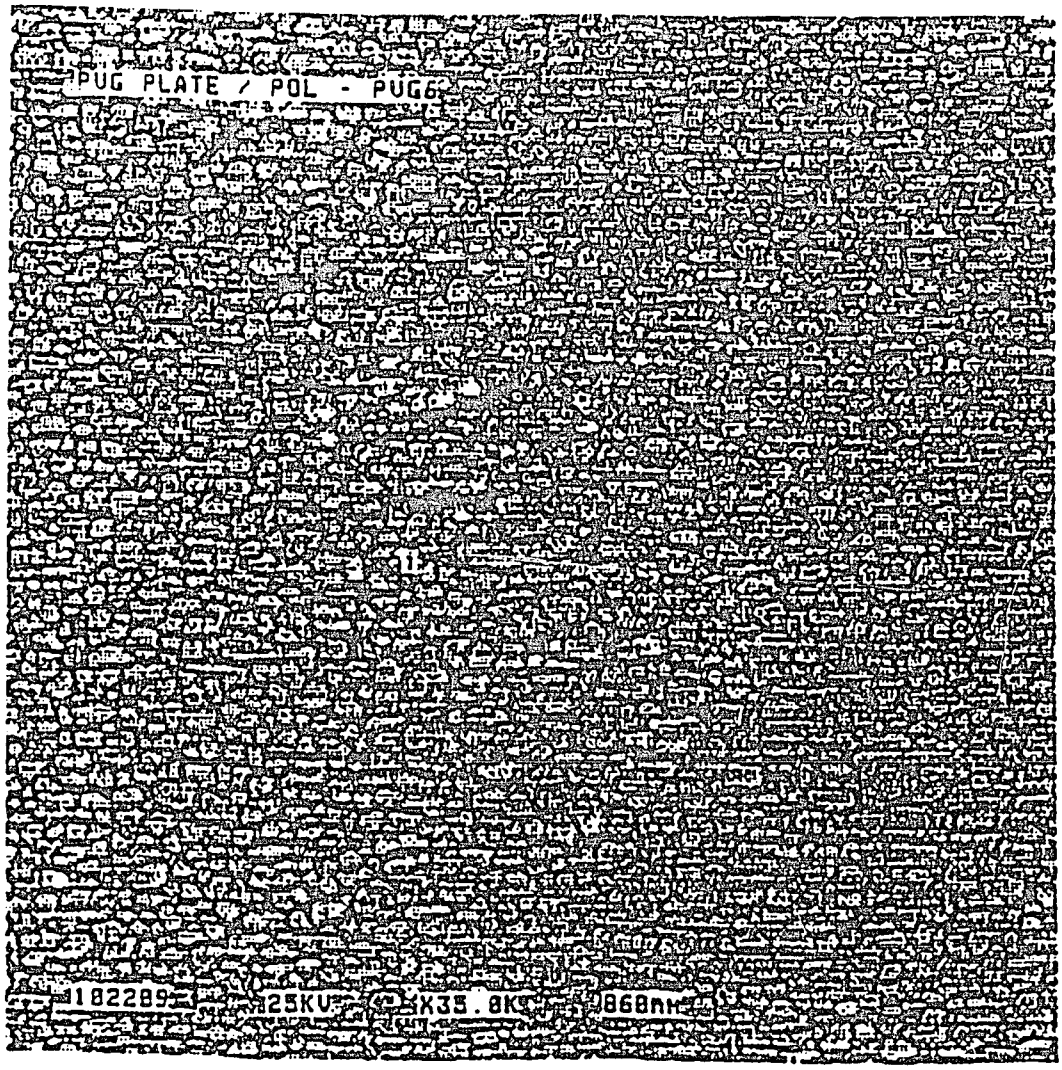

Figure 17. Scanning electron micrograph of calcined PVG

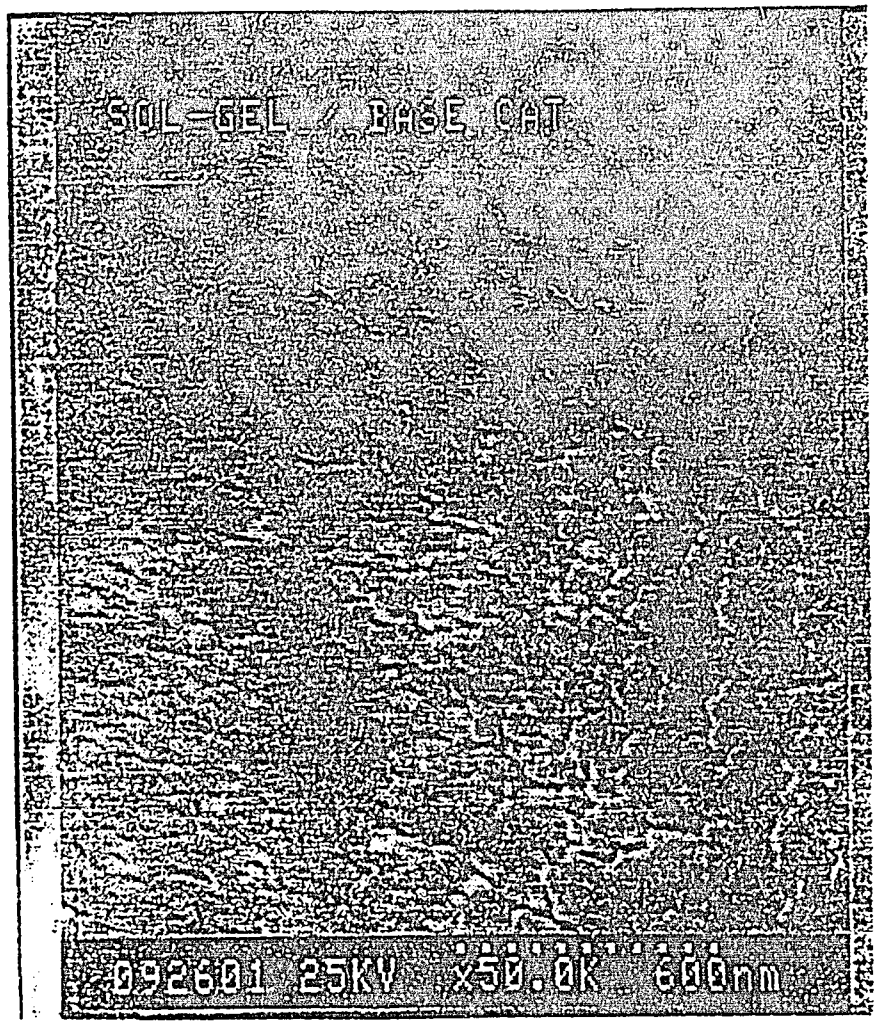

Figure 18. Scanning electron micrograph of calcined sol-gel

gel glass reveal a nodular surface composed of silicate nodules with intervening crevices. The intervening spaces in PVG, which in total correspond to a void volume of ca. 35%, range from 40 to 100 Å.[104] Figure 17 and Figure 18 illustrate the typical SEM photographs of calcined PVG and sol-gel glass.

3. 2. Photoinduced Methanation of CO_2 with $W(CO)_6$(ads) and WO_3(ads)

3. 2. 1. Distribution of Adsorbed $W(CO)_6$ and WO_3

The distribution of the chemical adsorbates was determined spectrally. Electronic spectra of the adsorbed complex or the oxide recorded at five different locations on a 25 mm x 25 mm x 2 mm sample are identical within experimental error, i.e.,± 0.1 absorbance unit. The spectral agreement establishes that impregnation by solution adsorption leads to a uniform distribution of the compounds on the surface of PVG.

The cross-sectional distribution of VIB hexacarbonyls adsorbed onto PVG has been previously studied in this laboratory.[88,125-126] With loading ≤ 10^{-5} mol/g, $W(CO)_6$ penetrates 0.4 ± 0.02 mm in the 25 mm x 20 mm x 4 mm PVG.[88] Assuming that $W(CO)_6$ penetrates the same depth in the 25 mm x 25 mm x 2 mm PVG, the penetration depth corresponds to ca. 40% of the total sample volume. The fractional surface coverage, Θ, is given by equation 3.1.

$$\Theta = A_m / W_g A_g \qquad (3.1)$$

where A_m is the total planar projected area of the adsorbate, W_g is the weight of glass impregnated, and A_g is the surface area per gram of the glass. For plate PVG, W_g is 40 % of the sample weight since the complex impregnated ca. 40% of the total sample volume. For powdered PVG, impregnation is uniform since impregnation depth, 0.4 ± 0.02 mm, exceeds the average particle diameter (≤ 0.074 mm). In this case, Wg equals sample weight.

Taking 0.3 nm as the radius of $W(CO)_6$, 0.2 nm as the radius of WO_3,[127-130] and 183 ± 15 m^2/g as the surface area of PVG, [89,103,131-132] the fractional surface coverages of the samples examined in the methanation experiments are summarized in Table III.

It is important to note that, even with the highest loading, 1.7 x 10^{-5} mol of WO_3/g of PVG, the samples examined in the experiments have the fractional surface coverages of ≤ 2%. The majority of the glass surface of the samples examined here is vacant, and other reagents are more likely to adsorbed onto the glass than directly onto the adsorbed metal complex or oxide.

3. 2. 2. Spectral Properties of Adsorbed $W(CO)_6$ and WO_3

Consistent with previous experiments in this laboratory,[87,98] the electronic and infrared spectra of adsorbed $W(CO)_6$ closely resemble those of

Table III. Fractional Surface Coverage of $W(CO)_6$ and WO_3 on PVG

Impregnate	Moles Adsorbed (10^{-6} mol/g)	Sample Type	Surface Coverage (Θ)
$W(CO)_6$	0.89	plate	0.20
$W(CO)_6$	1.5	plate	0.16
$W(CO)_6$	1.9	plate	0.45
$W(CO)_6$	2.7	plate	0.63
$W(CO)_6$	12.0	powder	1.12
WO_3	3.8	plate	0.39
WO_3	2.9	plate	0.30
WO_3	2.7	plate	0.28
WO_3	1.9	plate	0.20
WO_3	1.5	plate	0.16
WO_3	1.1	plate	0.11
WO_3	17.0	plate	1.76
WO_3	2.6	powder	0.11
WO_3	3.8	powder	0.16
WO_3	4.3	powder	0.18
WO_3	15.0	powder	0.62
WO_3	17.0	powder	0.70
WO_3	46.0	powder	1.91
WO_3	53.0	powder	2.20

the complex in n-hexane (Table IV). The electronic spectrum of $W(CO)_6$ (ads), as shown in Figure 19, exhibits an intense band at 287 nm. The lower energy, ligand field transition, which appears as low intensity shoulder on the 287 nm charge transfer transition in solution spectra (Figure 20), appears as unresolved tail in the 300-350 nm region. DRIFT spectra of $W(CO)_6$ (ads) show a band centered at 1986 cm^{-1}(Figure 21), characteristic of the CO stretching vibration in the hexacarbonyl.[87]

To spectroscopically characterize the photoproducts of the complex obtained in the glass, the spectroscopic properties of possible metal oxide products were examined. In aqueous solution, the structure of the tungstate ion is pH dependent and described by the following equilibrium (equation 3.2)

$$WO_4^{2-} + 12\ H^+ \text{ ---------> } W_{12}O_{42}^{12-} + 6H_2O \qquad (3.2)$$

In neutral and alkaline solutions, tungsten exists exclusively as the tetrahedral WO_4^{2-} ion.[133-134] Figure 22 illustrates the electronic spectra of aqueous solutions of WO_3 as a function of pH. The spectrum of a solution of pH 8 exhibits an intense absorbance at ca. 210 nm, therefore, this band is assigned to the monomeric, tetrahedral oxotungsten ions. Upon adsorption from an aqueous NH_4OH solution, pH 8, a slight red shift of the absorbance occurs in the electronic spectra of WO_3(ads). The red shift increases with loading, and the spectrum approaches that of bulk WO_3 which is octahedrally coordinated with a maximum absorbance in the 300-320 nm range.[160] As shown in Figure 23, a sample containing 1.9×10^{-6} mol WO_3/g PVG, for

Table IV. UV-Visible and Infrared Absorption of $W(CO)_6$ and $Ru_3(CO)_{12}$

Complex	Medium	nm	cm^{-1}
$Ru_3(CO)_{12}$	Hexane	238, 395	2062, 2033, 2018, 2012
	PVG	240, 395	2065, 2032, 2018
$W(CO)_6$	Hexane	290	1984
	PVG	287	1986

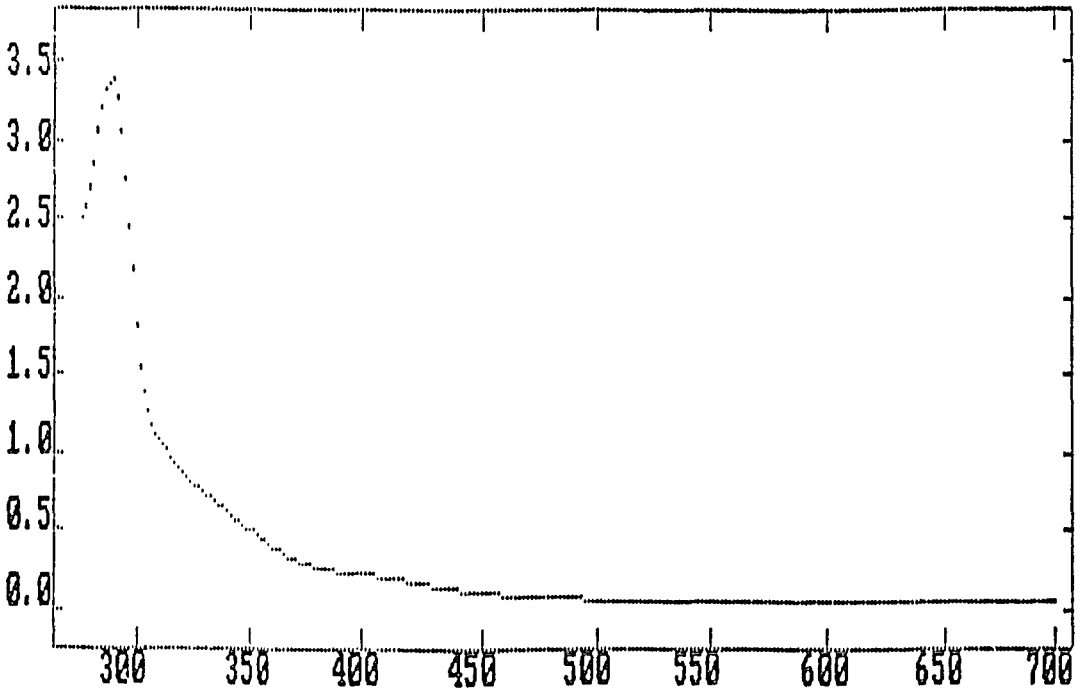

Figure 19. Electronic spectrum of 4.0×10^{-6} mol of $W(CO)_6$ /g of PVG

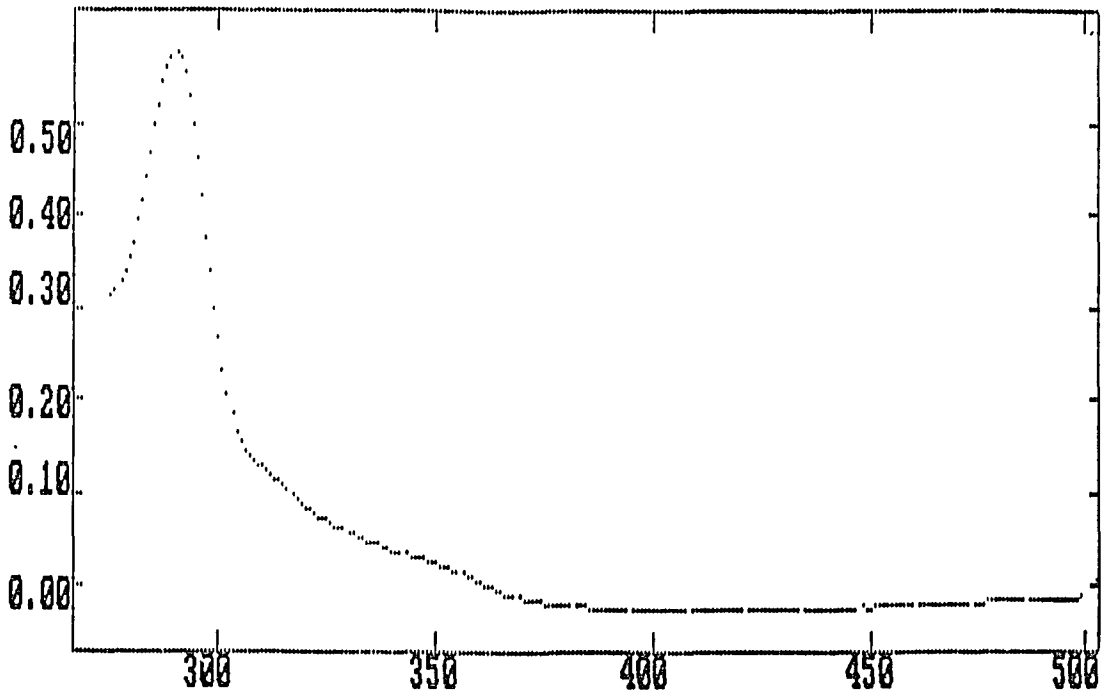

Figure 20. Electronic spectrum of $W(CO)_6$ in hexane, 1.2×10^{-5} M

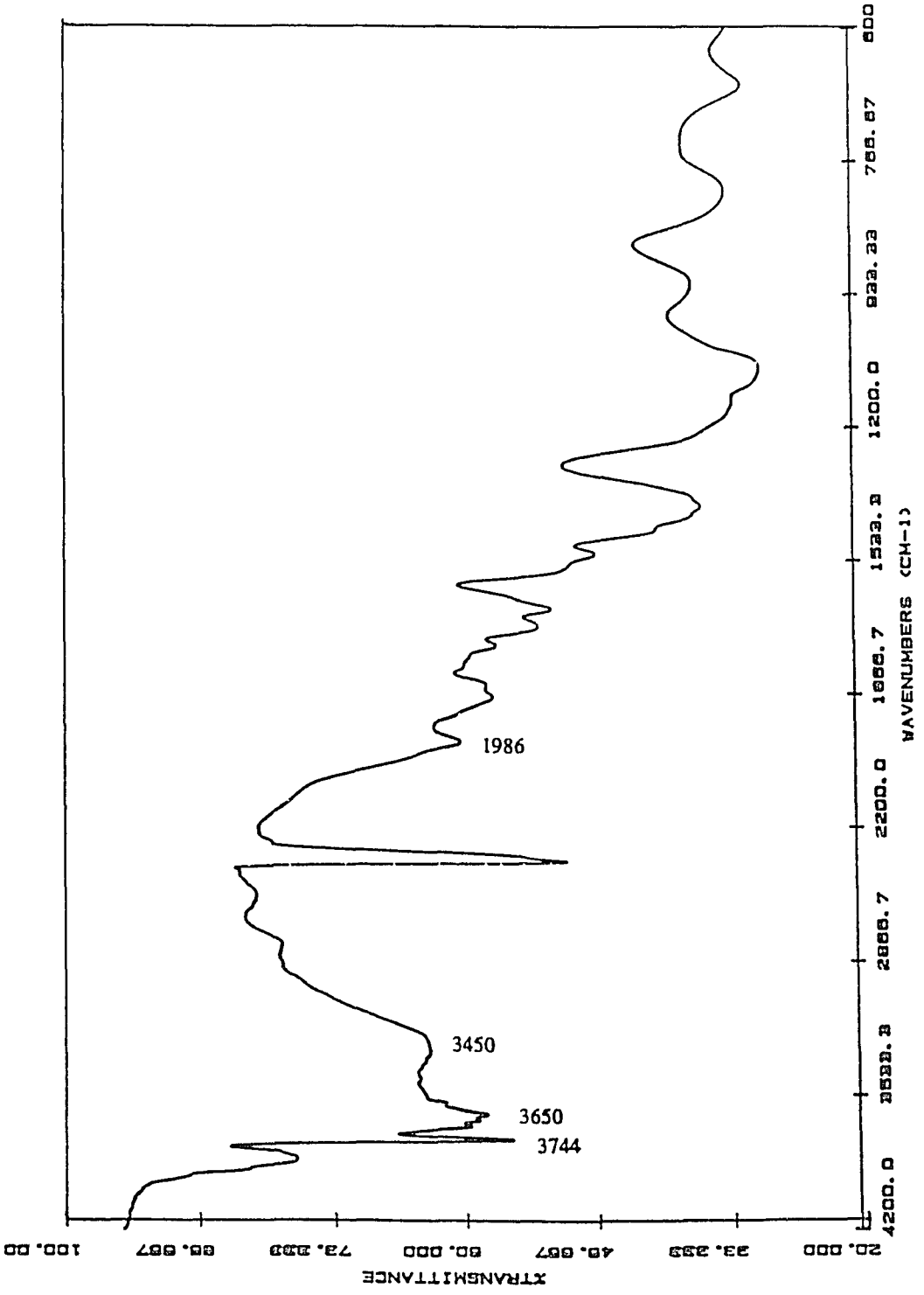

Figure 21. DRIFT spectrum of 1.2×10^{-5} mol of $W(CO)_6$ /g of PVG

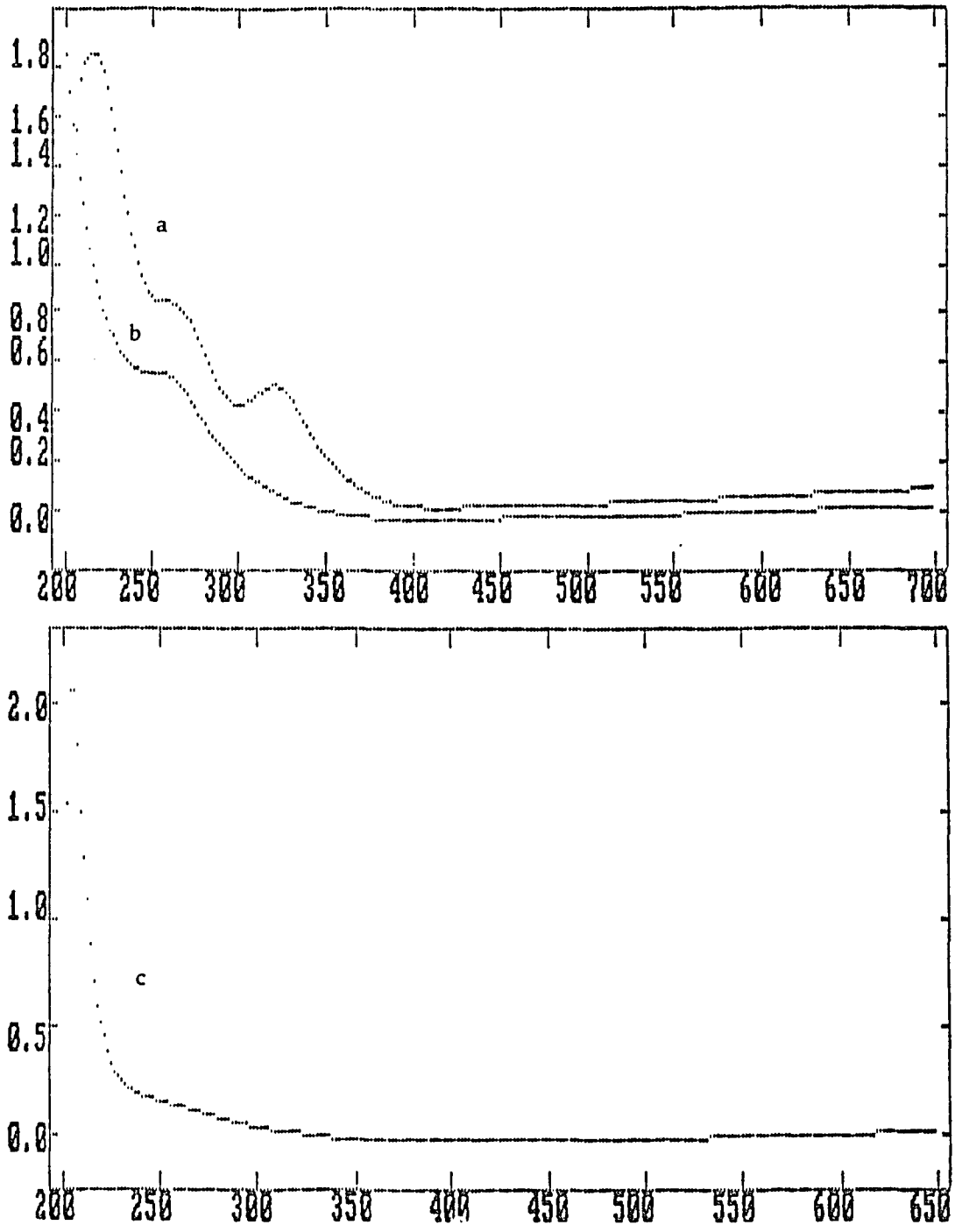

Figure 22. Electronic spectra of WO_3 aqueous solutions: a) pH = 2, b) pH = 6, c) pH = 8.

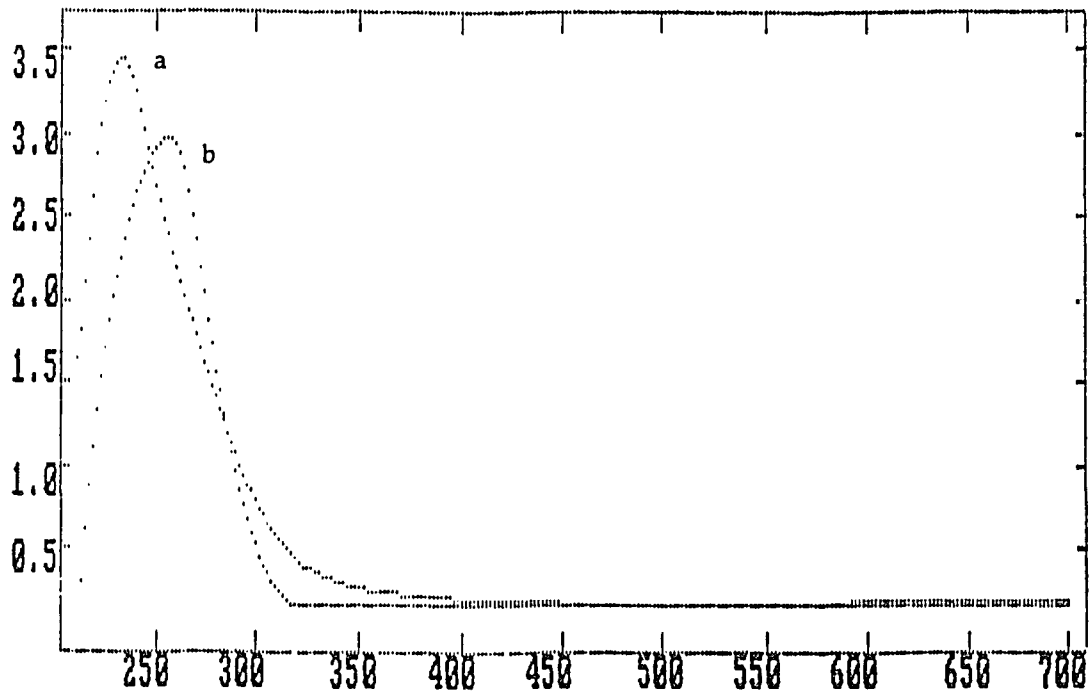

Figure 23. Electronic spectrum of WO_3 (ads): a) loading 3.8×10^{-6} mol of WO_3/g of PVG, b). loading 1.7×10^{-5} mol of WO_3/g of PVG.

example, exhibits an intense absorbance at 232 nm, while a sample with a loading of 1.7×10^{-5} mol WO_3/g PVG, exhibits an intense absorbance at 255 nm.

When WO_3 is adsorbed onto PVG, the intensity of the free silanol group band at 3744 cm^{-1} declines. The DRIFT spectrum of a sample contained 1.5×10^{-5} moles of WO_3 / g PVG (Figure 24), shows the intensity of 3744 cm^{-1} band declines about 40 % relative to that of a calcined PVG (Figure 2). The decline increases with loading, but it is not proportional to the amount of WO_3 loaded. As shown in Figure 25, when the loading increased from 2.6×10^{-6} to 5.3×10^{-5} mol of WO_3/g PVG, the intensity of 3744 cm^{-1} band declined 12 % to 46 % relative to the calcined PVG (Table V). On the other hand, the intensity of 3450 cm^{-1} band, assigned to chemisorbed water, increases in the spectra of WO_3(ads). The significance of this change is not clear since the increase may be attributed to water adsorbed during the impregnating process. The IR absorptions of bulk WO_3 crystalline at 876 and 780 cm^{-1} could not be resolved due to the strong absorptions of PVG in these low wavenumber regions.[135]

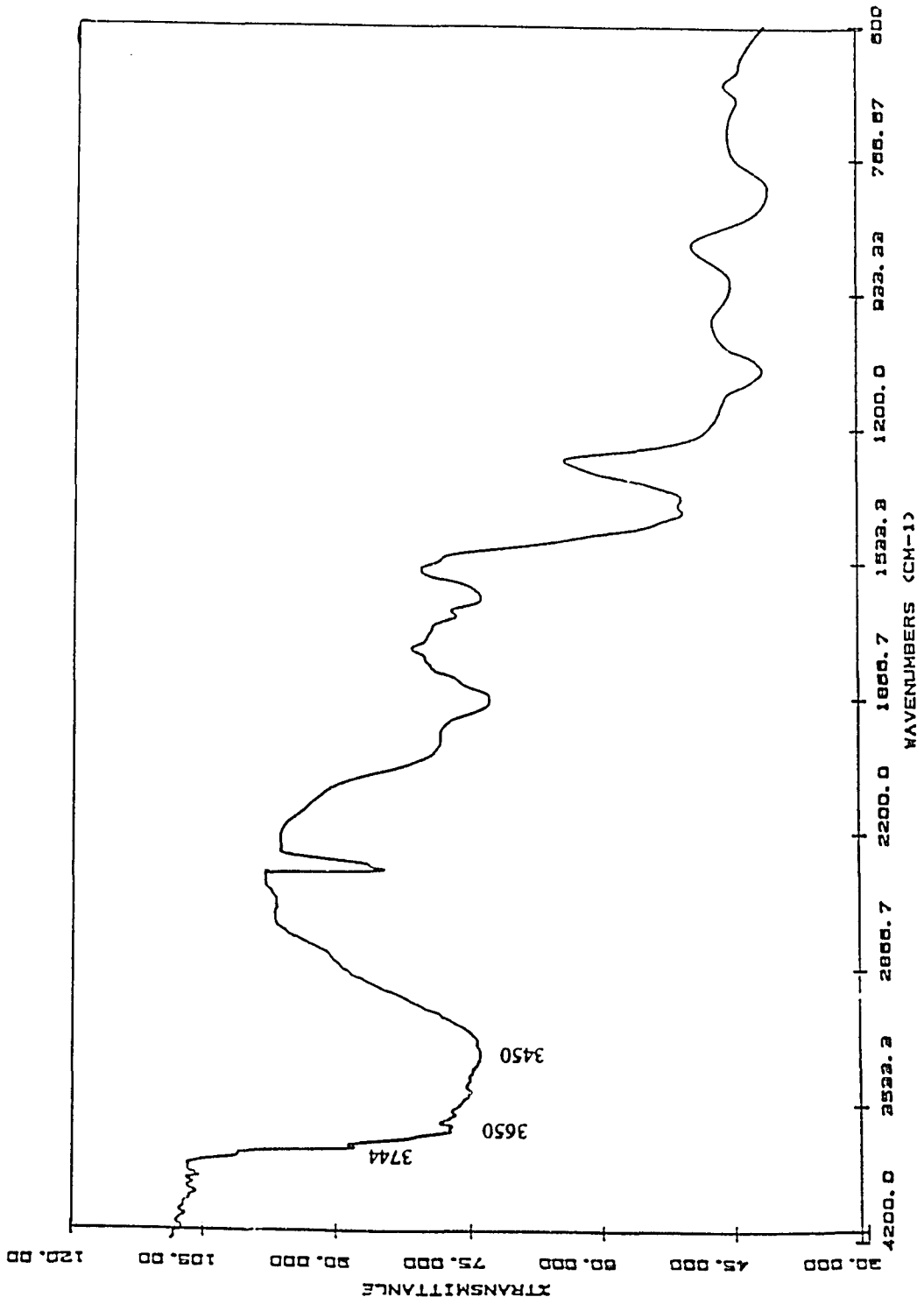

Figure 24. DRIFT spectrum of 1.5×10^{-5} mol of WO_3 /g of PVG

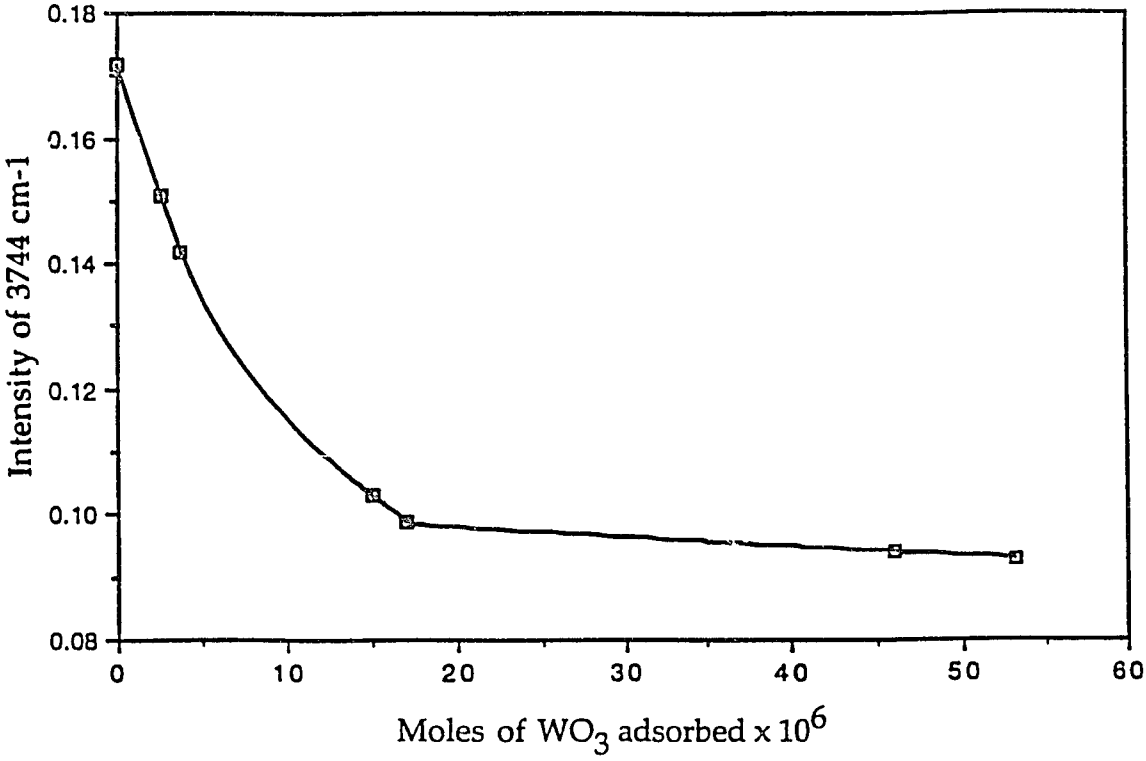

Figure 25. Intensity of the 3744 cm^{-1} free silanol band as a function of WO_3(ads) loading

Table V. Changes of Intensity of Free Silanol Band (3744 cm^{-1}) in the Spectra of PVG Impregnated with WO_3.

Impregnate	Moles Adsorbed (10^{-6} mol/g)	Intensity(log Io/I) 3744 cm^{-1}	Retained Intensity % 3744 cm^{-1}
PVG	0.0	0.172	100
$W(CO)_6$	2.7	0.171	99.4
$W(CO)_6$	12.0	0.173	100.6
WO_3	2.6	0.151	87.8
WO_3	3.8	0.142	82.6
WO_3	15.0	0.103	60.0
WO_3	17.0	0.099	57.6
WO_3	46.0	0.094	54.7
WO_3	53.0	0.092	53.5

3. 2. 3. Photoinduced Methanation of CO_2

A 254 - nm photolysis of a sample containing 4.2 x 10^{-6} moles of $W(CO)_6$ /g PVG in vacuo causes immediate spectral changes. As illustrated in Figure 26, the 287 nm absorption characteristic of the hexacarbonyl declines with a concurrent growth of a new band at 405 nm which has been assigned to tungsten pentacarbonyls.[87] Prolonged UV photolysis over a period of days shows that both 287 nm and 405 nm absorptions disappear, and a new intense band appears in the 230 - 250 nm region corresponding to the absorbance of WO_3(ads).

Corresponding to the spectral changes, period GC analyses indicate that 254-nm photolysis of the sample, which initially contains 4.2±0.2 x 10^{-6} mol of $W(CO)_6$, in vacuo yields 6.4±0.2 x 10^{-6} moles of CO without CH_4 evolution during the initial 2.5 hours. Continuing the photolysis for 24 hours, the photoreaction produces 1.1 x 10^{-5} mol of CO and 8.5 x 10^{-6} mol of CH_4, and after 96 hours, the reaction yields 1.3 x 10^{-4} mol of CH_4 and 2.4 x 10^{-5} mol of CO. This amount of CO corresponds to the recovery of 95 % of the originally coordinated CO. As mentioned in the introduction, these experiments reconfirmed that the formation of methane is due to the methanation of C_1 impurity in the PVG, and not due to the hydrogenation of coordinated CO.

When a sample containing 2.8 x 10^{-6} mole of $W(CO)_6$(ads) (Table VI, sample 1) , which has been photolyzed for 24 hours in vacuo, and then

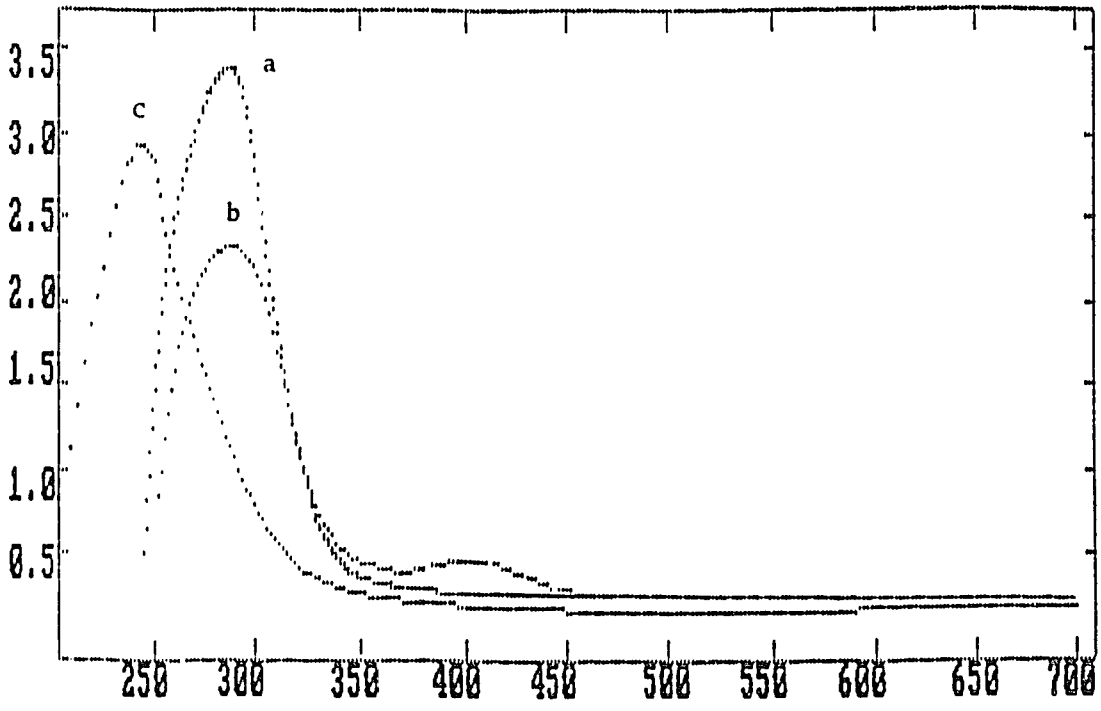

Figure 26. Spectral changes during 254 nm photolysis of 4.2×10^{-6} mol of $W(CO)_6$(ads)/g of PVG in vacuo. Photolysis time (a) 0.0 hour, (b) 1.0 hours, (c) 96 hours

Table VI. Rates of CO and CH_4 Evolution During 254 nm Photolyses of PVG Impregnated with $W(CO)_6$ or WO_3

Impregnate	Moles adsorbed [a] x 10^{-6}	Moles $^{13}CO_2$ x 10^{-4}	Rates (mol/h) ^{12}CO x 10^{-8}	$^{12}CH_4$ x 10^{-8}	^{13}CO x 10^{-8}	$^{13}CH_4$ x 10^{-8}	Turnover Frequency [e] x 10^{-6}
$W(CO)_6$	2.8 (1.9)	2.0	5.6	15	0.85	0.32	0.32
$W(CO)_6$	3.1 (1.9)	8.0	7.2	37	1.0	0.54	0.38
$W(CO)_6$	2.8 (1.9)	2.0	13	28	0.69	0.27	0.27
$W(CO)_6$ [b]	4.0 (2.7)	2.0	8.9	60	7.0	1.8	1.3
$W(CO)_6$ [b]	4.2 (2.7)	2.0	19	35	7.7	4.1	2.7
$W(CO)_6$	4.2 (2.7)	0.0	19	35			
$W(CO)_6$	2.3 (1.5)	0.0	12	26			
WO_3	1.4 (1.1)	1.6	3.2	16	2.8	0.52	1.0
WO_3 [b]	1.4 (1.1)	1.6	3.1	12	14.0	1.6	3.0
WO_3 [b]	1.6 (1.1)	1.6	3.5	14	9.3	1.7	3.0
WO_3 [b]	2.8 (1.9)	1.6	2.3	18	4.8	3.3	3.2
WO_3 [c]	2.6 (1.9)	1.6	2.3	14	3.8	1.8	1.9
WO_3 [d]	2.2 (1.9)	1.6	0.30	2.5	11.2	0.23	0.3
WO_3	24 (17)	1.6	26	29	65	23	2.7
WO_3 [c]	2.2 (1.5)	0.0	4.2	12			
WO_3	2.3 (1.5)	0.0	4.5	14			
WO_3	4.2 (2.9)	0.0	18	47			
WO_3	5.3 (3.8)	0.0	20	58			
WO_3	120 (78)	0.0	42	75			

a). Total moles adsorbed, numbers in parenthesis are moles adsorbed/g of PVG.

b). $^{13}CO_2$ was added after depleting the carbonaceous impurities (see text).

c). The sample was exposed to water vapor.

d). Extensively dehydrated by evacuation at 650 ° C, P ≤ 10^{-4} torr for 15 hours.

e). Turnover frequencies for $^{13}CH_4$ evolution, (sec^{-1}).

evacuated to ≤ 1 x 10^{-5} torr, is exposed to 25 torr of $^{13}CO_2$, 2.0 x 10^{-4} moles, the gas rapidly equilibrates between the adsorbed and gas phases. However, UV photolysis does not result in immediate $^{13}CH_4$ evolution. Instead, $^{12}CH_4$ initially accompanies CO evolution, but small amounts of ^{13}CO and $^{13}CH_4$ appear after 24 hours of photolysis (Figure 27). Increasing the $^{13}CO_2$ pressure to 100 torr, 8.0 x 10^{-4} moles, does not significantly enhance the initial rate of $^{13}CH_4$ evolution (Table VI, sample 2). However, prolonged photolysis of a sample containing 2.8 x 10^{-6} mol $W(CO)_6$(ads) (Table VI, sample 3) under 25 torr of $^{13}CO_2$ shows that the rate of $^{13}CH_4$ evolution slowly increases from 2.7 x 10^{-9} mol/h to 6.4 x 10^{-9} mol/h in 7. 2 x 10^5 seconds (Figure 28). After that point, the rate of $^{13}CH_4$ increases to 1.4 x 10^{-8} mol/h. Correspondingly, prolonged photolysis of a sample containing 2.8 x 10^{-6} mol of $W(CO)_6$(ads) (Table VI, sample 1) in vacuo, the rate of $^{12}CH_4$ declines from 1.5 x 10^{-7} mol/h to 9.2 x 10^{-9} mol/h in 7.5 x 10^5 seconds (Figure 29). The immediate appearance of $^{12}CH_4$ in all experiments with $W(CO)_6$, regardless of the initial $^{13}CO_2$ pressure, which ranged from 20 to 100 torr, suggests that the carbonaceous impurity is more easily hydrogenated than CO_2(ads). Depleting the carbon source in the glass by prior photolysis leads to immediate $^{13}CH_4$ evolution. For example, sample 5 (Table VI) was photolyzed until the rate of CH_4 evolution was below the detection limit of the GC (Gow-Mac 69-100,

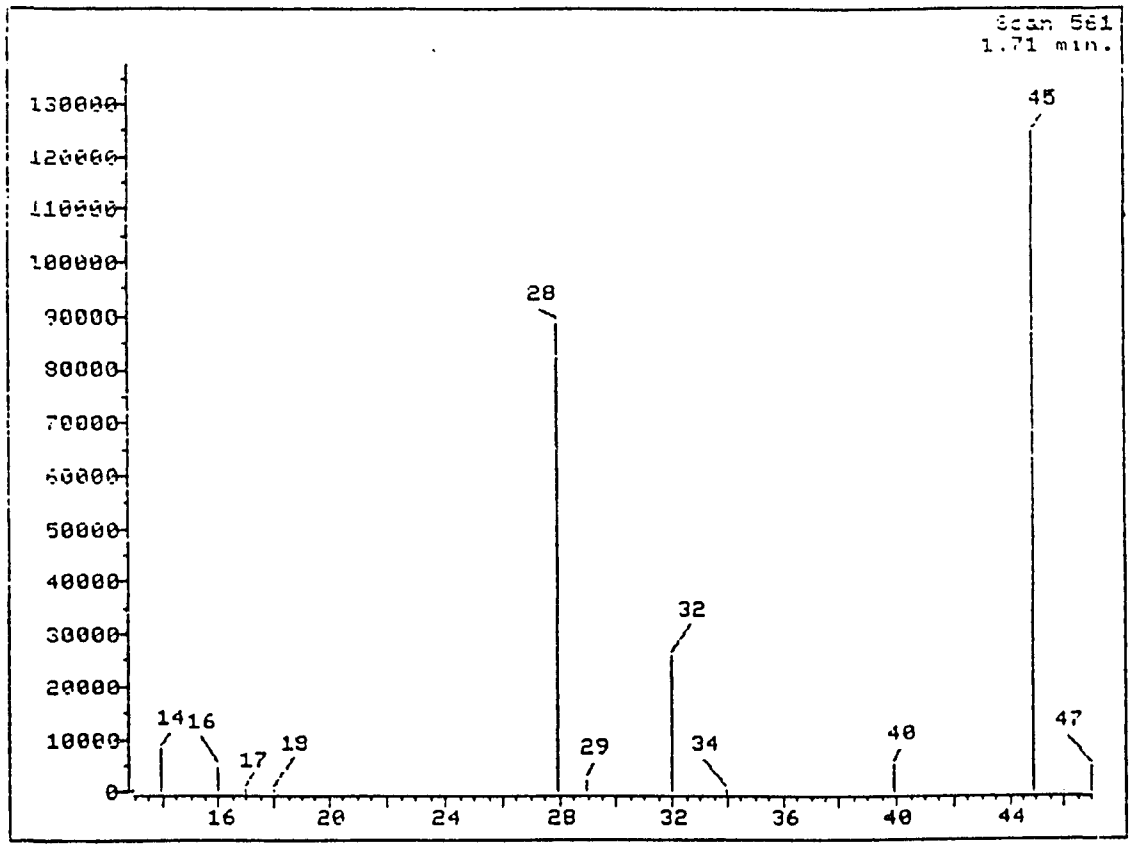

Figure 27a. GC-MS spectrum of gaseous products generated from 254 nm photolysis of a sample contained 2.8×10^{-6} mol of $W(CO)_6$ (ads) under 2.0×10^{-4} mol $^{13}CO_2$ in 8.6×10^4 sec. ($^{13}CH_4$: m/e= 17, ^{13}CO: m/e = 29)

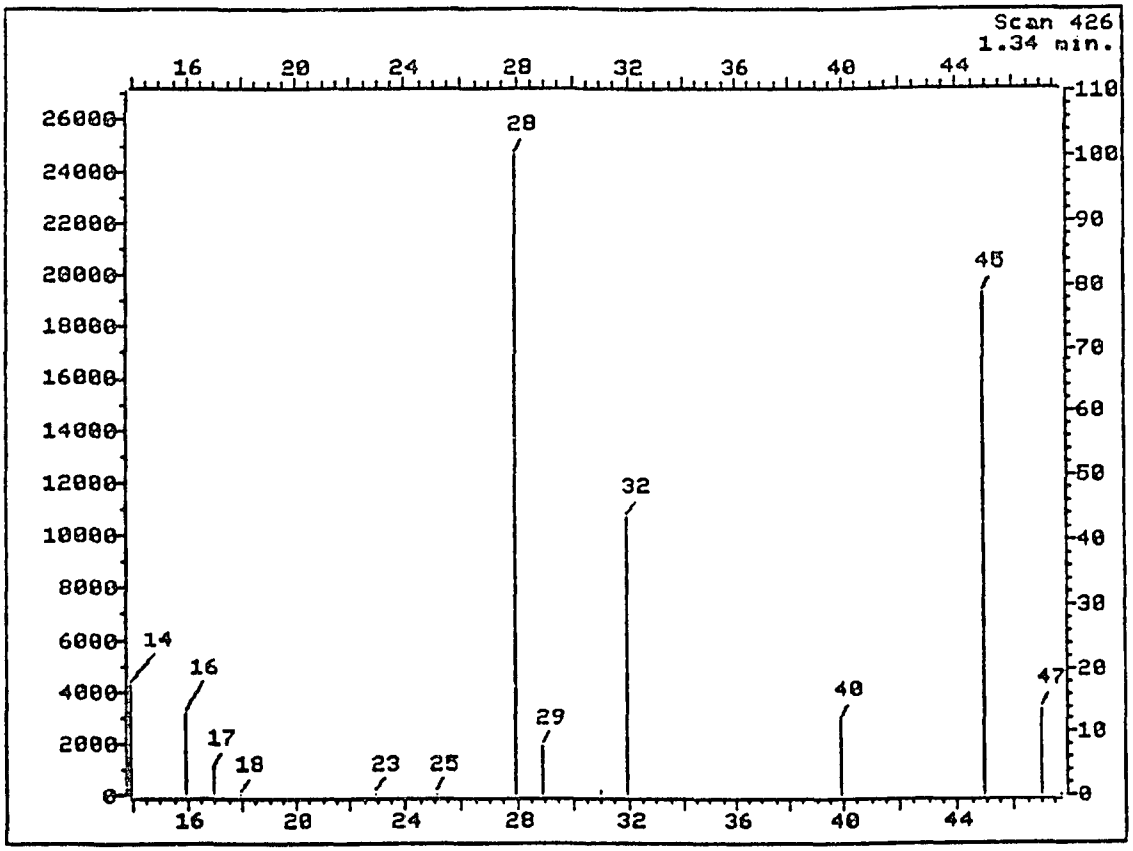

Figure 27b. GC-MS spectrum of gaseous products generated from 254 nm photolysis of a sample contained 2.8×10^{-6} mol of $W(CO)_6$ (ads) under 2.0×10^{-4} mol $^{13}CO_2$ in 8.8×10^5 sec. ($^{13}CH_4$: m/e= 17, ^{13}CO: m/e = 29)

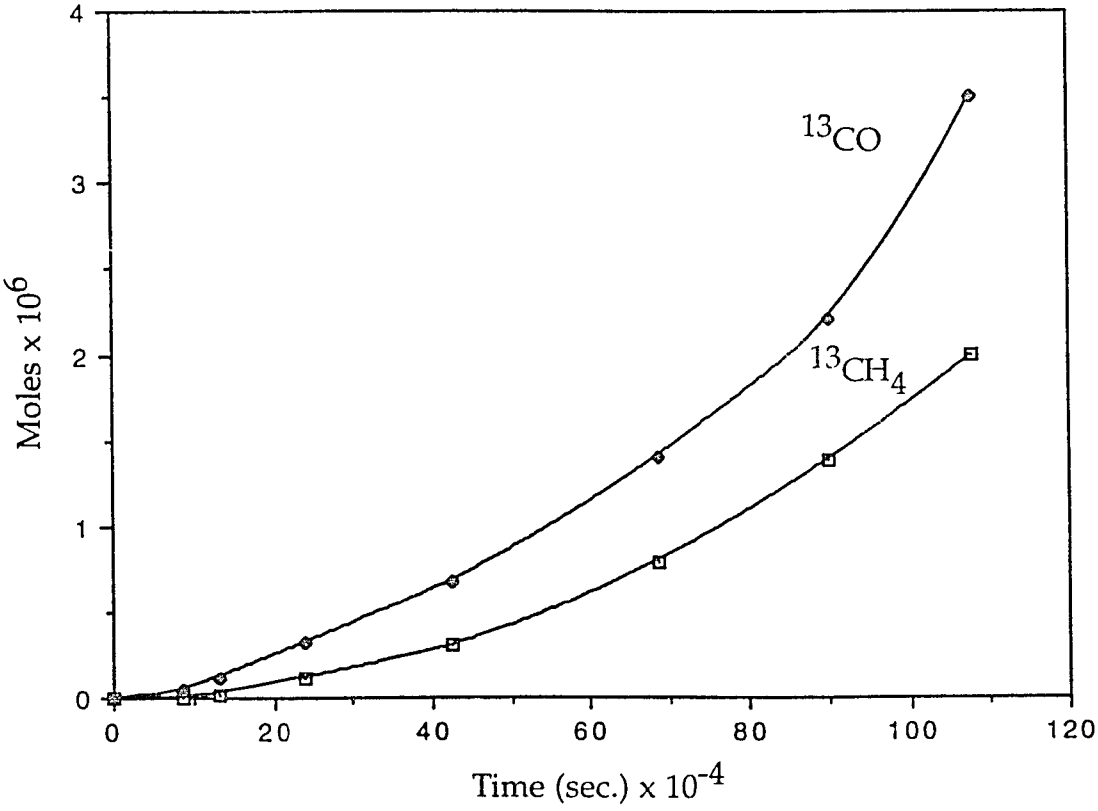

Figure 28. Yields of $^{13}CH_4$ and ^{13}CO during 254 nm photolysis of 2.8 x 10^{-6} mol of $W(CO)_6$(ads) in 2.0 x 10^{-4} mol of $^{13}CO_2$

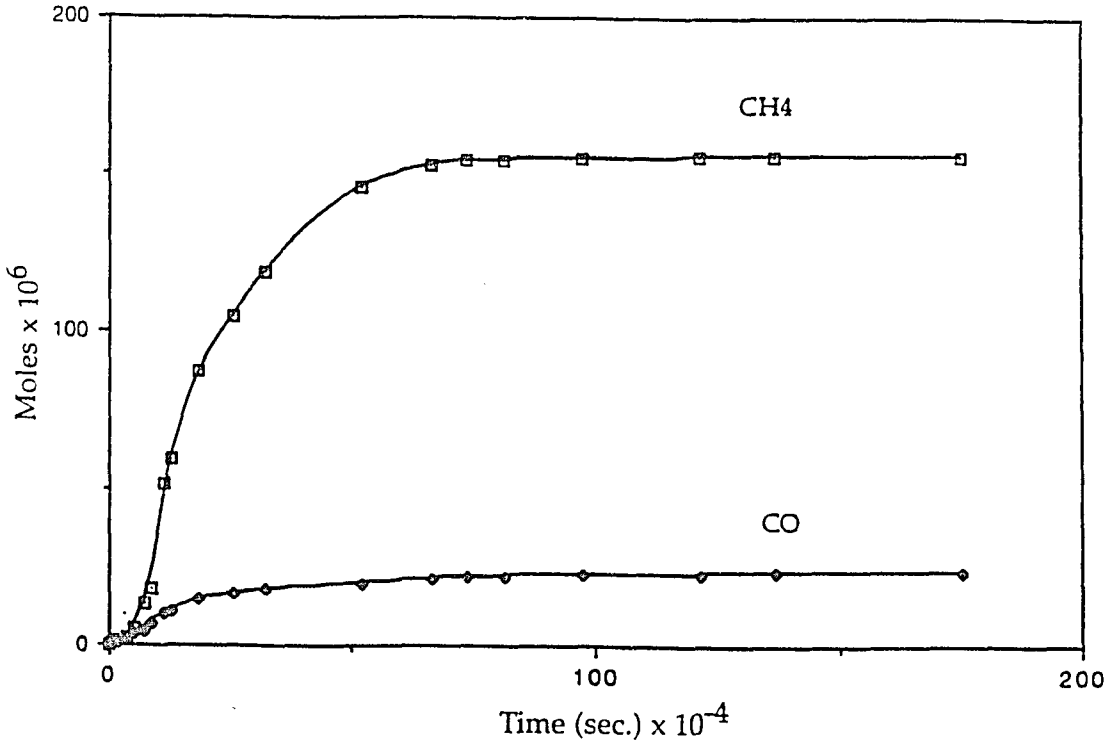

Figure 29. Yields of CH_4 and CO during 254 nm photolysis of 2.8 x 10^{-6} mol $W(CO)_6$(ads) in vacuo

10^{-8} mol). At that point, the sample was evacuated (P $\leq 10^{-5}$ torr), charged with 25 torr of $^{13}CO_2$ and photolyzed. After 2 hours photolysis, GC/MS analysis of the surrounding gas phase indicates that reaction generates 8.2×10^{-8} mol of $^{13}CH_4$ and 1.5×10^{-7} mol of ^{13}CO.

DRIFT spectra recorded during photolysis show that the 1986 cm^{-1} band of the hexacarbonyl disappears during $^{12}CH_4$ evolution. When $^{13}CH_4$ evolution occurs, the electronic spectra of the adsorbate consist of a strong UV absorbance in the region of 230 - 250 nm with a weak shoulder at ca. 350 nm. The spectrum is essentially equivalent to the spectrum of WO_3(ads) as illustrated in Figure 30. Therefore, experiments were carried out with samples directly impregnated with WO_3. As found with the metal carbonyl, irradiation under 20 torr of $^{13}CO_2$ leads to $^{12}CH_4$ evolution initially, followed by $^{13}CH_4$ evolution. Depleting the carbonaceous impurity by prior irradiation also leads to immediate $^{13}CH_4$ evolution (Table VI, sample 8-10).

The quantum yields for the formation of CH_4 are summarized in Table VII. Competitive absorption of the 254 nm excitation by the glass precludes an exact determination of the quantum yield of CH_4 evolution. The listed data are computed from the initial rates of CH_4 evolution and the excitation intensity incident on the impregnated sample calculated according to equation 2.3.

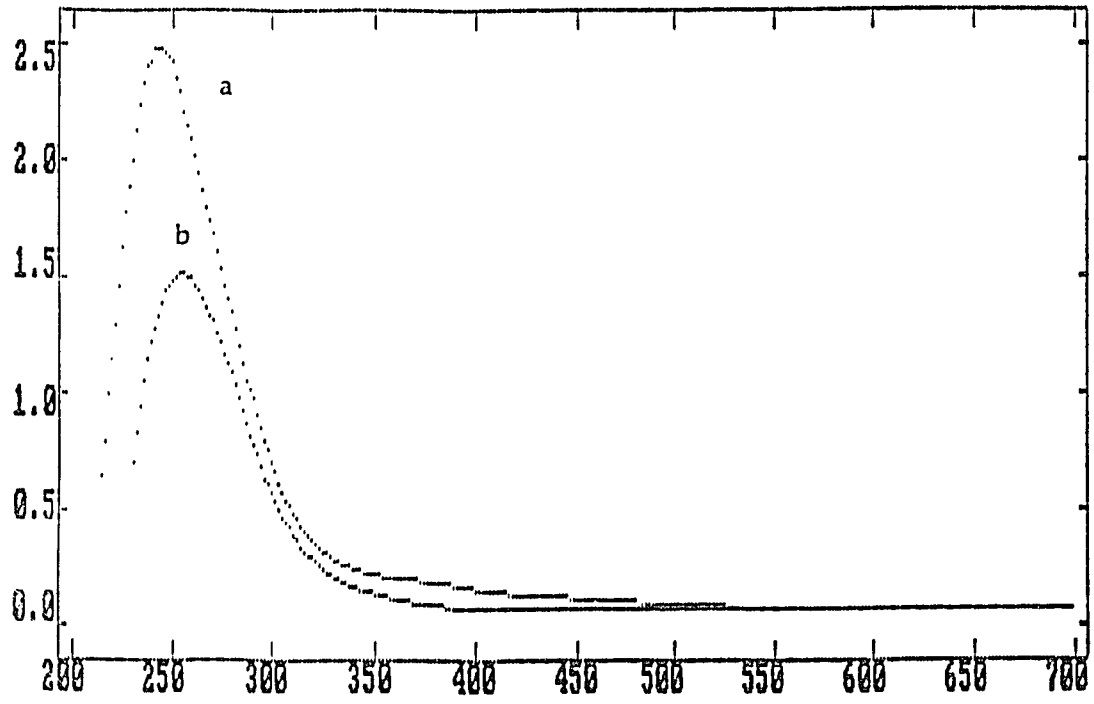

Figure 30. UV spectrum of (a) 2.7×10^{-6} mol of WO_3/g of PVG, (b) the final photoproduct of 1.9×10^{-6} mol $W(CO)_6$/g of PVG.

Table VII. Quantum Yield Data

Impregnate	Moles adsorbed	Light adsorbed	Quantum Yield $^{12}CH_4$	Quantum Yield $^{13}CH_4$	Quantum Yield pentene cis-	Quantum Yield pentene trans-
	10^{-6} mol/g	Einstein/sec	10^{-3}	10^{-4}		
$W(CO)_6$	1.9	4.95×10^{-9}	8.4	1.8		
$W(CO)_6$	1.9	5.48×10^{-9}	22.2	3.2		
$W(CO)_6$	1.9	4.95×10^{-9}	15.7	1.5		
$W(CO)_6$	2.7	4.62×10^{-9}	36.1	10.8		
$W(CO)_6$	2.7	5.11×10^{-9}	19.0	22.2		
WO_3	1.1	5.28×10^{-9}	6.3	8.4		
WO_3	1.1	6.06×10^{-9}	6.4	7.8		
WO_3	1.9	5.06×10^{-9}	9.9	18.1		
WO_3	17	4.73×10^{-9}	15.3	135.1		
$Ru_3(CO)_{12}$	0.12	4.42×10^{-9}			0.16	0.24
$Ru_3(CO)_{12}$	0.29	4.84×10^{-9}			0.42	0.71
$Ru_3(CO)_{12}$	0.45	4.65×10^{-9}			0.48	0.85
$Ru_3(CO)_{12}$	0.78	5.17×10^{-9}			0.65	1.27
$Ru_3(CO)_{12}$	0.78	5.52×10^{-9}			0.72	1.38
$Ru_3(CO)_{12}$	0.45	8.25×10^{-9} *			0.43	0.77
$Ru_3(CO)_{12}$	0.78	1.02×10^{-8} *			0.78	1.44

* Irradiated at 350 nm light.

The impregnated PVG samples used in the $^{13}CO_2$ methanation experiments contain ≤ 2.7 x 10^{-6} mol of $W(CO)_6$/g PVG and ≤ 1.7 x 10^{-5} mol WO_3(ads)/g PVG, which correspond to a fractional surface coverage of ≤ 2 % in the impregnated volumes of the glass. Nevertheless, the fact that the rate of CH_4 evolution increases with tungsten content (Table VI), and the absence of $^{13}CH_4$ evolution during 254 nm photolysis of an unimpregnated, calcined PVG under 20 torr of $^{13}CO_2$ for 24 hours confirm that tungsten is essential to the conversion.

Electronic spectra recorded during photolysis of the hexacarbonyl, the stoichiometry of CO evolution, and the fact that equivalent behavior occurs with samples impregnated with WO_3 indicate that photolysis converts the $W(CO)_6$ to a tungsten oxide. Consequently, a tungsten oxide surface species is the photocatalytic reagent in the conversion of $^{13}CO_2$ to $^{13}CH_4$. Electronic spectra show no change in the oxide during the reaction, and GC-MS analyses indicate no loss of activity in the 5 periodic evacuation and recharging with 20 torr $^{13}CO_2$ (Table VIII).

Deuterium labeling experiments indicate that the hydrogen source is either the silanol or chemisorbed water.[87] Calcined (600°C) PVG contains small amounts of chemisorbed water, and methane evolution is dependent, although in a complex way, on the amount of adsorbed water. Extensive

Table VIII. Photocatalytic Activity of WO_3/PVG Catalysts for the Methanation of CO_2 during Periodic Evacuation and Recharging with 20 Torr $^{13}CO_2$ (wavelength=254 nm, period=10 hours)

Impregnated WO_3 (mol)	Rate of $^{13}CH_4$ Formation (10^{-8} mol/h)					
	Initial	Period 1	Period 2	Period 3	Period 4	Period 5
1.6×10^{-6}	1.7	1.3	1.9	1.8	1.5	1.9
2.8×10^{-6}	3.3	3.5	3.0	3.2	2.8	3.1

dehydration of a sample containing 2.2×10^{-6} mol of WO_3(ads) under vacuum ($P \leq 6 \times 10^{-4}$ torr) at 650°C for 15 hours, for example, reduces the rate of $^{13}CH_4$ evolution by an order of magnitude during subsequent photolysis under 20 torr of $^{13}CO_2$. On the other hand, increasing the water content by exposing a calcined sample containing 2.6×10^{-6} mol of WO_3(ads) to water vapor also decreases the rate of $^{13}CH_4$ evolution by 40% relative to an unexposed sample (Table VI), but no significant decrease in the rate of $^{12}CH_4$ evolution occurs. Apparently water is an essential reactant, but in excess, it competes with the adsorption of $^{13}CO_2$ onto the active sites. This is suggested by the fact that the rate of $^{12}CH_4$ evolution, where the $^{12}CH_4$ derives from a C_1 oxide currently occupying the active site, is uneffected by exposing to H_2O.

In addition to acting as a hydrogen source, water could be the source of the reducing equivalents. Indeed, GC analyses of the photoproducts indicate that oxygen forms in the methanation of CO_2. As shown in Table IX, the ratio of peak height of nitrogen to oxygen reduces from 3.2 ± 0.1 to 1.9 ± 0.4 after 10 hours photolysis. According to the equations (3.3) and (3.4),

$$CO_2 + 2H_2O \text{ ------> } CH_4 + 2O_2 \qquad (3.3)$$

$$CO_2 + H_2O \text{ -------> } H_2 + CO + O_2 \qquad (3.4)$$

three moles of O_2 are expected per mole of CH_4 and CO formed. As demonstrated in Table X, however, the actual number of moles of O_2

Table IX. Peak Height of N_2 and O_2 Obtained during 254 nm Photolysis of PVG Samples Containg $W(CO)_6$ or WO_3

Impregnate	Moles adsorbed	Peak Height (cm) (before photo)		Peak Height (cm) (after photo)	
		N_2	O_2	N_2	O_2
$W(CO)_6$	4.0×10^{-6}	4.2	1.3	4.5	2.2
WO_3	1.6×10^{-6}	3.5	1.1	3.6	2.1
WO_3	2.8×10^{-6}	3.3	1.0	3.7	2.5
WO_3	2.6×10^{-6}	3.8	1.2	4.2	1.8

Table X. Theoretical and Experimental Yield of O_2 Obtained during 254 nm Photolysis of PVG Samples Containing $W(CO)_6$ or WO_3

Impregnate	Moles adsorbed	O_2 (Theoretical) (Moles)	O_2 (Experimental) (Moles)
$W(CO)_6$	4.0×10^{-6}	1.1×10^{-6}	4.8×10^{-7}
WO_3	1.6×10^{-6}	1.3×10^{-6}	6.0×10^{-7}
WO_3	2.8×10^{-6}	1.1×10^{-6}	7.9×10^{-7}
WO_3	2.6×10^{-6}	7.4×10^{-7}	2.7×10^{-7}

Calculation:

A. O_2 Theoretical Yield = 2 x Yield of $^{13}CH_4$ + Yield of ^{13}CO

B. O_2 Experimental Yield= $[(O_2)_{\text{after photo.}} - (O_2)_{\text{befor photo.}}]$

C. O_2 before photo. = (Peak Height of $O_2)_{\text{before photo.}} \times 1.6 \times 10^{-7}$ mol/cm x 4*

D. O_2 after photo. = (Peak Height of O_2/Peak Height of $N_2)_{\text{after photo.}}$ x (Peak Height of $N_2)_{\text{before Photo.}} \times 1.6 \times 10^{-7}$ mol/cm x 4*

* Multiply 4 here since each injection equales one forth of amount of gases in the photoreactor.

detected experimentally ranged from ca. 40% to 75% of these theoretical yields. The reason for this discrepancy is not clear. One of the possibilities is that the reaction stoichiometry is biased by the reaction 3.5,

$$CO_2 + 4H_2 \text{------>} CH_4 + 2H_2O \qquad (3.5)$$

where some H_2 formed in reaction 3.4 hydrogenates CO_2 directly. On the other hand, 254 nm photolysis of WO_3(ads) with a mixture of CO_2 and H_2 at ratio of 1 : 4 does not increase the rate of CH_4 evolution, as shown in Table XI.

The IR spectrum of CO_2 adsorbed on the WO_3/PVG is similar to the spectrum of CO_2 adsorbed on unimpregnated PVG. The results are consistent with the low WO_3 surface coverage (≤ 2%). As shown in Figure 31, when the PVG sample containing 1.9 x 10^{-6} mol of WO_3/g is exposed to CO_2, the silanol group bands at 3744, and 3650 cm^{-1} shift to 3730 and 3632 cm^{-1}, and a new band appears at 3599 cm^{-1}. Also, bands indicative of physisorbed CO_2 appear at 2360, and 671 cm^{-1}, and a series of weak bands appear in the 1700-1200 cm^{-1} region. The 14-18 cm^{-1} red shifts of surface hydroxyl bands indicate that a interaction between CO_2 and surface silanol groups occurs. Similar red shifts of hydroxyl group bands have been observed on SiO_2 with various gases like nitrogen, oxygen, methane, acetone and water,[136,156] where the interaction between the adsorbates and surface hydroxyl groups is attributed to a hydrogen-bonding interaction.[156] The IR bands indicative of physisorbed

Table XI. Effect of H_2 on the Rates of CO and CH_4 Evolution

Impregnate	Moles adsorbed [a] x 10^{-6}	Moles CO_2 x 10^{-4}	Moles H_2 x 10^{-4}	Rates (mol/h) ^{12}CO x 10^{-8}	$^{12}CH_4$ x 10^{-8}	^{13}CO x 10^{-8}	$^{13}CH_4$ x 10^{-8}
WO_3	1.4 (1.1)	1.6	0.0	3.2	1.4		
WO_3	1.4 (1.1)	1.6	6.4	2.9	1.2		
WO_3	1.6 (1.1)	1.6 [b]	0.0			9.3	1.7
WO_3	1.6 (1.1)	1.6 [b]	6.4			5.6	1.5

a). Total moles adsorbed, numbers in parenthesis are moles adsorbed/g of PVG.

b). Charged with $^{13}CO_2$.

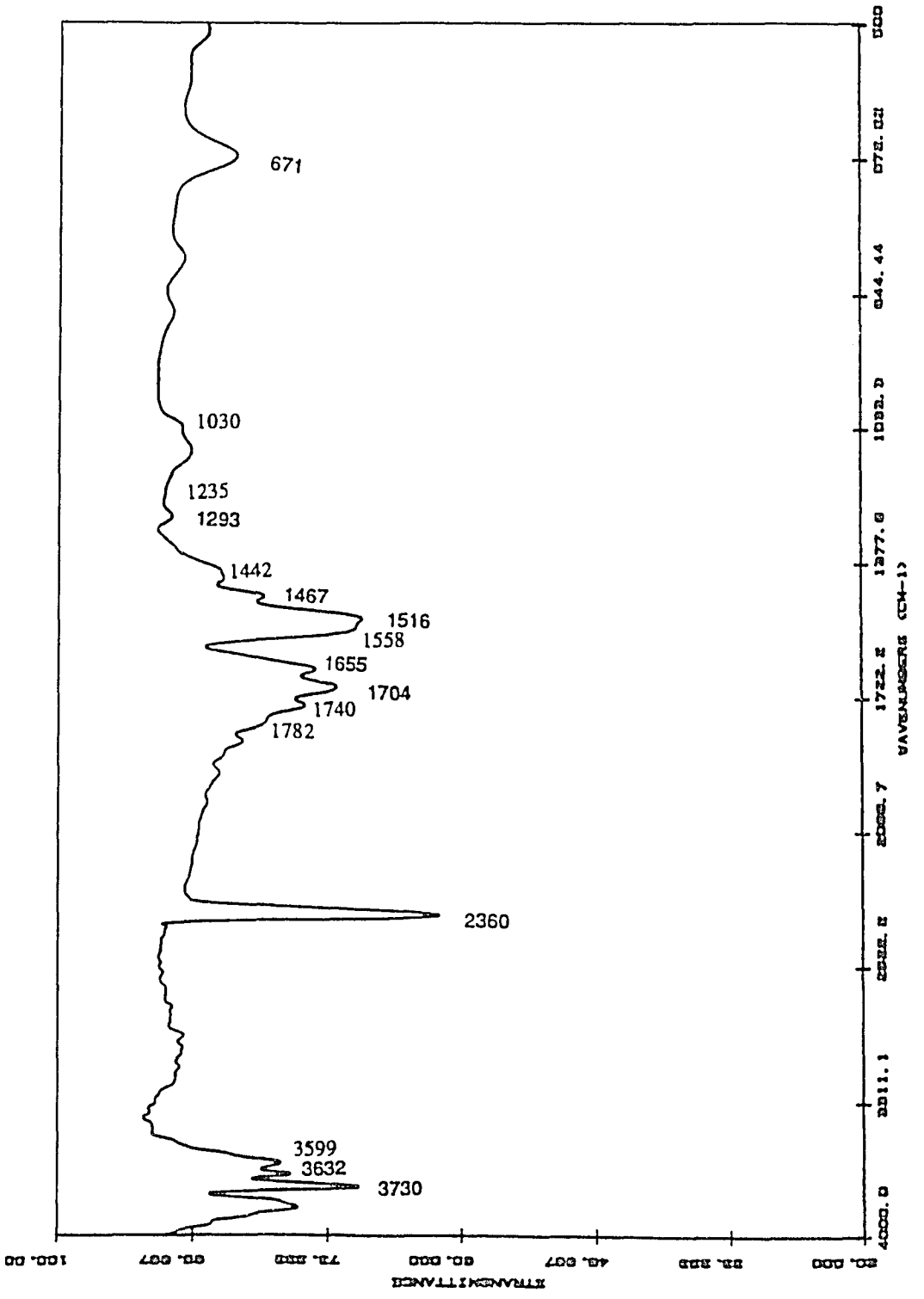

Figure 31. DRIFT spectrum of PVG containing 1.9×10^{-6} mol of WO_3/g exposed to 25 torr of CO_2.

CO_2 and perturbed silanol groups at 3730, 3632, and 3599 cm^{-1} decline immediately on evacuation ($P \leq 10^{-3}$ torr), while the silanol group band at 3744 cm^{-1} reappears. However, the intensities of the bands in the 1700-1200 cm^{-1} region are independent of the pressures of CO_2 and do not change on evacuation.

The bands in the 1700 - 1200 cm^{-1} range in the IR spectra of CO_2 on many metal and metal oxide surfaces have been assigned to carbonate and bicarbonate species by many researchers.[137-138] The assignments of the IR absorptions of CO_2 on Al_2O_3 and SiO_2 are summarized in Table XII. In the 1700-1200 cm^{-1} region, the 1655 and 1558 cm^{-1} bands agree with the absorptions of CO_2 adsorbed on SiO_2.[138a] The other bands, which appear at 1704, 1516, and 1293 cm^{-1} agree with bands that assigned to surface carbonate when CO_2 is adsorbed onto Al_2O_3, while the weak bands at 1467 cm^{-1} and 1442 cm^{-1} are similar to the bands of bicarbonate on Al_2O_3 surface.[138a] In addition to Si-OH Brønsted acid sites, PVG also possesses 2.6 ± 0.1% of electron deficient Lewis acid sites in the form of B_2O_3 or B-OH.[104] The spectrum of CO_2 adsorbed onto these sites would be more analogous to that adsorbed onto Al_2O_3 than that adsorbed onto SiO_2.

On the other hand, Diem and coworkers found that water vapor shows

Table XII. Assignment of Infrared Bands for Adsorbed CO_2 in the Range of 1000 cm^{-1} - 1800 cm^{-1}

Adsorbent	Frequency (cm-1)	Assignment	reference
Cr_2O_3/Al_2O_3	1630-1610	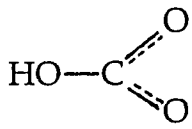 -	124
	1750	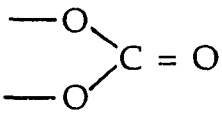	
	1430	CO_3^{2-}	
General	1780 1260 1020	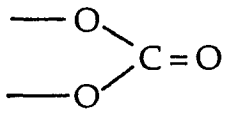	124
Al_2O_3	1708 1513 1309	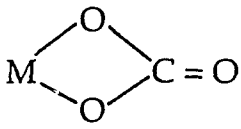 or	138a
		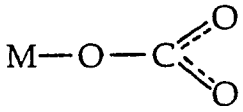	
	1649 1451 1433 1230	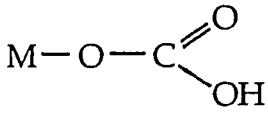	
	1597 1395 1379	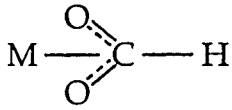	

Table XII. (continue)

Adsorbent	Frequency (cm-1)	Assignment	reference
SiO_2	1660 1581	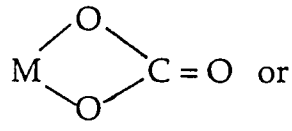 or	138a
		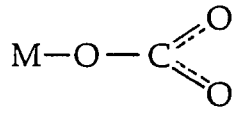	
	1625	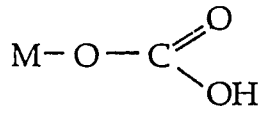	

a series of bands in the 1700 - 1200 cm^{-1} region.[138b] The IR bands of water vapor at 1750, 1714, 1664, 1562, 1527, 1473, 1446, 1286 cm^{-1} very close to those observed in the spectra of CO_2 on WO_3/PVG. The spectral agreement suggest that the bands in the 1700 - 1200 cm^{-1} region in the spectra of CO_2 on WO_3/PVG could be due to moisture. The moisture could come from transferring of CO_2 since CO_2 was directly introduced into the cell from container without predrying. At this moment, it seems to be difficult to decide these bands belongs to carbonate species or water.

Tying up the B_2O_3 Lewis acid sites through a reaction with NH_3 reduces the rate of CH_4 evolution substantially. NH_3 physisorbs onto PVG by H-bonding with surface hydroxyl groups, and chemisorbs by forming the donor-acceptor complex, H_3N-B_2O_3, with the Lewis acid sites.[122] Physisorbed NH_3 exhibits IR bands at 3400 and 3320 cm^{-1}, and desorbs under vacuum ($P \leq 10^{-2}$ torr) at room temperature, whereas chemisorbed NH_3, which exhibits IR bands at 3365 and 3280 cm^{-1}, desorbs only at temperatures $\geq$ 80 °C under an equivalent vacuum.[161] The difference in desorption conditions offers a means of selectively tying up the Lewis acid sites. Two pieces of PVG, each containing 1.7 x 10^{-5} mol of WO_3, were investigated in the experiment. Sample A was exposed to 1 atm NH_3 for 30 minutes then evacuated to 7 x 10^{-5} torr, and maintained under this dynamic vacuum for three hours at room

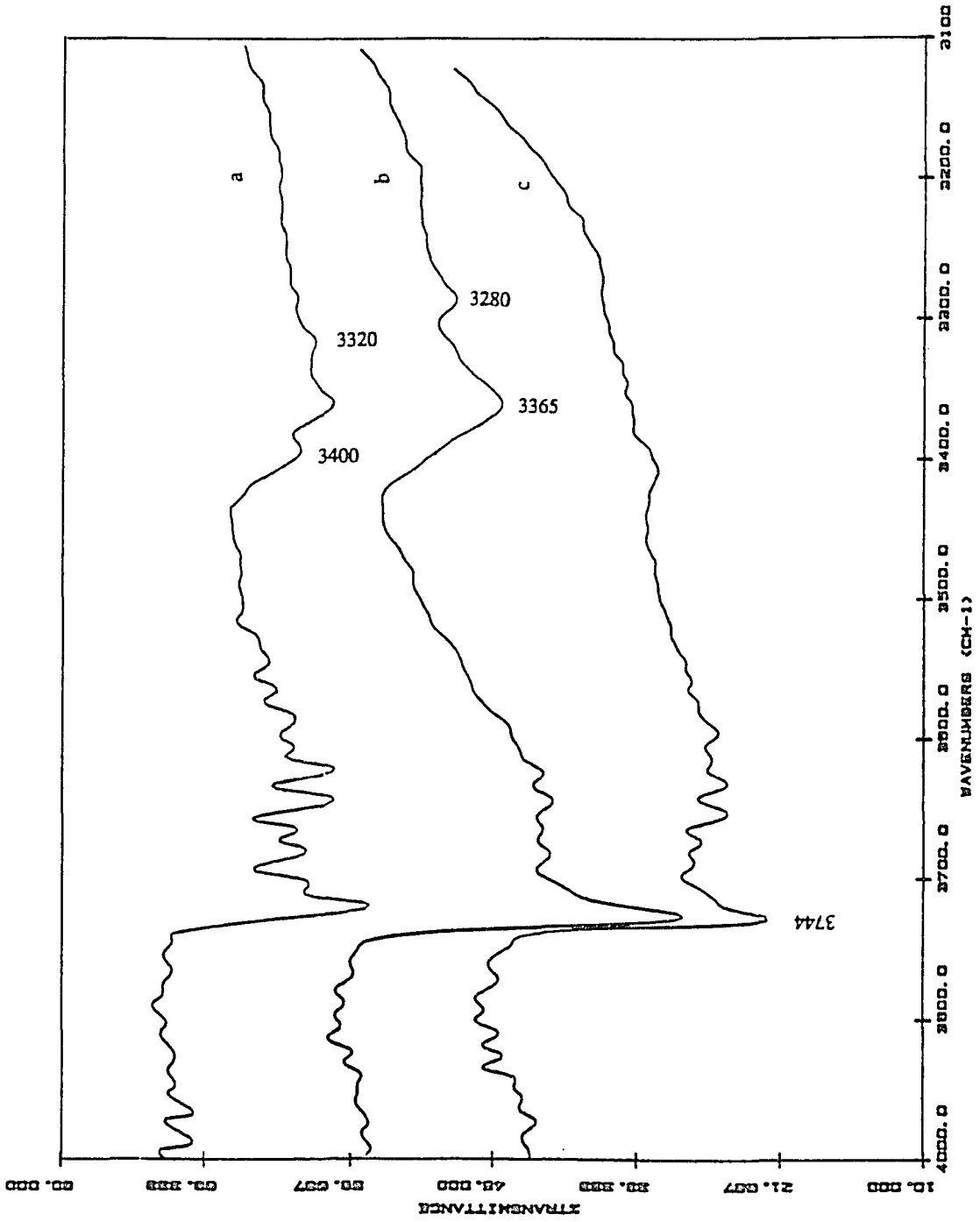

Figure 32. DRIFT spectra of NH_3 adsorbed on PVG contained 1.7 x 10^{-5} mol of WO_3. (a) exposed to 1 atm of NH_3, and evacuated for 10 minutes, (b) evacuated for 3 hours, (c) evacuated at 80 °C for 16 hours.

temperature. DRIFT spectra show that the 3400 and 3320 cm^{-1} bands indicative of physisorbed NH_3 disappear, while the 3365 and 3280 cm^{-1} bands of chemisorbed NH_3 are unaffected (Figure 32). Sample B was not exposed to NH_3, but evacuated to 7 x 10^{-5} torr, and maintained under this dynamic vacuum for three hours. After evacuation, both samples were exposed to 20 torr of CO_2, and irradiated with 254-nm light for 24 hours. The results listed in Table XIII demonstrate that exposing the sample to NH_3 reduces the rate of CH_4 evolution by ca. a factor of nine, and reduces the rate of CO evolution by a factor of two. Removing the chemisorbed NH_3 by evacuating and maintaining the sample under a dynamic vacuum of 8 x 10-5 torr at 80 °C for 16 hours increases the rate CH_4 evolution. GC-MS analyses show that, after removal of the chemisorbed NH_3, similar reaction rates of $^{13}CH_4$ and ^{13}CO evolution occur with both samples when irradiated with 254 nm light under 15 torr of $^{13}CO_2$ (Table XIII).

A decrease in reaction rate is also observed on uncalcined WO_3/PVG samples. As shown in Table XIV, 254-nm photolysis of a sample dried at 50 °C in vacuo (P≤ 300 torr) and loaded with 4.5 x 10^{-6} mol of WO_3 exhibits rates of 7.2 x 10^{-8} mol/h for CH_4, and 4.8 x 10^{-8} mol/h for CO. Under identical conditions, UV photolysis of a sample loaded 4.2 x 10^{-6} mol of WO_3, except in this case, the sample was calcined at 600 °C for 50 hours after drying, results in evolution rates of 4.7 x 10^{-7} mol/h for CH_4, and 1.8 x 10^{-7} mol/h for CO. These samples were prepared by impregnation of the PVG in 40 mL of

Table XIII. Effects of NH_3 on the Rates of CO and CH_4 Evolution

Sample	Impregnated	Mole Adsorbed $x10^{-5}$	NH_3	Rate (mol/hr) CO $x10^{-7}$	CH_4 $x10^{-7}$	^{13}CO $x10^{-7}$	$^{13}CH_4$ $x10^{-7}$
A.	WO_3	1.7	Yes	1.2	0.33	6.5	1.5
B.	WO_3	1.7	No	2.6	2.9	6.5	2.3

* Sample A was exposed to 1 atm NH_3 for 30 min before photolysis.
* Rates of CO and CH_4 evolution were determined for the reaction under 20 torr of CO_2.
* Rates of ^{13}CO and $^{13}CH_4$ evolution were determined for the reaction under 15 torr of $^{13}CO_2$ after removing chemisorbed NH_3.

Table XIV. Effect of Sample Prepration on the Rates of CO and CH_4 Evolution

Impregnate	Moles adsorbed [a] x 10^{-6}	Rates (mol/h) ^{12}CO x 10^{-8}	Rates (mol/h) $^{12}CH_4$ x 10^{-8}
WO_3 [b]	4.5 (2.9)	4.8	7.2
WO_3	4.2 (2.9)	17.5	46.8

a). Total moles adsorbed, numbers in parenthesis are moles adsorbed/g of PVG.
b). The sample was not calcined after impregnation.

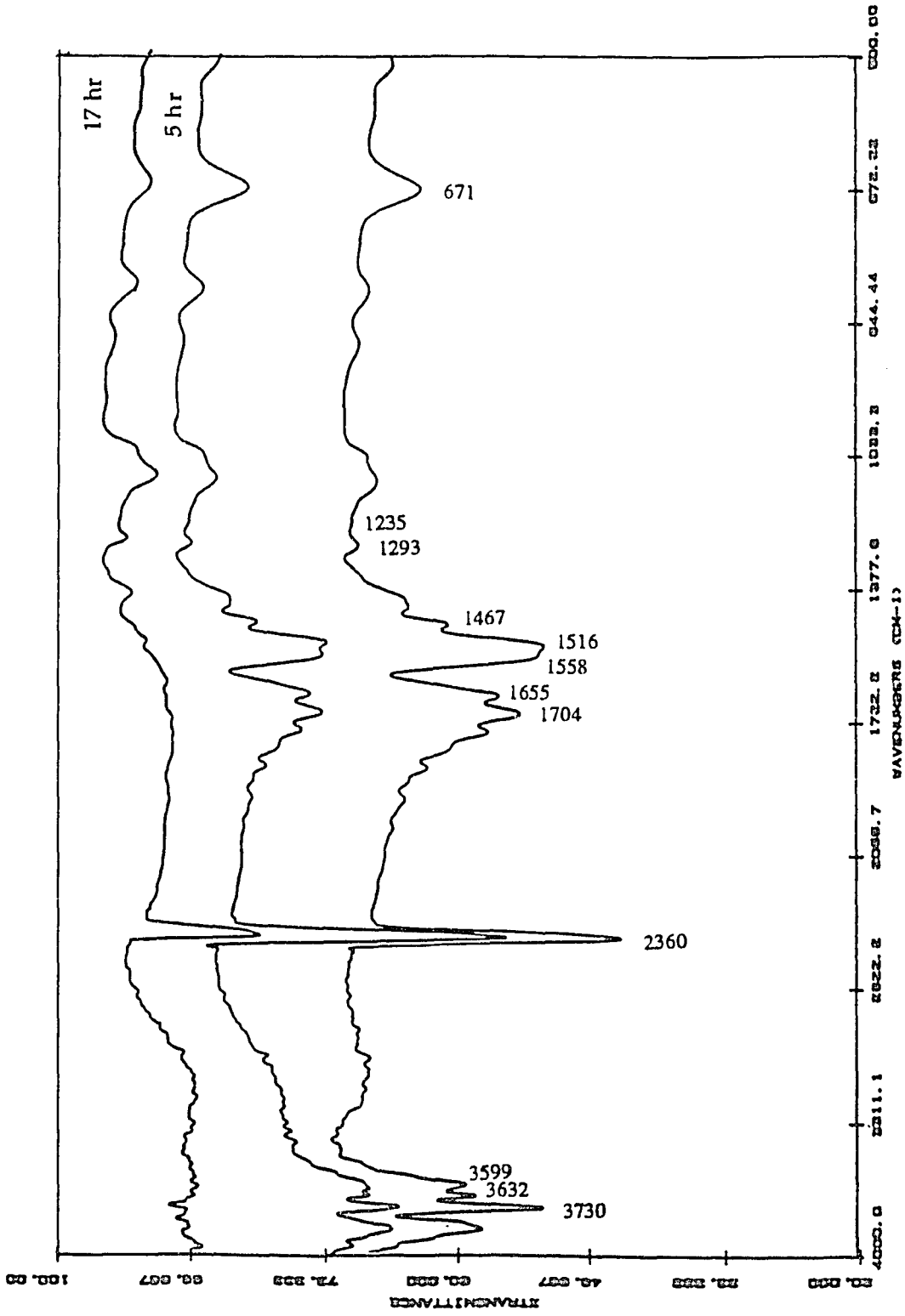

Figure 33. DRIFT spectra changes during 254 nm photolysis of 1.5×10^{-5} mol of WO_3(ads)/g of PVG after exposed to 20 torr CO_2. Numbers designate photolysis times in hours.

aqueous NH_4OH solution, at pH 8, containing 2.7 x 10^{-3} M WO_3. Consequently, the decline in gas evolution rates may reflect ammonia retained on the uncalcined sample, or the presence of excess chemisorbed water. The effect of NH_3 on the reaction rates will be further discussed in the section of quenching of the tungsten oxide emissions.

During UV irradiation, the IR bands of CO_2 absorbed onto WO_3/PVG samples decline concurrently with CH_4 evolution. As illustrated in Figure 33, a sample containing 1.5 x 10^{-5} mol of WO_3/g PVG was exposed to 20 torr of CO_2 for 30 minutes, and evacuated to 0.1 torr in the IR chamber. 254-nm photolysis causes progressive declines in the 3730-3599 cm^{-1} and 1700-1200 cm^{-1} regions, and the bands in both regions disappear after 17 hours irradiation. C-H vibrations in the 2900-3000 cm^{-1} region are not resolved from background in these experiments, but they are observed in DRIFT spectra recorded during 254 nm photolysis of a sample containing 2.1 x 10^{-5} mol of $W(CO)_6$/g PVG.[87] The fact that methane is the sole hydrocarbon product leads to an assumption that the methanation of CO_2 proceeds through a formaldehyde and methanol intermediates. To investigate these possible intermediates, base catalyzed TMOS/CH_3OH/H_2O sol-gel were used as a support instead of PVG. Calcined TMOS/CH_3OH/H_2O sol-gels are similar to PVG, but contain small amount of methoxyl groups, and do not have the B_2O_3 sites. In a typical trial, 0.65 g calcined sol-gel loaded with 3.9 x 10^{-6} mol

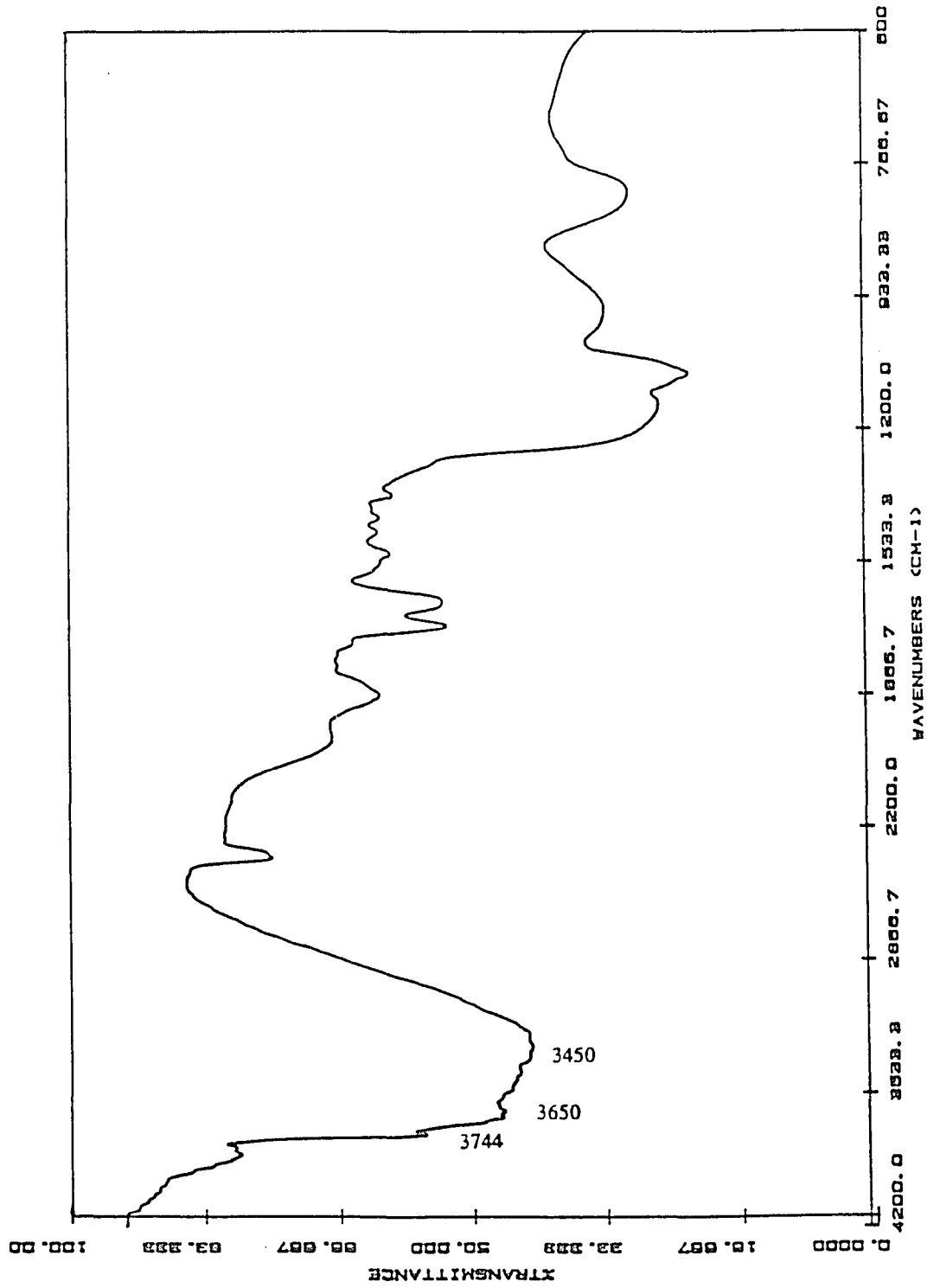

Figure 34. DRIFT spectrum of sol-gel contained 3.9 x 10^{-6} mol of WO_3 after 2 hours photolysis with 254 nm light in vacuo.

WO_3 was irradiated under a vacuum of 4 x 10^{-5} torr for 24 hrs. Under these conditions, photolysis produced 1.44 x 10^{-6} mol CH_4 without CO evolution. Evacuating the reaction cell and rephotolyzing for 24 hours failed to produce more CH_4. DRIFT spectra of WO_3/gel recorded during 254 nm photolysis show that IR bands in 2850-2970 cm^{-1} region due to C-H stretching vibration in Si-OCH_3 group disappear after 2 hours irradiation (Figure 34). In contrast, exposing the WO_3/sol-gel sample to 50 torr of CO_2 and irradiated with 254 nm light for 24 hours leads to 5.6 x 10^{-7} mol of CO and 2.3 x 10^{-7} mol of CH_4 evolutions. Since Si-OCH_3 is the exclusive carbon source in the absence of CO_2, and also no CO is detected in the absence of CO_2, it is concluded that surface -OCH_3 group is reduced to CH_4, and the CH_3O- groups could be the intermediate in the CO_2 methanation.

3. 2. 4. Photoluminescence Studies of WO_3(ads)

Because of the high sensitivity and nondestructive nature of photoluminescent analysis,[139] the photoluminescence of metal oxides have been used to investigate the nature, structure and properties of active sites on supported catalysts. Photoluminescence of WO_3(ads) occurs when samples are excited with light ≤ 300 nm. Figure 35 shows a typical luminesence spectrum and corresponding excitation spectrum of powdered WO_3/PVG sample containing 4.6 x 10^{-5} mol WO_3 /g PVG at 298 K under 4 x 10^{-3} torr vacuum. Two emission bands with maxima at 405 nm and 460 nm are present in the spectrum of the WO_3/PVG sample. The excitation spectrum

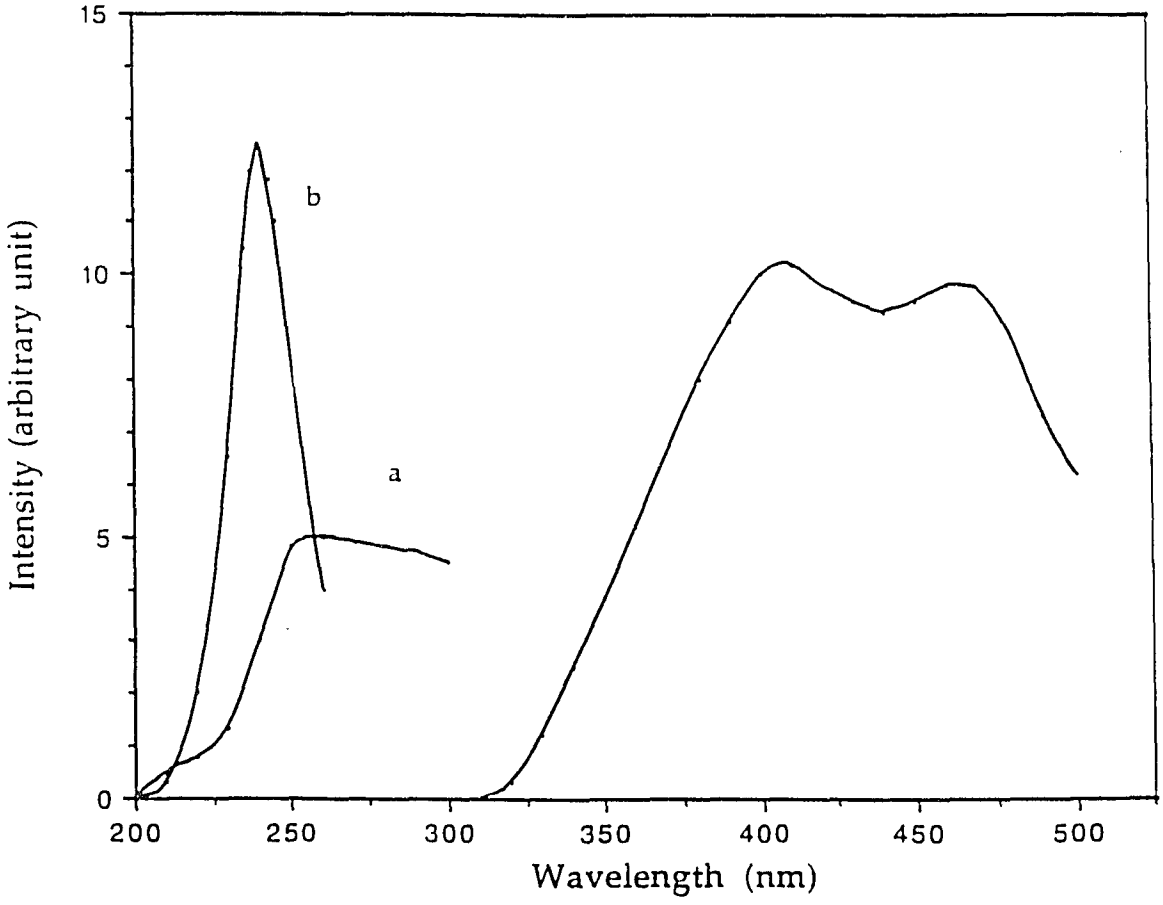

Figure 35. Photoluminescence spectrum of powdered WO_3/PVG (4.6×10^{-5} mol/g) and its excitation spectra at 298 K. (Excitation wavelength, 270 nm; slit width of excitation, 16 nm; slit width of emission, 24 nm; excitation spectra were monitored at (a) 410 nm, and (b) 470 nm respectively

corresponding to the 405 nm emission is broad with a maximum at ca. 250 nm, whereas that corresponding to 460 nm emission is a sharp, narrow band with a maximum at 235 nm. The large differences in the excitation spectra suggest that the different emissions arise from different species. The emission at 460 nm resembles to the phosphorescence band observed by Anpo and coworkers on MoO_3/PVG (450 nm),[140,143] V_2O_5/PVG(480 nm)[142] and CrO_3/PVG (480 nm) catalysts.[143-146] The excitation transition, is attributed to charge-transfer process associated with the metal-oxygen double bond.[140-146]

$$M^{n+} = O^{2-} \underset{h\nu'}{\overset{h\nu}{\rightleftharpoons}} (M^{(n-1)+} - O^{-})^*$$

At 77 K, both emission bands shift slightly to higher wavelength, the 405 nm band shifts to 410 nm, while 460 nm band shifts to 470 nm. The emission intensities increase greatly at 77 K as shown in Figure 36. Such features have been found on other highly dispersed metal oxides such as MoO_3/SiO_2 (440 nm to 470 nm),[147-149] MoO_3/PVG (450 nm to 470 nm),[150] and V_2O_5/PVG (480 nm to 500 nm) catalysts.[142] The increase of emission intensity is attributed to the temperature dependence of the nonradiative decay. The radiationless deactivation from the triplet state is less efficient at 77 K than that at 298 K, leading to an increase in phosphorescence intensity.

The emission spectra of powdered WO_3/PVG samples at 298 K excited with 230 nm and 270 nm light are shown in Figure 37, and the effects of excitation energy on phosphorescence yields are summarized in Table XV.

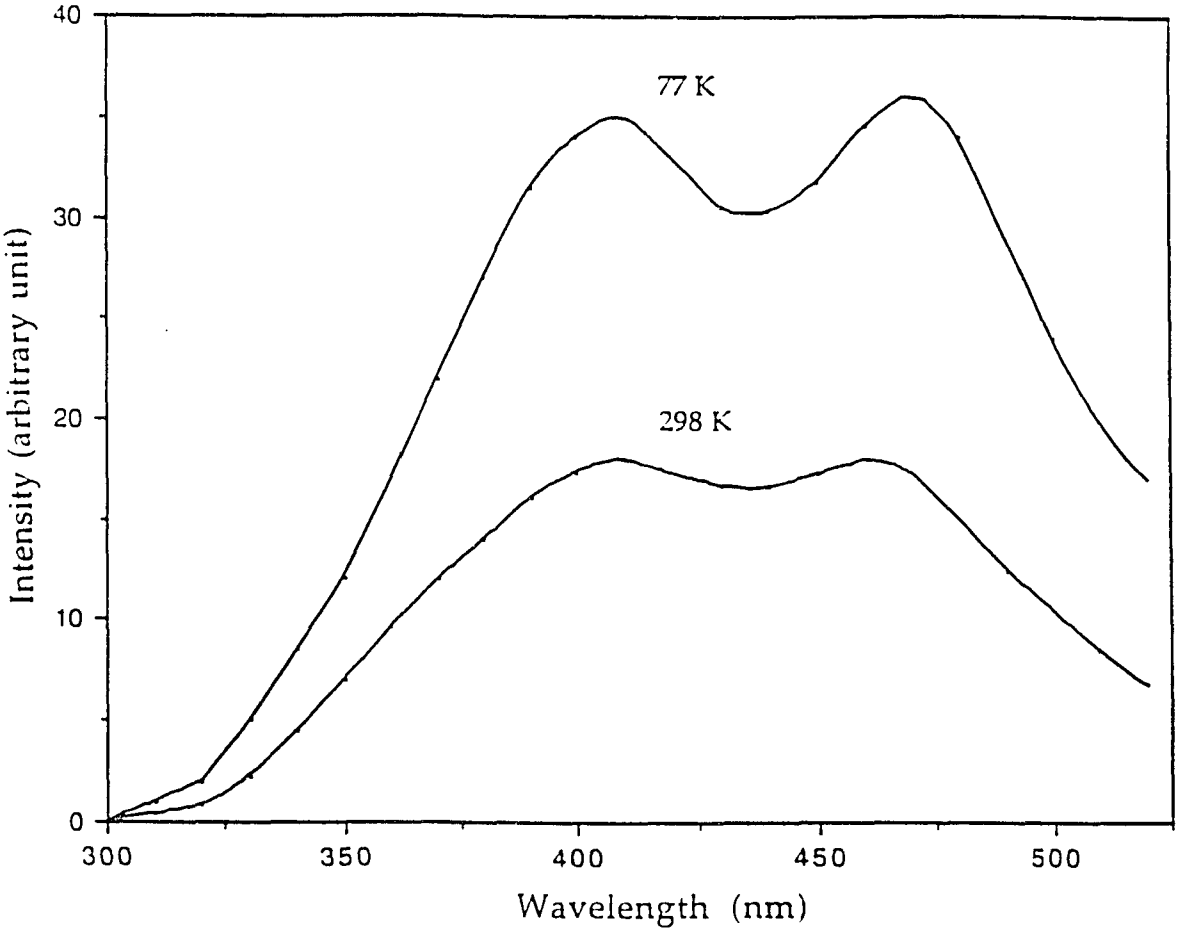

Figure 36. Effect of temperature on intensity and position of phosphorescence spectra of powdered WO_3/PVG sample (5.3×10^{-5} mol/g)

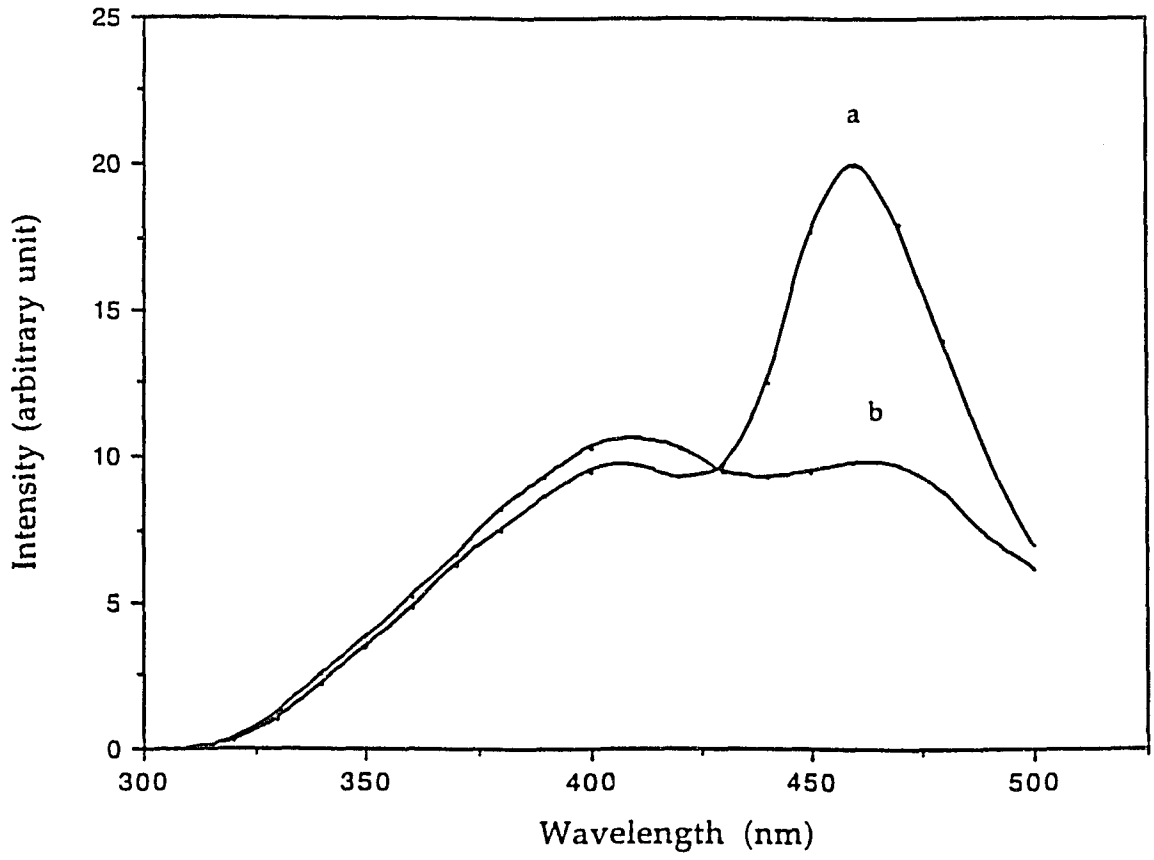

Figure 37. Effect of excitation energy on the intensity of phosphorescence spectrum of powdered WO_3/PVG sample (4.6×10^{-5} mol/g)
Excitation wavelength: (a) 230 nm, (b) 270 nm

Table XV. Effect of Excitation Energy on the Intensity of Emission Bands at 298 K for a Powdered WO_3/PVG Sample, 4.6×10^{-5} mol/g.

λ_{ex} (nm)	λ_{max} Intensity [a]	λ_{max} Intensity [a]
230	403 ± 3 (9.7)	460 ± 3 (20.0)
240	403 ± 3 (9.7)	460 ± 3 (18.0)
250	403 ± 3 (9.8)	460 ± 3 (13.0)
260	405 ± 5 (10.5)	460 ± 3 (10.5)
270	405 ± 5 (10.7)	460 ± 3 (9.8)
280	405 ± 5 (10.6)	460 ± 3 (9.7)
290	405 ± 5 (10.8)	460 ± 3 (9.7)
300	405 ± 5 (10.6)	460 ± 3 (9.7)

[a.] Values in parentheses are the relative intensity of the emissions.

The data demonstrate that the intensity of the band at 460 nm is dependent on the excitation wavelength. When the excitation wavelength increases from 230 nm to 300 nm, the intensity of the band at 460 nm decreases by more than half. In contrast, the intensity of the band at 405 nm is independent of excitation wavelength. The results are consistent with their excitation spectra shown in Figure 35, where a intense excitation band appears at 230 nm with emission wavelength at 460 nm, and a very broad band occurring between 240-290 nm appears with emission wavelength at 410 nm. On the other hand, the emission maxima of both bands are independent of the excitation energy. This result differs from that obtained by Anpo and coworkers with impregnated MoO_3/SiO_2 catalysts,[150] where the maximum of phosphorescence changes from 466.4 to 481.0 nm when the excitation wavelength decreases from 305.0 to 270.5 nm. In that case, the shift of emission maximum with excitation wavelength has been attributed to the presence of more than one type of emitting site on the surface of impregnated MoO_3/SiO_2 catalysts. In contrast, the intensity of 405 nm emission from WO_3/PVG is independent of excitation wavelength, whereas the intensity of 460 nm emission depends on excitation wavelength. This difference in excitation intensity dependence, and as previously noted, the difference in the shapes of the excitation spectra suggest that each emission corresponds to different emitting species.

The nature of these two emission sites were investigated by O_2, CO_2 and NH_3 quenching. O_2 is well-known as an efficient quenchers of excited triplet states.[142,150] Figure 38 shows the results of quenching by oxygen at 298

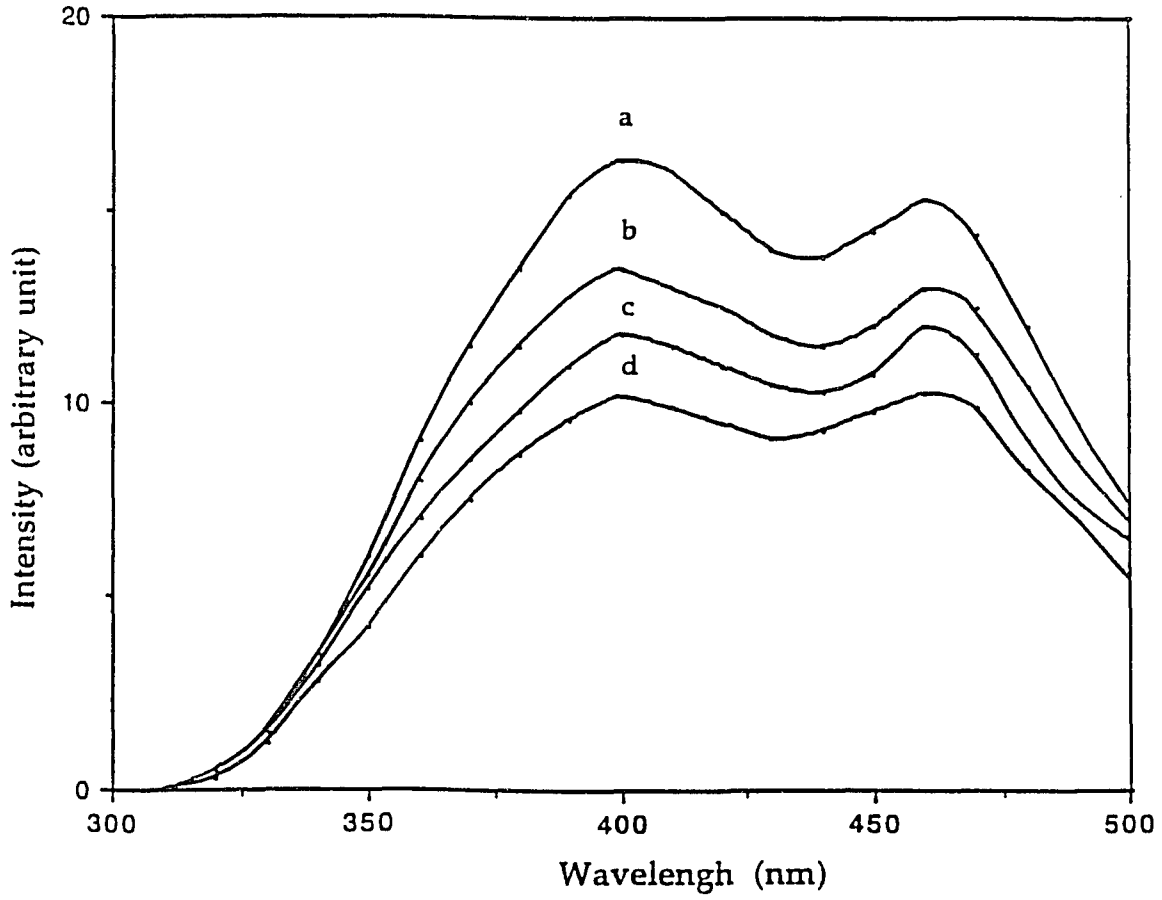

Figure 38. Change in the emission spectrum of powdered WO_3/PVG sample (4.6×10^{-5} mol/g) as a function of O_2 pressure at 298 K. Pressure of oxygen: (a) 0.0 torr (10^{-4} torr vacuum), (b) 99 torr, (c) 215 torr, (d) 385 torr.

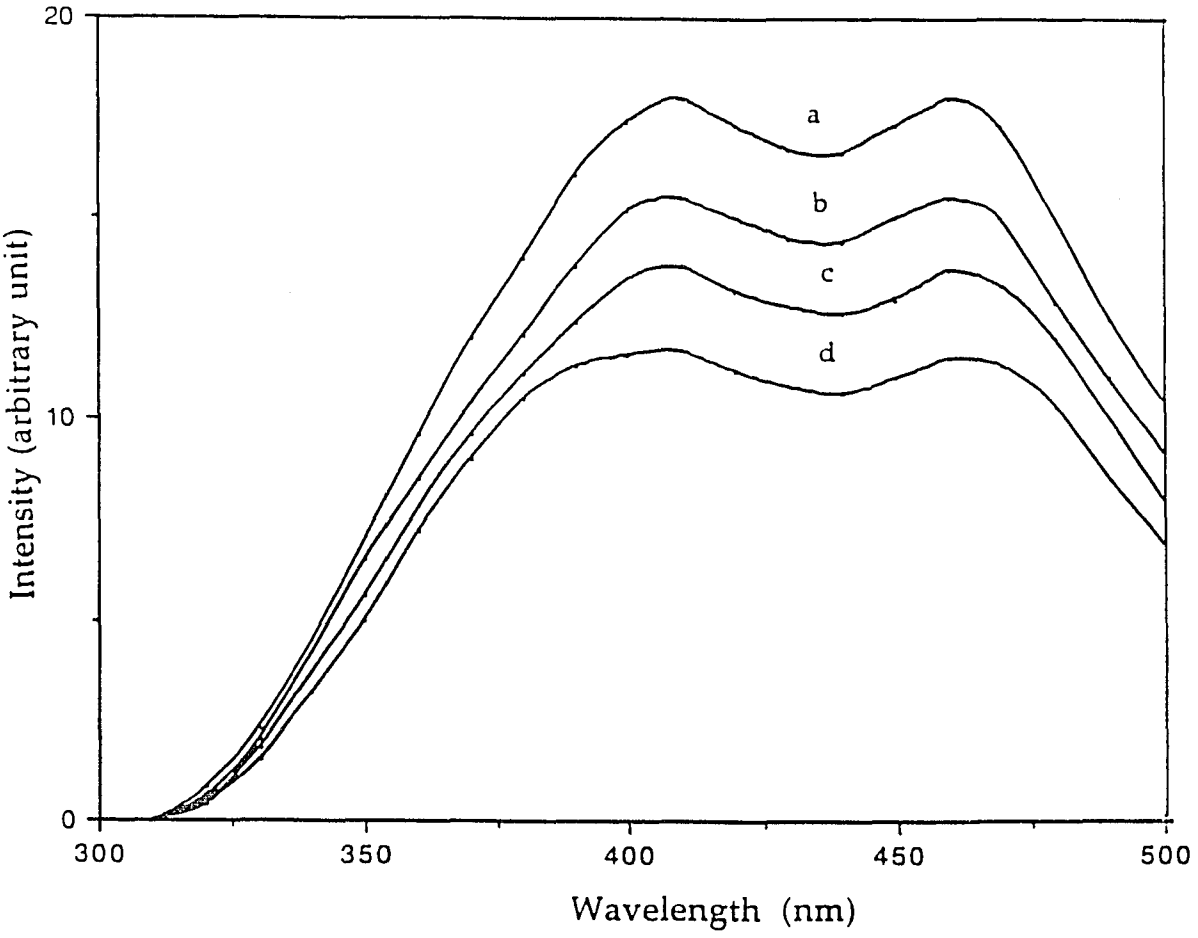

Figure 39. Change in the emission spectrum of powdered WO_3/PVG sample (4.6×10^{-5} mol/g) as a function of CO_2 pressure at 298 K. Pressure of CO_2: (a) 0.0 torr (10^{-4} torr vacuum), (b) 135 torr, (c) 181 torr, (d) 231 torr.

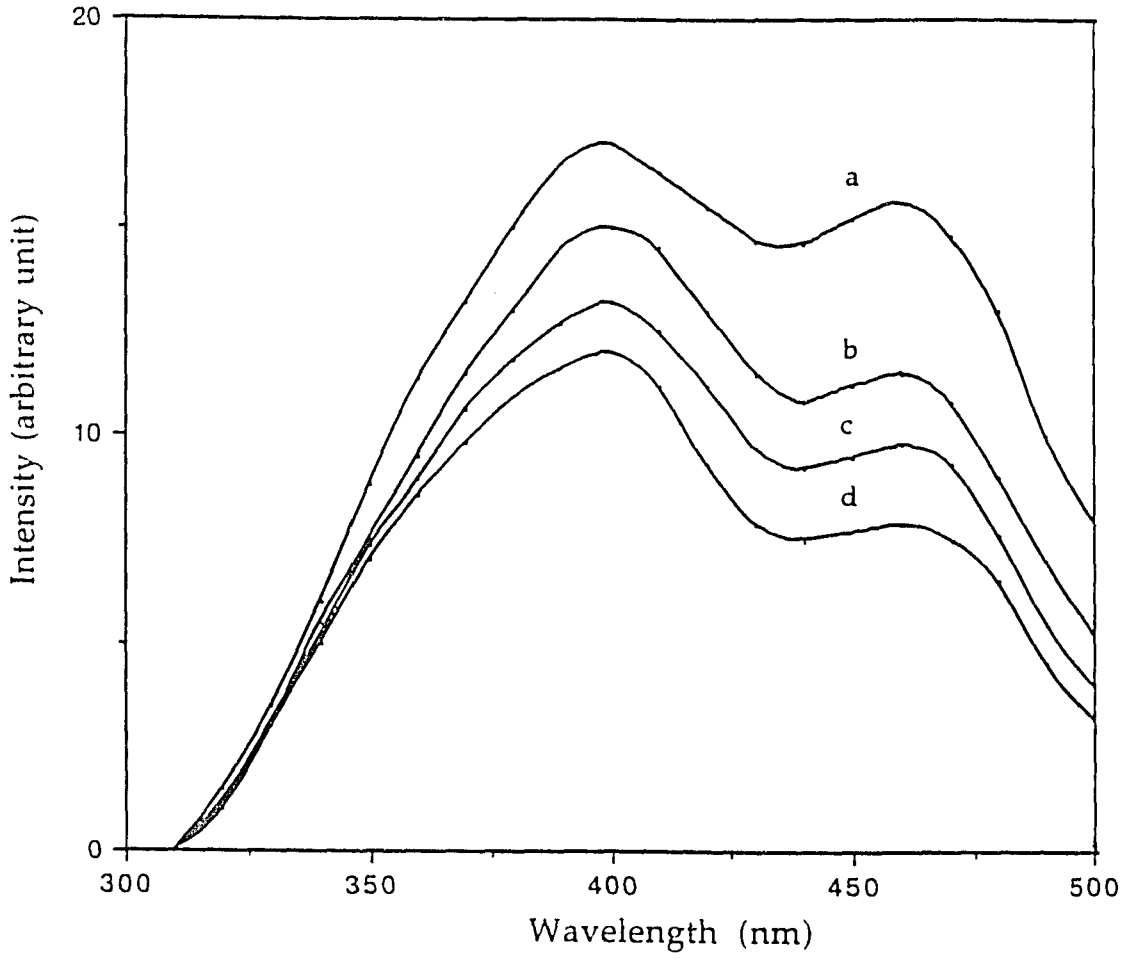

Figure 40. Change in the emission spectrum of powdered WO_3/PVG sample (4.6×10^{-5} mol/g) as a function of NH_3 pressure at 298 K. Pressure of NH_3: (a) 0.0 torr (10^{-4} torr vacuum), (b) 130 torr, (c) 255 torr, (d) 354 torr.

K on the WO_3/PVG (4.6×10^{-5} mol/g) catalysts. Quenching increases with increasing O_2 pressure, but does not completely quench the emission even in the presence of excess oxygen. Quenching with CO_2 results in similar changes in the emission spectra (Figure 39), while quenching with NH_3 shows that it more effectively quenches the phosphorescence at 460 nm than the emission at 410 nm (Figure 40). This quenching selectivity is evident in the Stern-Volmer plots in Figure 41, and the Stern-Volmer constants obtained for the quenching of 410 and 460 nm bands are listed in Table XVI.

With O_2 or CO_2 as the quencher, the phosphorescence is almost completely recovered after evacuation of the sample at room temperature for 30-60 min. The reversible nature of the quenching suggests that the O_2 and CO_2 molecules interact weakly with the active surface sites on the WO_3/PVG catalysts. In contrast, with NH_3 molecules, only ca. 35% of the 405 nm emission and ca.20% of the 460 nm emission are recovered after pumping out the NH_3 at 298 K for 60 minutes. Even after prolonged evacuation of the sample at 373 K for 100 minutes, only 80-85% of the original intensities of 405 nm emission and 65-74% of the 460 nm emission were recovered. This lack of complete recovery suggests that NH_3 interacts strongly with the active surface sites on the WO_3/PVG samples.

Figure 42 shows the effects of tungsten content upon the phosphorescence yields of WO_3/PVG catalysts at 298 K. When the tungsten content increases from 4.3×10^{-6} to 4.6×10^{-5} mol/g, which corresponds to ca. 0.1% to 1% W by weight, and a surface coverage from 0.2% to 1.9%, the emission

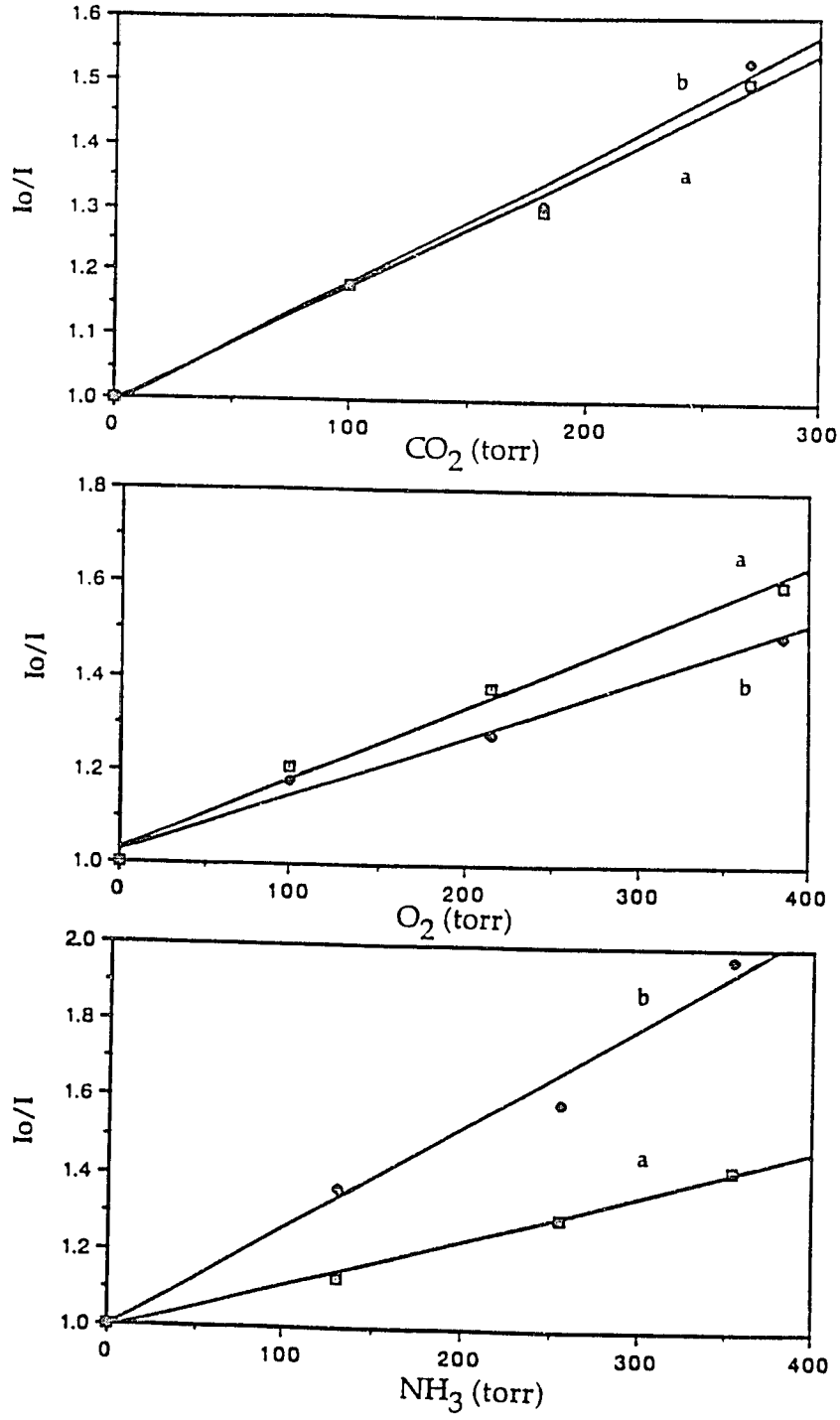

Figure 41. Stern-Volmer plots for powdered WO_3/PVG sample (4.6×10^{-5} mol/g) at 298 K. (a) 410 nm, (b) 460 nm.

Table XVI. Stern-Volmer Constant for Powdered WO_3/PVG Sample (4.6×10^{-5} mol/g) at 298 K

	K_{sv} ($torr^{-1}$)		
λ_{em} (nm)	O_2	CO_2	NH_3
410	1.53 ± 0.1 E-3	1.82 ± 0.2 E-3	1.19 ± 0.1 E-3
460	1.23 ± 0.2 E-3	1.93 ± 0.2 E-3	2.63 ± 0.2 E-3

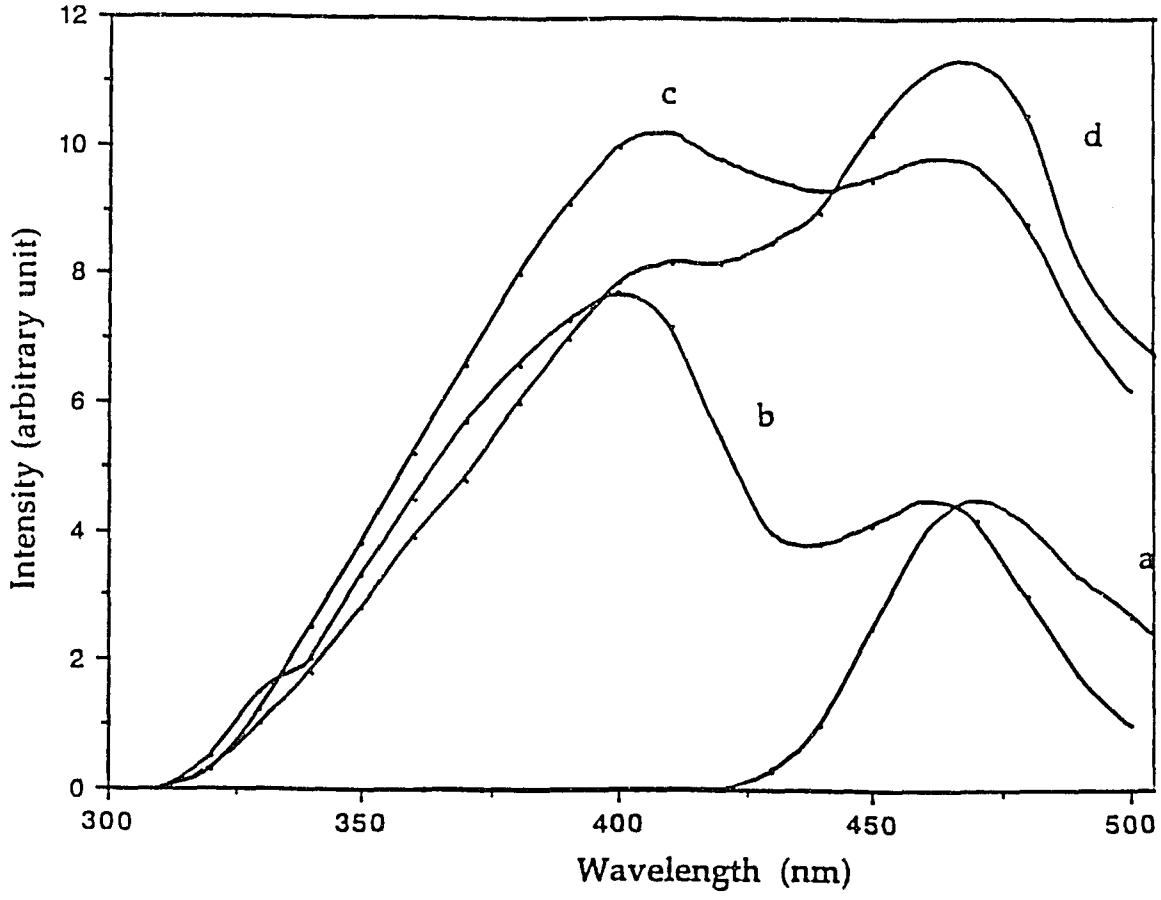

Figure 42a. Emission spectra of powder WO_3/PVG samples with different W contents at 298 K. (a) pure WO_3 powder, (b) 4.3×10^{-6} mol/g , (c) 4.6×10^{-5} mol/g , (d) 4.5×10^{-4} mol/g . (Excitation wavelength, 270 nm; slit width of excitation, 16 nm; slit width of emission, 24 nm)

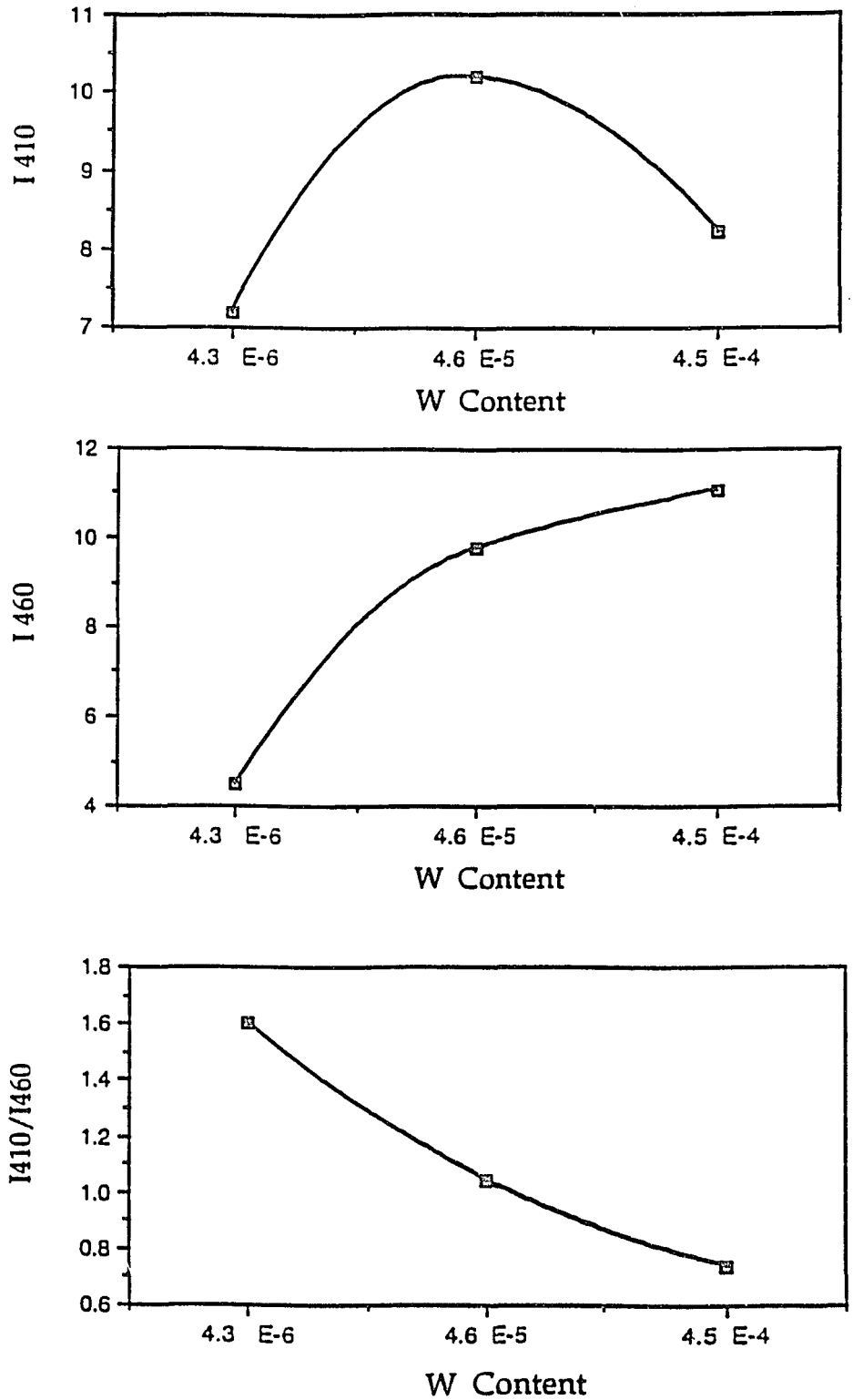

Figure 42b. Emission intensity with W content

intensity increases with the tungsten content. Although both band positions scarcely change, the intensity of the band at 460 nm increases faster than that of the 410 nm band. However, when tungsten content increases to 4.5×10^{-4} mol /g, which corresponds to ca. 10% W by weight, and a surface coverage of 18.7%, both band positions shift to the longer wavelength, and the intensity of band at 410 nm decreases, whereas the intensity of the band at 460 nm greatly increases. Since pure WO_3 exhibits an emission at 460 nm, the band at 460 nm, which dominates the spectrum at higher loading, is assigned to a octahedral species. The 405-nm emission is assigned to tetrahedral species since this emission is dominant at low loading and $CaWO_4$, which contains the WO_4^{2-} tetrahedral structure, exhibits an emission maximum at 435 nm and excitation maximum at 275 nm(Figure 43).

3.3 Photocatalyzed Isomerization of 1-Pentene

3. 3. 1. Photolysis of $Ru_3(CO)_{12}$ (ads)

Consistent with previous experiments in this laboratory, the electronic and DRIFT spectra of adsorbed $Ru_3(CO)_{12}$ closely resemble those of the complexe in n-hexane (Table IV). The results establish that the $Ru_3(CO)_{12}$ trimer physisorbs onto PVG without disruption or significant distortion of the complex. The impreganation depth of the $Ru_3(CO)_{12}$ was found to be 0.3 mm with loading $\leq 10^{-5}$ mol/g.[160] Taking 0.5 nm as the radius of $Ru_3(CO)_{12}$,[160] the fractional surface coverages of the samples examined in the isomerization are calculated by equation 3.1, and the results are listed in

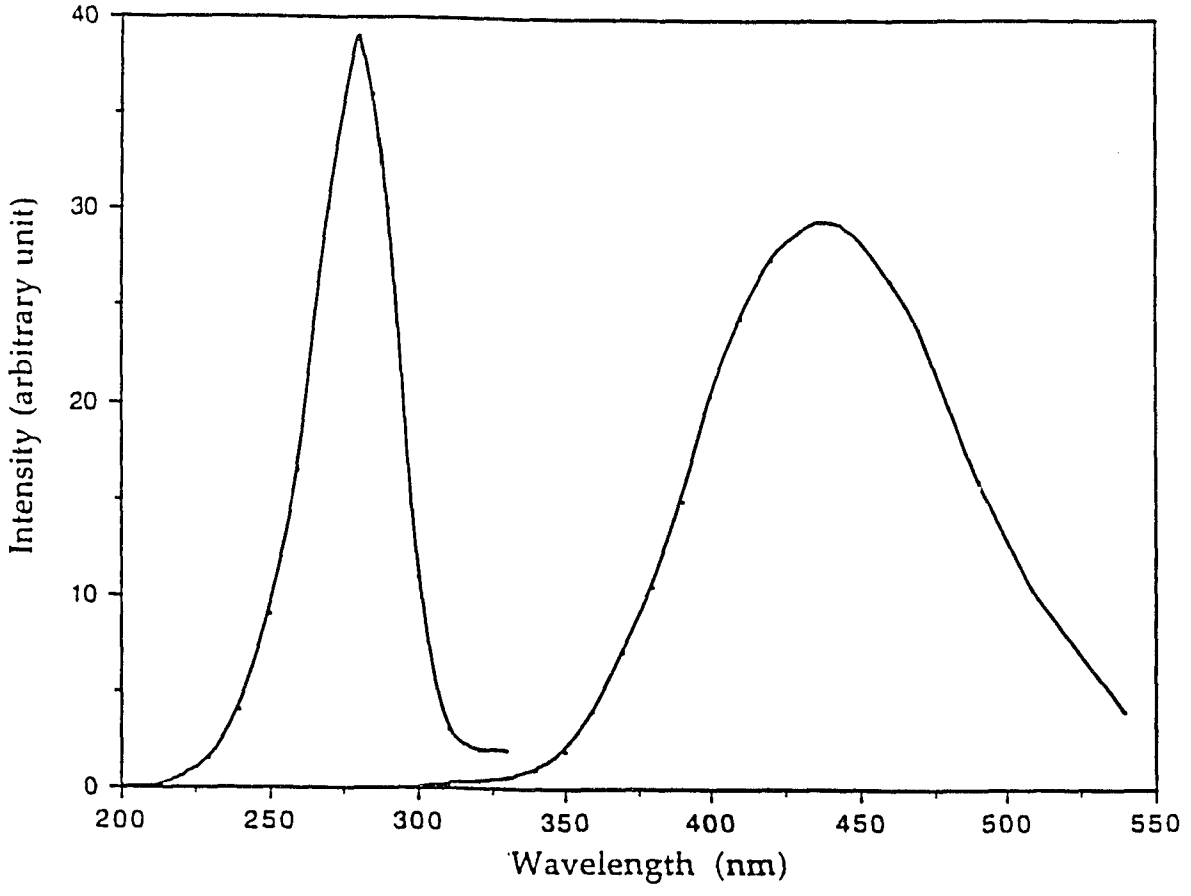

Figure 43. Photoluminescence spectrum of pure CaWO4 powder. (Excitation wavelength, 270 nm; slit width of excitation, 12 nm; slit width of emission, 12 nm. Excitation spectra were monitored at 420 nm)

Table XVII. Fractional Surface Coverage of $Ru_3(CO)_{12}$ on PVG

Moles Adsorbed (10^{-6} mol/g)	Sample Type	Surface Coverage (Θ)
0.32	plate	0.28
0.45	plate	0.39
0.70	plate	0.60
0.89	plate	0.77
1.2	plate	1.0
2.3	plate	2.0
2.7	plate	2.3
3.5	powder	0.9
4.5	powder	1.2
5.0	powder	1.3
45.0	powder	11.6

Table XVII.

UV photolysis of the physisorbed trimer, designated $Ru_3(CO)_{12}$ (ads), causes an immediate reaction. As illustrated in Figure 44, a decline of the trimer characteristic absorbance at 395 nm is accompanied by a concurrent increase in absorbance at 330 nm. DRIFT spectra show decline in the 2065, and 2035 cm^{-1} bands characteristic of the trimer, and the appearance of a weak band at 2109 cm^{-1}, two relatively intense bands at 2078 and 2068 cm^{-1}, and a broad band at 2035 cm^{-1} with a shoulder at 1999 cm^{-1}(Figure 45). These spectral changes are similar to those reported by Basset and coworkers for the oxidative addition product from thermal activation of physisorbed $Ru_3(CO)_{12}$ on silica gel.[95] This spectral similarity, as well as the stoichiometry of the photoreaction, i.e., 2 moles of CO evolved per moles of $Ru_3(CO)_{12}$ reacted, indicates a photoinduced oxidative addition of $Ru_3(CO)_{12}$ to the glass Si-OH groups to form the $(\mu\text{-H})Ru_3(CO)_{10}(\mu\text{-OSi})$, shown in Figure 1.

3. 3. 2. Photocatalyzed isomerization of 1-Pentene

Although stable for weeks in vacuo, the grafted complex is highly reactive. After removal of the photodetached CO, exposing $(\mu\text{-H})Ru_3(CO)_{10}(\mu\text{-OSi})$ to 400 torr of 1-pentene, for example, results in an immediate reaction. As shown in Figure 46, a decline in its characteristic 330 nm absorption is accompanied by a broad, nondescript increase in absorbance in the 300-450 nm region with a weak shoulder at ca. 310 nm. The corresponding changes in the

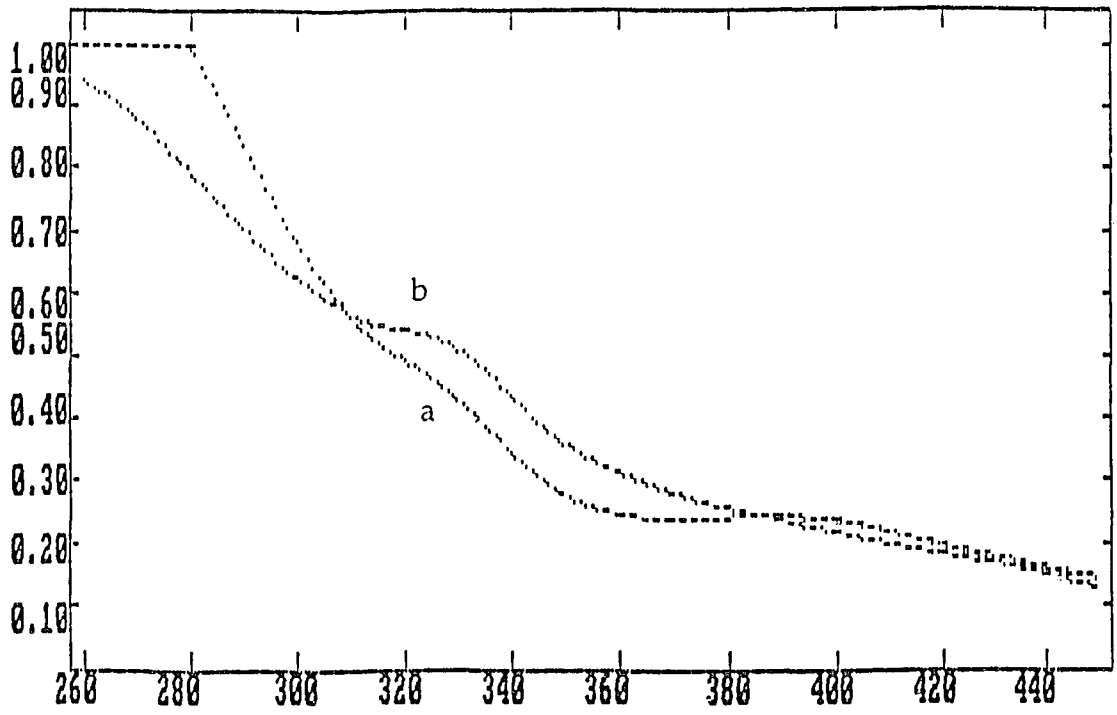

Figure 44. Electronic spectra of $Ru_3(CO)_{12}$ on PVG (7.0×10^{-7} mol/g), (a) before photolysis, (b) 254 nm photolysis for 60 minutes.

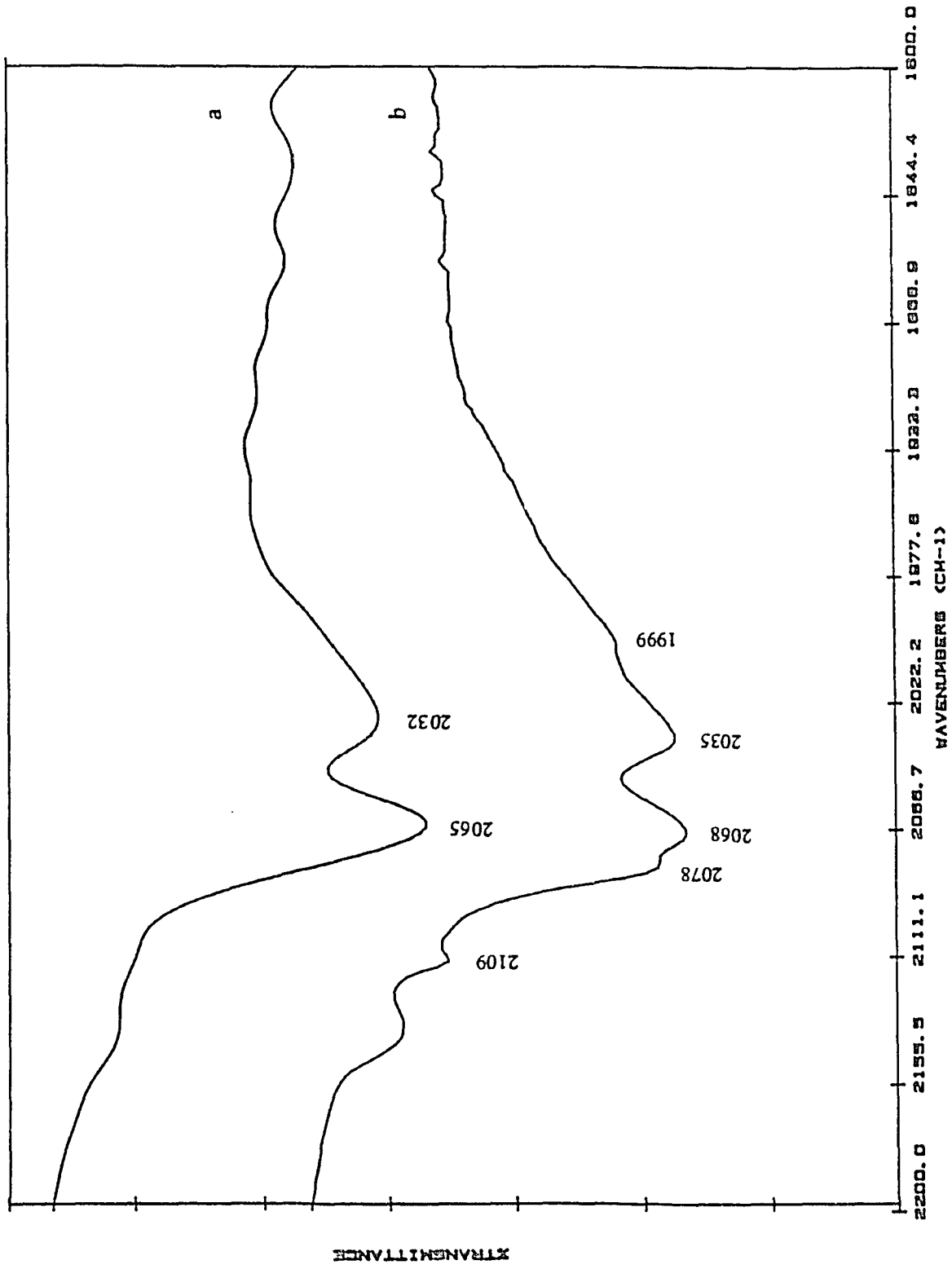

Figure 45. DRIFT spectra of $Ru_3(CO)_{12}$ on PVG (4.5×10^{-5} mol /g), (a) before photolysis, (b) 254 nm photolysis for 60 minutes.

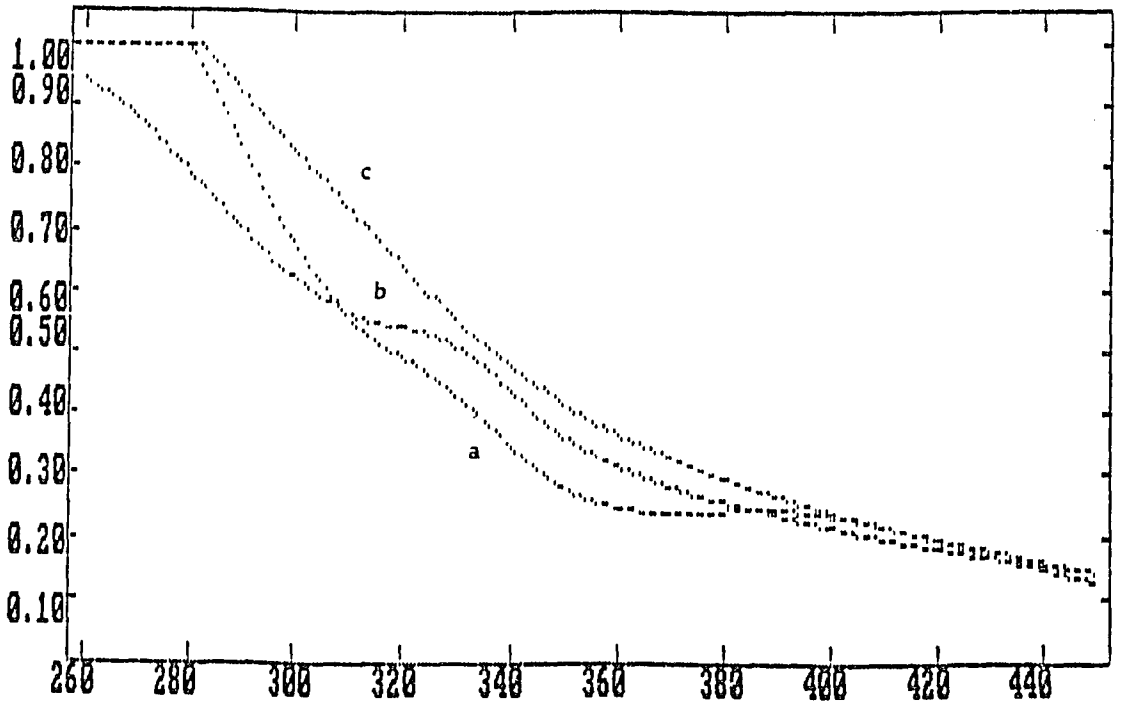

Figure 46. Electronic spectra of (a) physisorbed $Ru_3(CO)_{12}$ on PVG (7.0×10^{-7} mol/g), (b) (μ-H)$Ru_3(CO)_{10}$(μ-OSi), (c) (μ-H)$Ru_3(CO)_{10}$(μ-OSi) under 400 torr of 1-pentene.

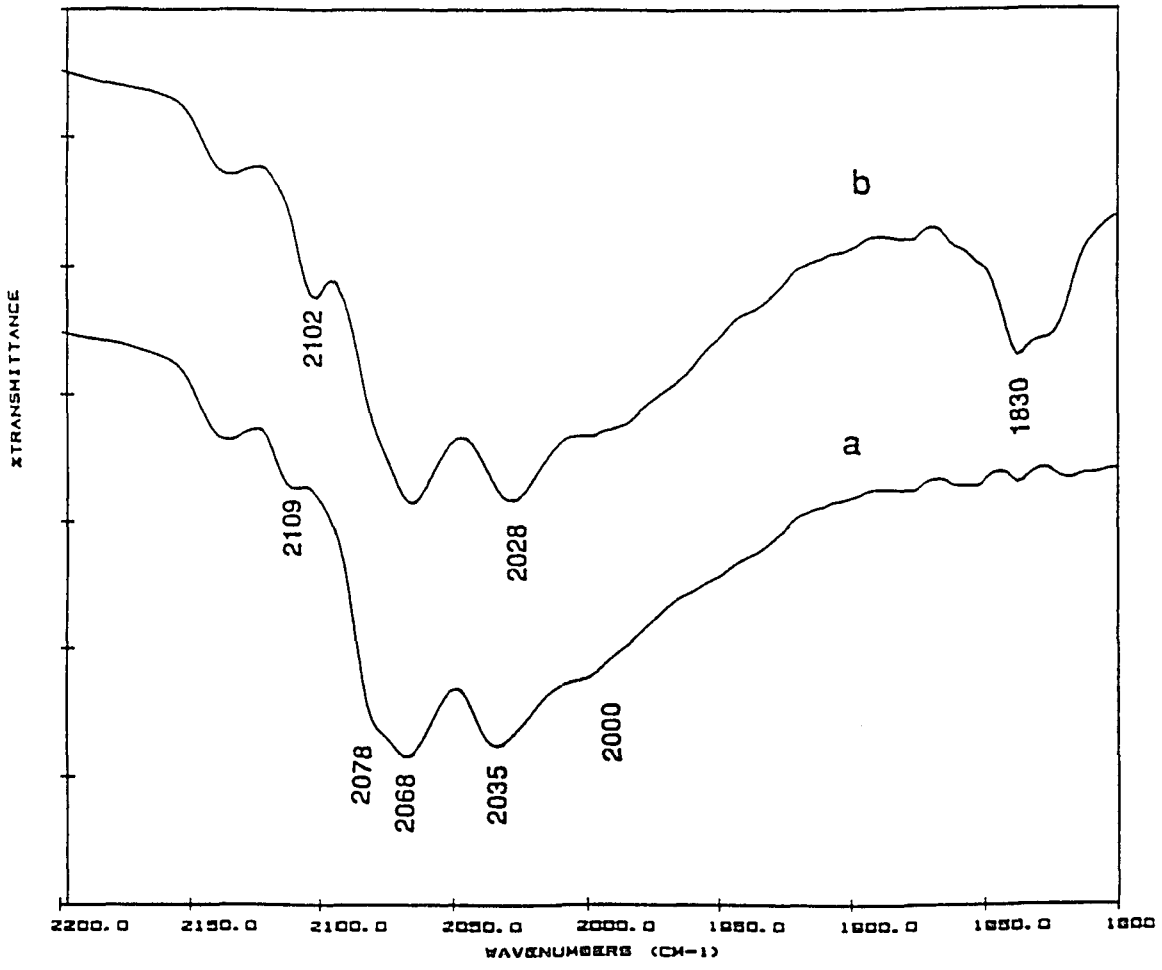

Figure 47. DRIFT spectra of (a) (μ-H)$Ru_3(CO)_{10}$(μ-OSi), and (b) (μ-H)$Ru_3(CO)_{10}$(μ-OSi) under 400 torr of 1-pentene.

DRIFT spectrum are illustrated in Figure 47.The bands at 2109 and 2078 cm^{-1} decline, while the 2068 cm^{-1} band declines slightly and shifts to 2066 cm^{-1}, and the 2035 cm^{-1} band shifts to 2028 cm^{-1}. Concurrent with these changes, two new bands appear at 2102 and 1830 cm^{-1}. GC analysis of the effluent from the reactor shows that exposing $(\mu\text{-H})Ru_3(CO)_{10}(\mu\text{-OSi})$ to 1-pentene does not result in CO evolution. In addition, the spectral changes are reversible. Evacuation of the cell to a pressure of 4×10^{-4} torr regenerates the IR spectrum of the oxidative addition product within four hours, and the increase in absorbance at 330 nm indicates ≥ 90% recovery of $(\mu\text{-H})Ru_3(CO)_{10}(\mu\text{-OSi})$. The ability to quantitatively cycle the system, and recover $Ru_3(CO)_{12}$(ads) in ≥ 90% yield, when $(\mu\text{-H})Ru_3(CO)_{10}(\mu\text{-OSi})$ is subsequently exposed to CO (1 atm), strongly suggests that the metal trimer remains intact during the reaction sequence. As expected, the addition of 1-pentene appears to disrupt the multicentered bonds binding the trimer to the glass surface, rather than the metal-metal or metal-carbonyl bonds.

Electronic and DRIFT spectra recorded during UV photolysis of $(\mu\text{-H})Ru_3(CO)_{10}(\mu\text{-OSi})$ under 400 torr of 1-pentene show relatively little change. A slight decline in the 2102 cm^{-1} band is accompanied by a corresponding increase in the 2078 cm^{-1} band characteristic of $(\mu\text{-H})Ru_3(CO)_{10}(\mu\text{-OSi})$. Nevertheless, periodic GC analyses of the surrounding vapor phase indicate the conversion of 1-pentene to cis- and trans-2-pentene. The quantum yields

of the isomerization are listed in Table VII. The values are computed from the initial rates of 2-pentene evolution and the excitation intensity incident on the impregnated sample. Initially, the trans-/cis- ratio is 1.5 ± 0.2, and increases to a relatively constant value of 2.5 ± 0.1 as the photolysis proceeds (Figure 48). The ratio is smaller than the thermodynamic ratio, 4.82, and smaller than that obtained with photolysis of $Fe(CO)_5$ on PVG. In that case, the trans/cis ratio increases from 1.6 ± 0.2 after ten minutes of photolysis to 3.7 ± 0.2 after 60 minutes.[155]

Periodic GC analyses give no indication of CO release during photolysis ($<10^{-8}$ mol), and introducing H_2 into the reactor neither increases the rate of isomerization, nor results in hydrogenation of 1-pentene. However, using (μ-D)$Ru_3(CO)_{10}$(μ-OSi), which is generated by photolysis of $Ru_3(CO)_{12}$ adsorbed onto deuterated PVG,[98] yields 10-15% deuterated olefins (Figure 49). Of the total deuterium incorporated, GC/MS indicates that ca. 90% is present in the 2-pentenes, while the remainder is present as 1-D-1-pentene. (Table XVIII).

GC-MS analysis indicates no deuterated pentene generated during 254-nm photolysis of a deuterated PVG under 400 torr 1-pentene for 24 hours. The results suggest that deuterated olefins result from the hydrogen-deuterium transfer between the olefin and grafted complex, rather than from the hydrogen-deuterium transfer between the olefin and deuterated PVG. Also, prolonged UV photolysis of 1-pentene with unimpregnated PVG does not result in olefin isomerization. UV (350-nm or 254-nm) photolysis of 1-pentene with physisorbed $Ru_3(CO)_{12}$ on PVG does not generate 2-pentene

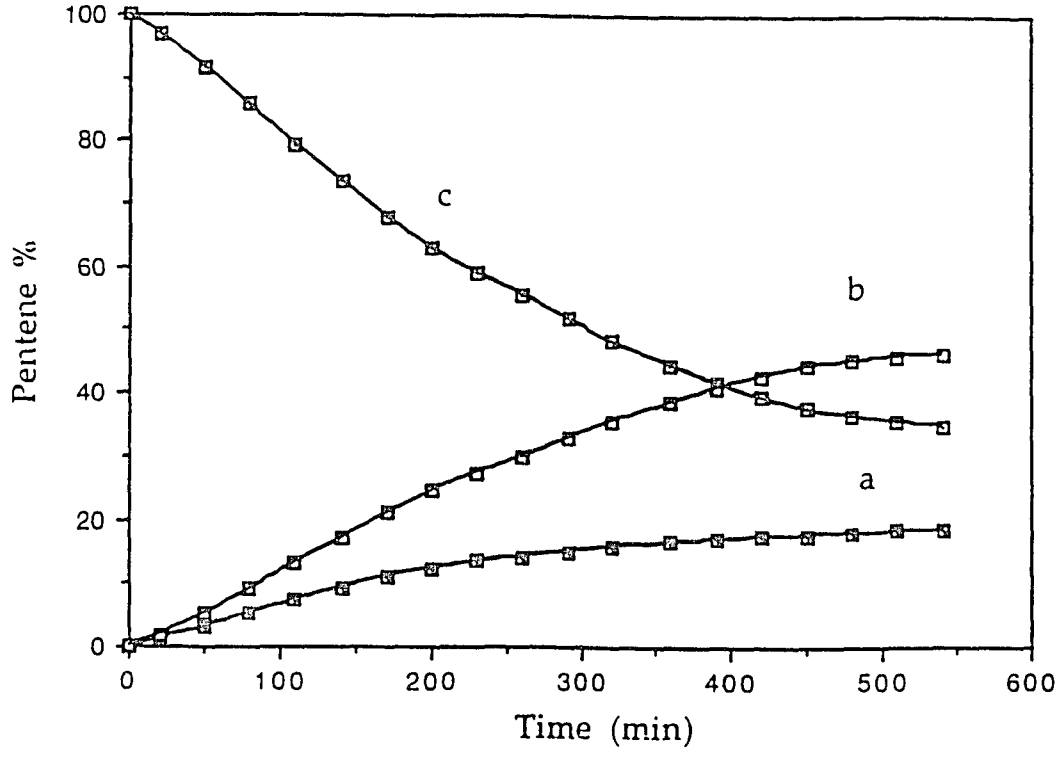

Figure 48. Profile of (a) cis-2-pentene, and (b) trans-2-pentene during 254 nm photolysis of (μ-H)$Ru_3(CO)_{10}$(μ-OSi) [loaded 1.5 x 10^{-6} mol of $Ru_3(CO)_{12}$] under (c) 400 torr of 1- pentene.

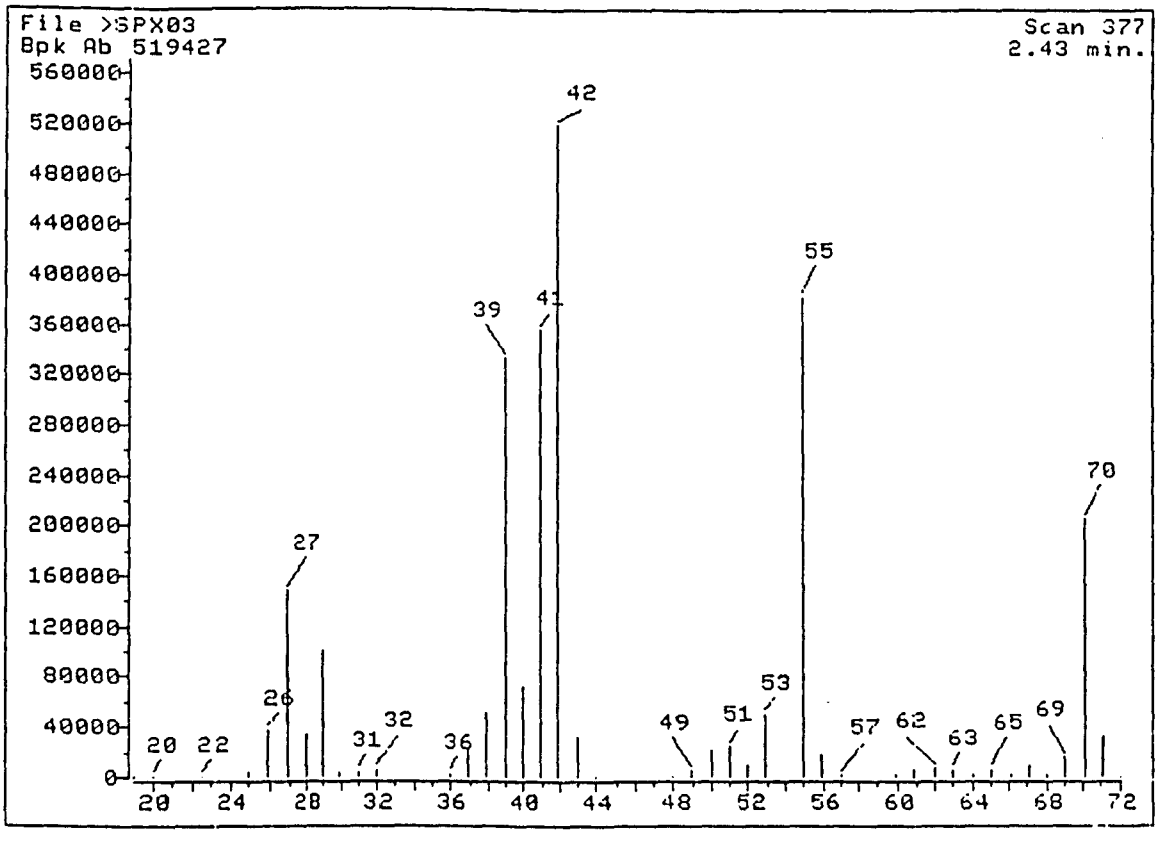

Figure 49. GC-MS spectrum of gaseous products generated from 254-nm photolysis of 400 torr of 1-pentene with (μ-D)$Ru_3(CO)_{10}$(μ-OSi).

Table XVIII. Assignment of Pentene Fragments in GC-MS Spectra

m/e	Assignment	Intensity
71	C_5H_9D	6.1
70	C_5H_{10}	39.5
57	$C_3H_7CD^+$	0.1
56	$C_3H_7CH^+$	3.5
43	$C_2H_5CD^+$	6.0
42	$C_2H_5CH^+$	100
29	CH_3CD^+	19.4
28	CH_3CH^+	6.6
15	CHD^+	2.2
14	CH_2^+	not available

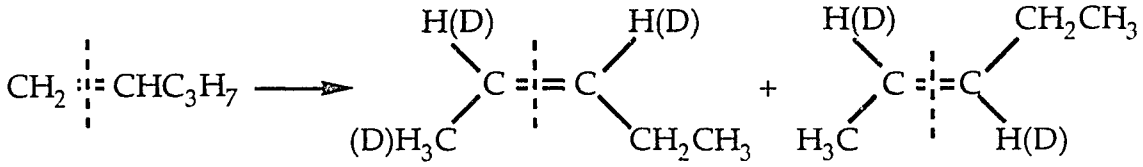

14 (15) 56 (57) 28 (29) 42 (43)

1-D-1-pentene = 15/(15 + 29 +43)

initially. However, continuing the photolysis leads to formation of (μ-H)$Ru_3(CO)_{10}$(μ-OSi) and induces the isomerization, although the reaction is at a lower rate relative to the rate of the reaction directly on the grafted complex (μ-H)$Ru_3(CO)_{10}$(μ-OSi) (Figure 50). These results establish that the grafted complex is essential to the conversion. Since isomerization ceases when photoexcitation ceases, the reaction appears to be a photoassisted catalytic process in which excitation of (μ-H)$Ru_3(CO)_{10}$(μ-OSi) or (μ-H)$Ru_3(CO)_{10}$(μ-OSi)-1-pentene adduct generates an excited state that promotes 1-pentene isomerization.

Exposing (μ-H)$Ru_3(CO)_{10}$(μ-OSi) to 500 torr of CH_2CH_2 results in spectral changes similar to those observed when (μ-H)$Ru_3(CO)_{10}$(μ-OSi) is exposed to 1-pentene. As illustrated in Figure 51, however, three new bands at 1915, 1889, and 1868 cm^{-1} appear in the DRIFT spectrum instead of the band at 1830 cm^{-1}, which is due to physisorbed 1-pentene. The three bands disappear immediately on evacuation, and are therefore assigned to physisorbed CH_2CH_2 on the glass. Exposing (μ-H)$Ru_3(CO)_{10}$(μ-OSi) to 500 torr of H_2 does not cause any spectral change, indicating no interaction between the grafted complex and H_2. UV photolysis of (μ-H)$Ru_3(CO)_{10}$(μ-OSi) under 500 torr of CH_2CH_2, or under a mixture of 300 torr of CH_2CH_2 and 300 torr of H_2 does not result in hydrogenation of the CH_2CH_2. Period GC analyses of the gaseous phase give no indication of CH_3CH_3 release during a 24 hours photolysis.

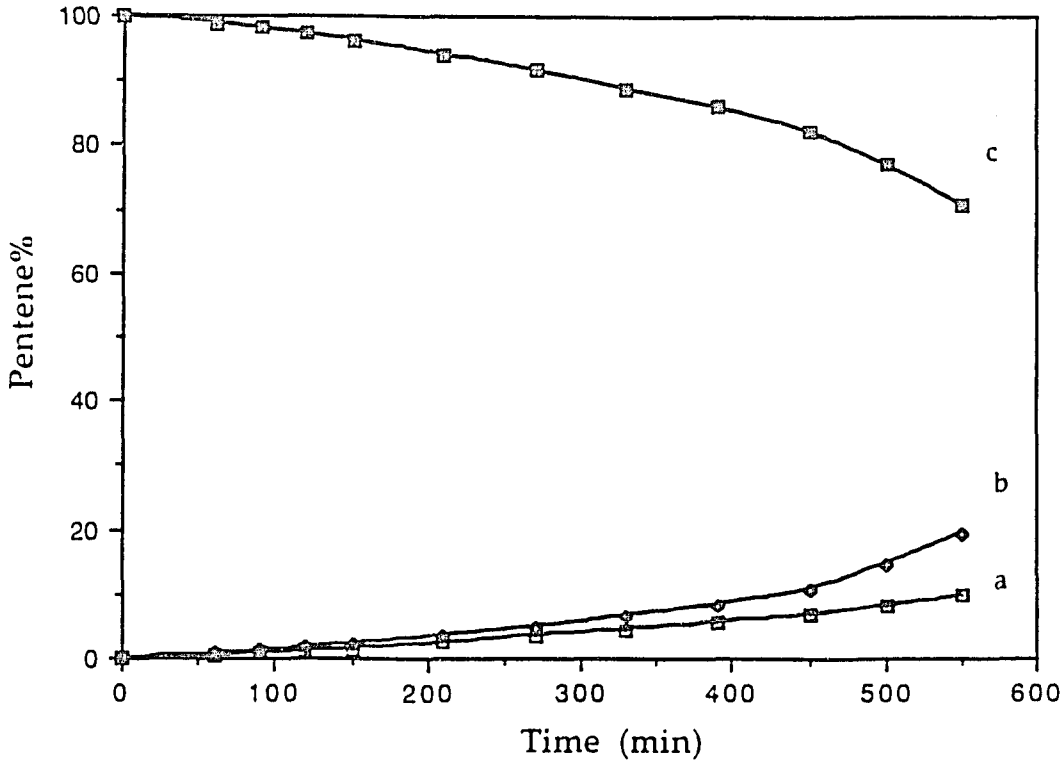

Figure 50. Yields of 2-pentenes during 254 nm photolysis of 1.2×10^{-6} mol of $Ru_3(CO)_{12}$ physisorbed onto PVG under 400 torr 1-pentene. (a) cis-2-pentene, (b) trans-2-pentene, (c) 1-pentene.

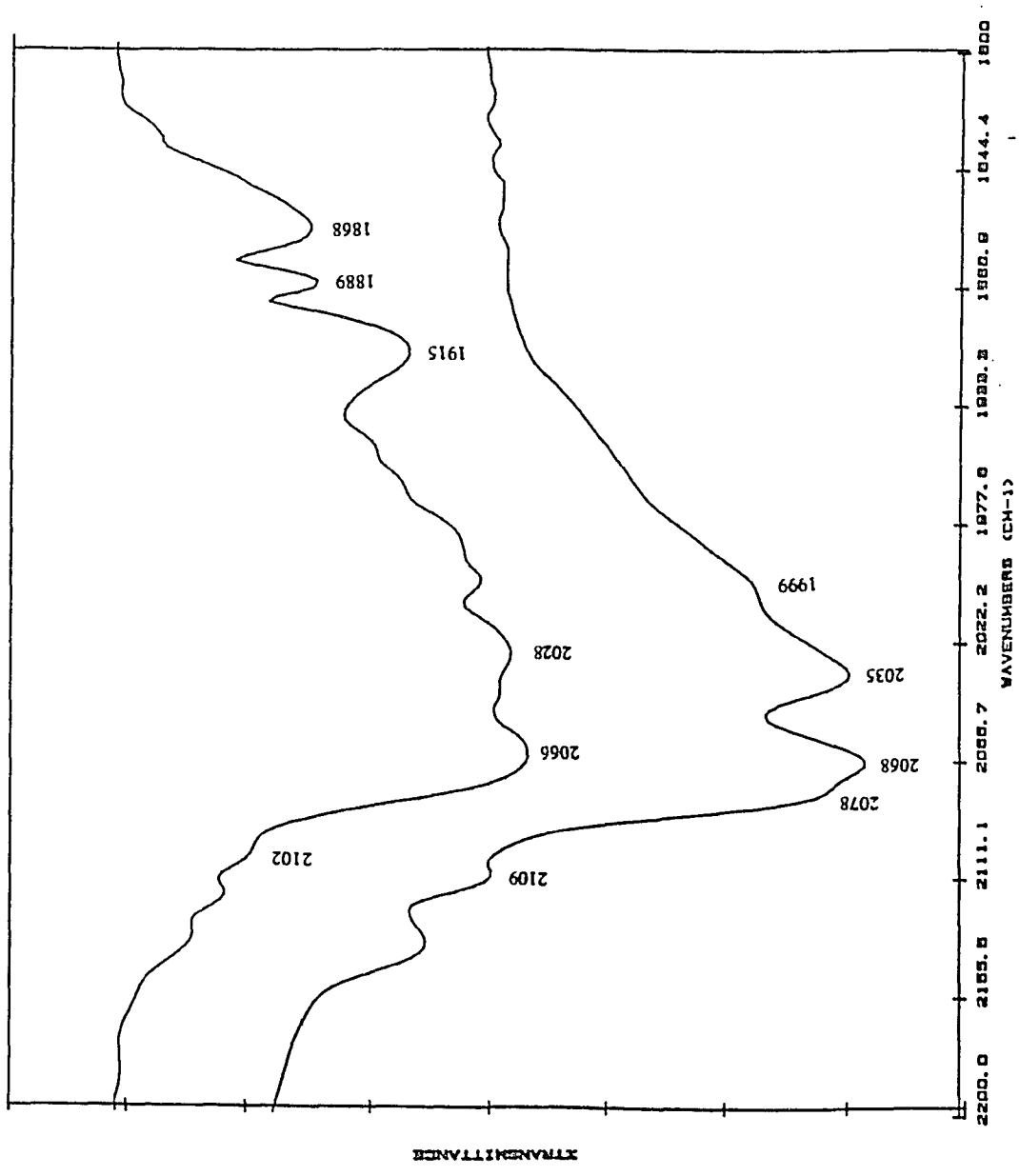

Figure 51. DRIFT spectra of (a) (μ-H)$Ru_3(CO)_{10}$(μ-OSi), and (b) (μ-H)$Ru_3(CO)_{10}$(μ-OSi) under 500 torr of CH_2CH_2.

Chapter 4. DISCUSSION

4. 1. Photoinduced Methanation of CO_2

The electronic spectrum of $W(CO)_6$ (ads) recorded during UV photolysis in vacuo, as illustrated in Figure 26, indicates that the primary photoprocess generates a coordinately unsaturated intermediate, $W(CO)_5$(ads). GC analysis of the gaseous product in the reactor indicates only CO evolution in the initial 2-3 hours of photolysis. The results establish that primary photochemical reaction is decarbonylation. However, continued UV photolysis leads to CH_4 evolution, and the previous stoichiometric measurements indicate that CH_4 evolution initiates when the complex achieves an average molecularity of $W(CO)_4$.[87] Nevertheless, continued CH_4 evolution after complete oxidation of the complex establishes that either an individual or agglomerated metal oxide on the glass surface photocatalyzes the hydrogenation of C_1 impurity in the PVG.

Depleting the carbon source in the $W(CO)_6$(ads) samples, and then irradiating the sample under $^{13}CO_2$ with UV light leads to $^{13}CH_4$ and ^{13}CO evolution immediately. The results indicate that the photogenerated tungsten oxide/PVG system is active in the methanation of CO_2. The electronic spectra of the final photoproduct of the hexacarbonyl agree with that of WO_3(ads) (Figure 30), and the studies of prolonged photolysis of $W(CO)_6$ trapped in O_2-doped Ar matrices establish WO_3 as the final photoproduct.[84] UV photolysis

of WO_3(ads) with $^{13}CO_2$ yields same products as that from continued photolysis of $W(CO)_6$(ads) under equivalent conditions. On the other hand, neither CH_4 nor $^{13}CH_4$ evolution is observed during UV photolysis of unimpregnated PVG under $^{13}CO_2$. These results establish that the supported WO_3 plays the role of catalyst in the methanation of CO_2.

The surface tungsten oxide species in the Al_2O_3 and SiO_2 supported catalysts has been examined with many different techniques in recent years.[161-169] When the loading is below monolayer coverage in WO_3/Al_2O_3 catalysts, Raman spectra indicate that the tungsten oxide is present as a highly dispersed oxide bound to the support surface. Salvati and coworkers proposed the WO_x species exist as tetrahedral WO_4^{2-}. [166] This assumption has been confirmed by Horsley and coworkers with X-ray absorption near edge spectroscopy (XANES).[163] The XANES spectrum indicates a distorted tetrahedral structure for the surface tungsten oxide at coverage less than 1/3 monolayer on alumina, in the absence of coordinated water. When the sample exposed to air, water molecules coordinate to the surface tungsten oxide species forming an octahedral species. At loadings approaching monolayer coverage, a significant fraction of the surface tungsten oxide sites appear to have a distorted octahedral environment.

Several groups have proposed that WO_3 on SiO_2 surface is present as a mixture of crystalline bulk oxide WO_3 and a tetrahedral WO_4^{2-} species at

monolayer coverage.[163,167 -169] The ratio of these species is a function of WO_3 content. The tetrahedral surface species is attributed to a strong chemical interaction between the active OH groups on the support surface and the metal ions as illustrated in the scheme I.

$$WO_3 + H_2O \rightleftharpoons H_2WO_4$$

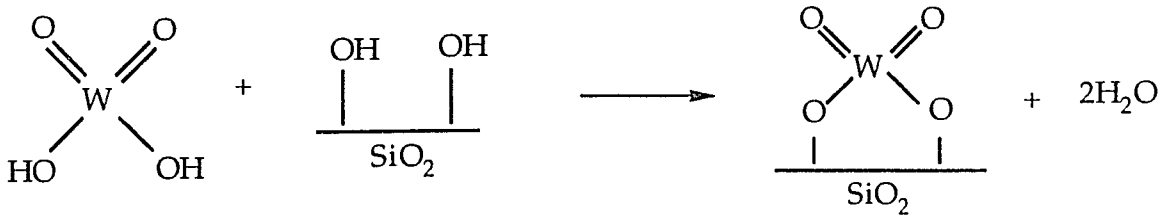

Scheme I

This interaction results in decrease of the concentration of free Si-OH group on the surface. The experimental evidence for this is a reduction in the intensity of SiOH line in ^{1}HMASNMR spectra upon impregnation with MoO_3 or WO_3.[169]

The principal constituent of PVG, 96% by weight, is SiO_2. Therefore, it is expected that the dispersion of WO_3 on PVG is expected to be similar to that found with WO_3/SiO_2 catalysts. FTIR spectra of WO_3/PVG samples show that the intensity of the 3744 cm^{-1}, free silanol band initially decreases with increasing WO_3 loading, as illustrated in Figure 25. However, when the loading reaches 1.7 x 10^{-5} mol/g, corresponding to a fractional surface coverage of 70%, further increases in tungsten loading causes only a slight decrease in the intensity of free silanol band (Figure 25). Even at much higher loading, about 50% of the intensity of the silanol groups remains (Table V). Similar phenomena have been observed with silica supported Mo and W oxides.[169] The decrease of the intensity of free silanol band suggests an interaction between the SiOH groups and the tungsten compound to form a tetrahedral surface species. While a considerable amount of silanol groups are left free suggests that a part of WO_3(ads) agglomerates before forming a monolayer on the surface.

The emission spectra of WO_3/PVG samples reveal that two types of emissive species are present on the catalysts. As shown in Figure 35, one emission band has a maximum at 405 nm with an excitation maximum at ca.

260 nm, while the other has a maximum at 460 nm with an excitation maximum at 230 nm. With a WO_3 loading of 4.3 x 10^{-6} mol/g, which corresponds to ca. 0.1% W by weight, and a surface coverage of 0.2%, the 405 nm band dominates the spectrum (Figure 42). Increasing the WO_3 loading to 4.6 x 10^{-5} mol/g, ca. 1% W by weight, and a surface coverage of 1.9%, the 405 nm band exhibits the highest intensity. Increasing the WO_3 loading to 4.5 x 10^{-4} mol/g, ca. 10% W by weight, and a surface coverage of 18.7%, changes the relative emission intensities. At this loading, the 460 nm emission dominates the spectrum. As mentioned above, the structure of the surface tungsten oxide species is dependent on the tungsten contents in WO_3/Al_2O_3 and WO_3/SiO_2 catalysts. Anpo and coworkers report a similar change in emission spectra with MoO_3/PVG catalysts. The authors claim that the decrease in the phosphorescence intensity in the high Mo content region ($\geq$ 0.4% by weight) is due to the change of coordination from tetrahedral to octahedral.[154] Since pure WO_3 exhibits an emission at 460 nm, the band at 460 nm, which dominates the spectrum at higher loading, is assigned to an octahedral structure. The 405 nm emission is assigned to a tetrahedral species since this emission is dominant at low loading, and $CaWO_4$, a compound containing WO_4^{2-} tetrahedral structure, exhibits an emission at 435 nm (Figure 43).

Both emissions are quenched by O_2, CO_2, and NH_3, but the quenching is not complete even in the presence of excess quenchers(50 $\pm$ 10 times more than the theoretical amounts). Anpo and coworkers report a similar phenomenon for impregnated MoO_3/SiO_2 catalysts.[150] They claim that the

emitting sites in the MoO_3/SiO_2 catalysts are tetrahedral Mo species, not octahedral Mo species, and the incomplete quenching in the MoO_3/SiO_2 catalysts arise from the presence of octahedral species on the surface. A part of the tetrahedral emitting sites is physically covered with aggregated Mo and/or polymolybdate species derived from octahedral Mo species. Therefore, these emitting sites cannot be quenched. The other part is not covered and located on the surface, and thus can be efficiently quenched. The proposed model describing the different Mo sites on the SiO_2 surface is illustrated in scheme II.

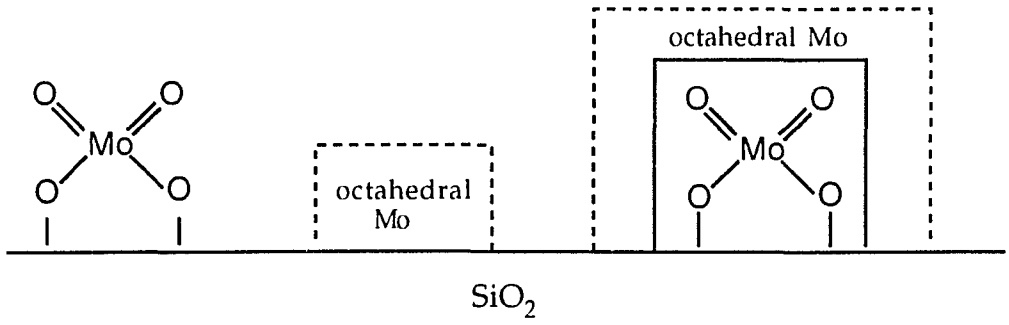

Scheme II

The reduction in the intensity of 3744 cm^{-1} free silanol band in DRIFT spectra of WO_3/PVG samples indicate an interaction between free silanol group and tungsten compound to form a tetrahedral tungsten species, and emission spectra indicate that both tetrahedral and octahedral tungsten oxide species present in the WO_3/PVG catalysts. Therefore, the incomplete quenching in WO_3/PVG could be explained with the similar model, i.e., a part of the emitting sites is physically covered with aggregated tungsten and/or polytungstate species, and connot be quenched.

It was found that NH_3 is somewhat selective in its ability to quench the two emitting sites. As shown in Figures 40 and 41, NH_3 quenches the 460 nm emission ca. 2.2 times more effectively than it quenches the 405 nm emission. Rate data, as listed in the Table XIII, indicate that NH_3 has ca. 4 times the effect on the rate of CH_4 evolution as it does on the rate of CO evolution. If reactions 3.3 and 3.4 occur at the same phtoactived catalytic site, NH_3 quenching should reduce the rate by the same amount. Therefore, the results raise an interesting question: Do the two emitting sites selectively catalyze the CO_2 reduction? That is, does the species giving rise to the 460 nm emission selectively photocatalyze CH_4 formation, while the species giving rise to the 405 nm emission selectively photocatalyze CO evolution?

Many researchers have proposed that methanation of CO_2 on solid catalysts starts with the dissociation of CO_2 into CO(ads) and O(ads), then follows the mechanism of CO methanation.[9,12,13,18,19,22] After exposing WO_3/PVG or blank PVG samples to CO_2, GC and GC-MS analyses of the

surrounding gas before photolysis indicate 2.5 - 3.1% of the CO_2 converts to CO before photolysis. Since unimpregnated PVG exhibits the same results as that from WO_3/PVG samples, the CO evolution before photolysis is attributed to the dissociative adsorption of CO_2 on the PVG. Actually, DRIFT spectra of CO_2 absorption on the WO_3/PVG samples closely resemble to the adsorption of CO_2 on unimpregnated PVG suggesting that CO_2 adsorbs on the uncovered PVG surface. Hall and coworkers reported a similar results on molybdena-alumina catalysts by IR measurements.[170] CO_2 is found to adsorb selectively on the uncovered alumina portion of the surface, while NO adsorbs on the molybdena portion of reduced molybdena-alumina catalysts.

The percentage of CO_2 dissociation on the WO_3/PVG or PVG is independent of CO_2 pressure in the range of 20 torr to 500 torr. The intensity of the IR bands in the 1700-1200 cm^{-1} region are also independent of CO_2 pressure. The independence suggests a limited number of adsorption sites on the surface of PVG.

Tying up the B_2O_3 Lewis acid sites with NH_3 reduces both rates of CH_4 and CO evolution (Table XII). The results suggest that the Lewis acid sites may be the active sites or at least involved in the photocatalyzed conversion. However, subsequent experiments with WO_3 supported on the base catalyzed TMOS/CH_3OH/H_2O xerogel, which are similar to PVG, but do not contain boron or B_2O_3 site,[104] show that irradiation with 254 nm light under 50 torr of CO_2 leads to 2.3×10^{-7} mol of CH_4 and 5.6×10^{-7} mol of CO evolutions in 24

hours. The data correspond to a rate of 1.0×10^{-8} mol/h for CH_4, and 2.3×10^{-8} mol/h for CO, i.e. the rates are in the same order as that on the WO_3/PVG samples. These data imply that even if the B_2O_3 Lewis acid site involved in the conversion, the adsorption or dissociation of CO_2 on these sites is not the rate - controlling step in the photocatalyzed reduction.

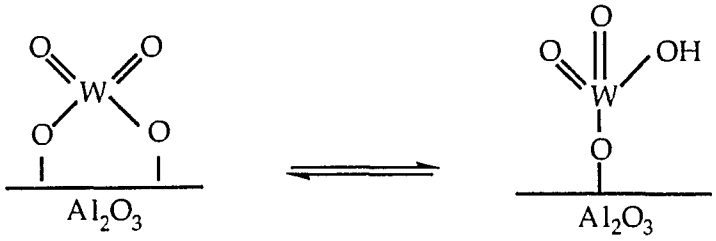

A B

Scheme III

Emission quenching experiments suggest that NH_3 reduces the rate of CH_4 evolution by quenching the photoexcited metal oxide. Bulk WO_3 acts as an acid in n-heptane hydrocracking,[171] olefin isomerization,[172] and alcohol dehydration reactions.[173] Supported on Al_2O_3, it is postulated that WO_3 could form either a Lewis acid or Brønsted acid sites on the surface.[174] As illustrated in Scheme III, the proposed configuration A represents the Lewis

acid site with a coordinatively unsaturated W center able to complex with a Lewis base. Configuration B, on the other hand, represents the Brønsted acid site with a proton available to react with base. The configuration A seems to be more favorable in WO_3/PVG samples, since it has a tetrahedral structure. NH_3 functions as a non-site-specific base,[174] it reacts with both Lewis and Brønsted acid sites in the supported WO_3. After exposing a sample containing 4.6×10^{-5} mol WO_3/g of PVG to NH_3 for 30 minutes, and then evacuating ($P \leq 10^{-4}$ torr) at 298 K for 60 minutes, about 35% of the initial phosphorescence intensity from the sample is recovered. The result indicates a strong interaction between NH_3 and supported WO_3, which could account for the reduction of the rate of CH_4 evolution.

The appearance of CH_3D and CH_2D_2 when the glass is deuterated,[87] the dependence of the rate of CH_4 evolution on H_2O content, and the appearance of O_2 as a reaction product indicate that water is both the hydrogen source and ultimately the source of reducing equivalents in the methanation of CO_2 on these WO_3/PVG catalysts. Recently, Anpo and Chiba report photocatalytic reduction of CO_2 with H_2O on anchored titanium oxide catalysts.[175] They find that UV irradiation of the anchored catalysts at 275 K in the presence of CO_2 and H_2O led to the photocatalytic formation of CH_4 with a minor amount of CH_3OH, but in the presence of CO_2 alone, only a very small amount of CH_4 produced. ESR measurements indicate that UV irradiation of the anchored titanium oxide catalyst in the presence of CO_2 and H_2O at 77 K leads to the formation of ·C radicals, H atoms and Ti^{3+} ions. The

ESR signals disappear once the temperature of the cell rises to 275 K, and the authors claim that CH_4 is formed by the reaction of ·C radicals, which are generated from the dissociation of CO_2. The ·C radicals then react with H atoms that are formed by the reduction of protons (H^+) from H_2O adsorbed on the catalyst.

Ogura and coworkers studied the visible light assisted decomposition of H_2O and photo-methanation of CO_2 over CeO_2-TiO_2 catalysts.[69] Under visible light irradiation, the reaction of CO_2 and H_2O on the catalyst produces H_2, O_2 and CH_4. The authors claim that the reaction proceeds through the stoichiometric photodecomposition of H_2O followed by the methanation of CO_2. Optical excitation of TiO_2 promotes the H_2O decomposition, while CeO_2 offers the active sites for the CO_2 methanation, i.e.,

$$TiO_2 + h\nu \text{ ----------> } TiO_2(e_{cb}^-, h_{vb}^+) \quad (4.1)$$

$$H_2O + 4h_{vb}^+ \text{ ----------> } 4H^+ + O_2 \quad (4.2)$$

$$4H^+ + 4e_{cb}^- \text{ ----------> } 4H_{ad} \quad (4.3)$$

$$2H_{ad} \text{ ----------> } H_2 \quad (4.4)$$

$$CO_2 + S + 4\,e_{cb}^- \text{ ---------> } S\text{-}C + 2O_{ad}^{2-} \quad (4.5)$$

$$S\text{-}C + 4H_{ad} \text{ ---------> } S\text{-}CH_4 \quad (4.6)$$

$$S\text{-}CH_4 \text{ ---------> } CH_4 + S \quad (4.7)$$

where S is the active site of CeO_2. Published reports suggest that H_2O functions as a source of hydrogen and reducing equivalents in the

photocatalytic reduction of CO_2 through photodecomposition of H_2O by the semiconductor TiO_2.[69,175] Semiconductors are efficient catalysts in the water photosplitting.[176] Adsorption of photons with energy greater than the semiconductor band gap leads to electrons (e^-) and positive holes (h^+). In order to retain electrical neutrality during a photocatalytic reaction, electrons are consumed by reducible species, while the holes react with oxidizable species. In the water photodecomposition, the electrons react with H^+ dissociated from H_2O to yield H_2, while the holes reacts with OH^{-1} to form O_2. The band gap of WO_3 is 3.2 eV,[177] which is comparable to the band energy of TiO_2 (3.2 eV). 254-nm irradiation of WO_3 supported on PVG in the presence of CO_2 leads to the evolution of CH_4, CO, O_2 and H_2. Although the amount of photo-formed H_2 was not quantitated, the fact that H_2 evolution precedes CH_4 evolution suggests that WO_3 may photocatalyze the water decomposition on the surface of WO_3/PVG catalysts prior to, or during the methanation of CO_2.

CO_2 dissociation has been suggested as the rate-limiting step for the methanation of CO_2.[19] However, the most popular belief is that CO(ads) dissociation or possibly C(ads) hydrogenation are the rate-limiting steps in the reduction.[14,21,178,179] Prairie and coworkers recently reported a low-temperature (≤ 200 °C) methanation of CO_2 over Ru supported on TiO_2 and Al_2O_3.[18] The authors claim that CO_2 methanation proceeds via adsorbed CO species formed from the reverse water-gas shift reaction, i.e.,

$$CO_2 + H_2 \text{ ----------> } CO(ads) + H_2O \qquad (4.8)$$

and the CO(ads) hydrogenation step is rate-controlling. As discussed previously, the effect of coadsorbed NH_3 shows that adsorption or dissociation of CO_2 on the B_2O_3 Lewis acid sites is not a rate-controlling step in the methanation of CO_2 over the WO_3/PVG catalysts. Pure WO_3 shows a high activity in the dissociation of CO_2 to CO and C in the presence of H_2 at temperature ≥ 573 K.[180]

Oades and coworkers report that on low surface area alumina (< 100 m^2/g) supported WO_3 catalysts exhibit a good activity for CO hydrogenation at pressure of H_2/CO (2 : 1) over a range of 1 - 30 atm, and temperature of 573 - 673 K.[181] The authors claim that excess WO_3 above the WO_3/Al_2O_3 monolayer is the active species for the CO hydrogenation. At loading over a monolayer coverage on Al_2O_3, tungsten oxide is present as a mixture of tetrahedral and octahedral species.[163,166] For the photocatalyzed methanation of CO_2 over the WO_3/PVG catalysts, rate data indicate that CH_4 evolution increases with tungsten loading (Table VI). Emission measurements indicate that the octahedral tungsten oxide species increases with WO_3 content, and NH_3 quenching experiments suggest that the octahedral tungsten oxide species selectively photocatalyzes CH_4 formation. These results suggest that methanation of CO_2 on the WO_3/PVG catalysts occurs via dissociation of CO_2, and follows the CO hydrogenation mechanism

since the octahedral tungsten oxide species appears to be the active species for the CO hydrogenation.[181]

If the rate-controlling steps of CO_2 methanation involves hydrogenation of CO(ads) or the active carbon, the localized, relative hydrogen-rich environment at the active sites would be expected to increase the methane formation. Extensively dehydrating the WO_3/PVG catalysts reduces the rate of CH_4 evolution, which suggests that a minimun amount of water is necessary for the conversion. On the other hand, introducing H_2 into the reactor does not increase the rate of methane formation(Table XI). The results suggest that active hydrogen atoms are primarily from photocatalyzed splitting of H_2O, not from the dissociation of H_2.

The rate of CH_4 evolution on WO_3/PVG catalysts is independent of the CO_2 pressure in the range of 20 to 100 torr. A lack of dependence of methanation rate on CO_2 partial pressure has also been observed on Ru/TiO_2 catalysts.[18] The absence of correlation between CO_2 pressure and methanation rate suggests that hydrogenation of CO_2 or dissociated CO proceeds only on a small number of highly active sites. It is noted that $^{12}CH_4$ appears immediately in all experiments with WO_3/PVG catalysts, regardless of the initial $^{13}CO_2$ pressure. Furthermore, the rate of hydrogenation of the carbonaceous impurity in the PVG exceeds the rate of hydrogenation of CO_2 on the catalysts(Table VI). The results suggest that the active sites are those initially containing the C_1 oxide impurity, and the first events are the

conversion of the C_1 impurity to $^{12}CH_4$. As the impurity sites are depleted, $^{13}CO_2$ adsorbs onto the vacated sites, and continued photolysis of WO_3 leads to $^{13}CH_4$. Consistent with this hypothesis, depleting the carbon source by photolysis prior to exposure to $^{13}CO_2$ leads to immediate $^{13}CH_4$ evolution.

Based on the above discussion, the reaction mechanism for the methanation of CO_2 on WO_3/PVG catalysts are postulated as following:

$$WO_3 + hv \text{ ----------> } WO_3(e^-, h^+) \quad (4.9)$$

$$H_2O + 4h^+ \text{ ----------> } 4H^+ + O_2 \quad (4.10)$$

$$4H^+ + 4e^- \text{ ----------> } 4H(ads) \quad (4.11)$$

$$2H(ads) \text{ ----------> } H_2 \quad (4.12)$$

$$CO_2 + 2S \text{ ----------> } S\text{-}CO + O\text{-}S \quad (4.13)$$

$$S\text{-}CO + 2H(ads) \text{ ----------> } H_2CO\text{-}S \quad (4.14)$$

$$H_2CO\text{-}S + 4H(ads) \text{ -------> } CH_4 + H_2O + S \quad (4.15)$$

$$O\text{-}S + 2H(ads) \text{ ----------> } H_2O + S \quad (4.16)$$

where S represents the active site on PVG. DRIFT spectrum of the photoproduct recorded during 254-nm photolysis of 2.06×10^{-5} mol $W(CO)_6$/g PVG exhibis a strong absorption at 2966 cm^{-1} with a shoulder at 2945 cm^{-1} and a broad absorption in the 3210-3450 cm^{-1} region,[87] which agrees with the spectrum of formaldehyde adsorbed onto PVG. Also, no ESR signal attributable to ·C occurs during photolysis of CO_2 with WO_3/PVG catalysts.

Therefore, the formaldehyde species, reaction 4.14, is proposed as an intermediate. This intermediate is then further reduced to methanol which is then reduced to CH_4.

4.2. Photoinduced Isomerization of 1-Pentene

The electronic and DRIFT spectra of $Ru_3(CO)_{12}$ adsorbed onto PVG agree with the spectra of the trimer in n-hexane (Table IV). The results establish that $Ru_3(CO)_{12}$ physisorbs onto PVG without disruption or significant distortion of the complex. In contrast to its photochemistry in solution, however, UV photolysis of the adsorbed $Ru_3(CO)_{12}$ leads to oxidative addition of a surface silanol group across an Ru-Ru bond and formation of the surface grafted species $(\mu\text{-H})Ru_3(CO)_{10}(\mu\text{-OSi})$.

After removal of the released CO, exposing $(\mu\text{-H})Ru_3(CO)_{10}(\mu\text{-OSi})$ to 1-pentene leads to spectral changes that indicate an immediate interaction between the grafted species and 1-pentene. GC analyses of the reactor contents show that the reaction with 1-pentene does not result in CO evolution, and evacuating the cell regenerates the spectra of the oxidative addition product, which can then be converted to $Ru_3(CO)_{12}$(ads) in $\geq$ 90% yield when $(\mu\text{-H})Ru_3(CO)_{10}(\mu\text{-OSi})$ is subsequently exposed to CO (1 atm). These results establish that the metal trimer remains intact during the reaction sequence, and that addition of 1-pentene disrupts the multicentered bonds binding the trimer to the glass surface.

On exposure to 1-pentene, three reaction products are possible: disruption of an Ru-O bond (I), an Ru-H bond (II), or both (III). Basset and coworkers proposed a structure analogous to I in $Os_3(CO)_{12}/SiO_2$ catalyzed olefin hydrogenation.[183] Although IR spectra recorded in our experiments do not exhibit a distinct absorption in the 1960-2060 cm^{-1} region that could be assigned to a terminal Ru-H vibration,[184] the product of 1-pentene addition is tentatively assigned to III. This assignment is based solely on the stability of the $(\mu\text{-H})Ru_3(CO)_{10}(\mu\text{-OSi})$-olefin product. The adduct persists for hours at room temperature, and the observed stability seems more consistent with a species in which the Ru atoms are formally 18-electron species. Consequently, the bands at 2109, 2078, 2066, 2028, and 2102 cm^{-1} are assigned to III. Although shifted, the band at 1830 cm^{-1} is assigned to 1-pentene adsorbed on the glass, because 1-pentene adsorbed onto calcined PVG exhibits a relatively intense band at 1850 cm^{-1} [157], and the 1830 cm^{-1} band disappears under vacuum much more rapidly than those assigned to III.

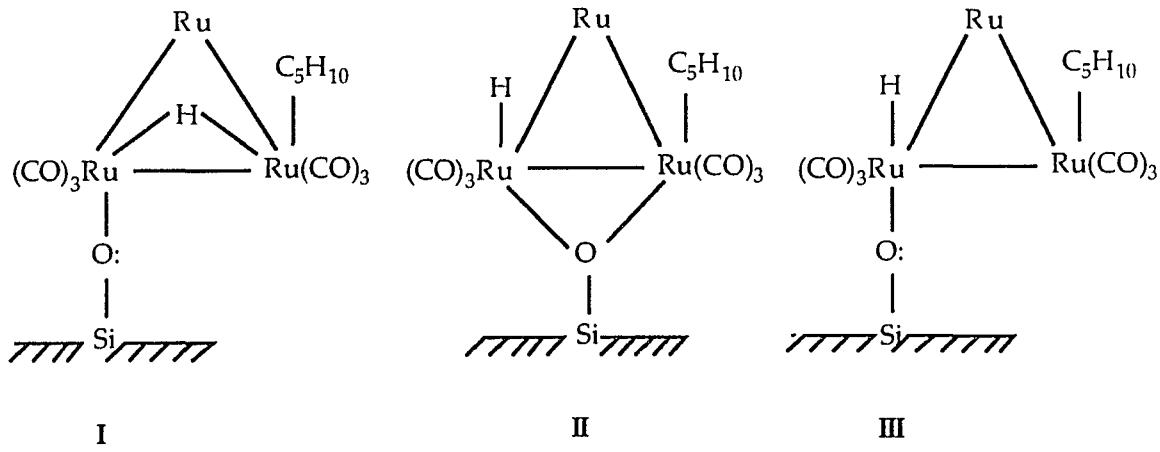

Scheme IV

UV photolysis of (μ-H)$Ru_3(CO)_{10}$(μ-OSi)-1-pentene leads to conversion of 1-pentene to cis- and trans-2-pentenes. The trans/cis- 2-pentene ratio is initially 1.5 ± 0.2, and increases to a relatively constant value of 2.5 ± 0.1 as the photolysis proceeds. The ratio is considerably smaller than the thermodynamic ratio, 4.82. One possible explanation is that the topology of the glass surface to which the complex is bound biases the isomer ratio. However, if this were the sole determinant of the trans/cis ratio, it would be expected that a ratio similar to that obtained in the photocatalyzed isomerization of 1-pentene by $Fe(CO)_5$ on PVG. In this case, the ratio is 3.7 ± 0.2, which is larger and closer to the thermodynamic ratio.[155] In the photoactivation of $Fe(CO)_5$, the photochemical reaction generates a thermally activated ground-state catalyst. In the Ru-PVG system, however, the

isomerization ceases when photoexcitation ceases. The reaction appears to be a photoassisted catalytic process in which the photoactivation generates an excited state that promotes olefin isomerization. Consequently, the smaller ratio found with the Ru-PVG system appears to be a function of the specific catalytic species present on the glass surface, rather than the topology of the surface, or since it is a photo process.

GC-MS analyses indicate that UV photolysis of 1-pentene on (μ-D)$Ru_3(CO)_{10}$(μ-OSi) generates deuterated olefins. The pentene fragments of 29 (m/e) and 43 (m/e) establish the formation of 1-D, 2-D, and 3-D-2-pentenes (Table XVIII). The formation of deuterated 2-pentenes suggests that the excited state may be similar to a pi-allyl complex, as shown in Scheme V. In this configuration, the carbons in the 1-, 2- and 3- positions are susceptible to deuterium substitution. The displaced olefin hydrogen can be transferred to the metal complex to regenerate the surface grafted cluster, which then reacts with 1-pentene to re-form III.

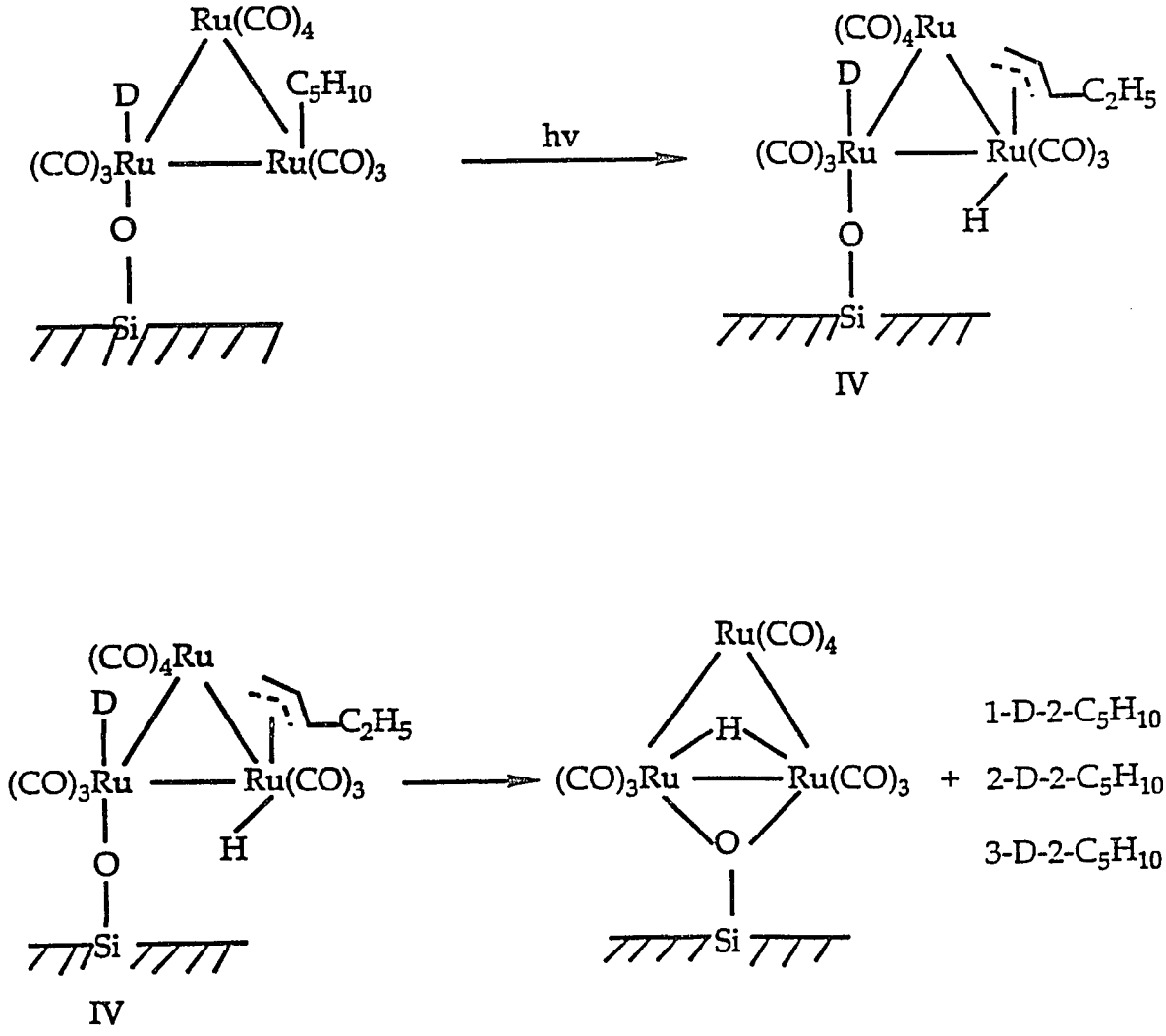

Scheme V

UV photolysis of (μ-H)$Ru_3(CO)_{10}$(μ-OSi) with 1-pentene does not result in hydrogenation even in the presence of H_2. Exposing (μ-H)$Ru_3(CO)_{10}$(μ-OSi) to a mixture of CH_2CH_2 and H_2 does not result in hydrogenation of CH_2CH_2 either. IR spectrum of CH_2CH_2 on (μ-H)$Ru_3(CO)_{10}$(μ-OSi) is similar to the spectrum of 1-pentene adduct (Figure 51). However, UV and IR measurements indicate that exposing (μ-H)$Ru_3(CO)_{10}$(μ-OSi) to H_2 does not cause any spectral change, that is, no indication of an interaction between H_2 and the grafted complex. The details of the inactivity of the catalyst to olefin hydrogenation is not clear. Nevertheless, the high selectivity of the grafted complex to olefin isomerization is an attractive property.

In conclusion, the photogenerated grafed complex, (μ-H)$Ru_3(CO)_{10}$(μ-OSi), possess a high selectivity and activity to 1-pentene isomerization. The trans-cis ratio observed, 2.5 ± 0.1, is considerably smaller than the thermodynamic ratio, 4.82. The smaller ratio found with this system is attributed to the specific species present on the glass surface, i.e., (μ-H)$Ru_3(CO)_{10}$(μ-OSi), rather than steric effects induced by the topology of the PVG surface.

Reference

1. Pamela S. Zurer, C & EN News, April 1, 7 (1991).
2. Lunde, P. J. & Kester, F. L. J. Catal. 30, 423-429 (1973).
3. Phyng Quack, T. Q. & Rouleau, D. J. appl. Chem. Biotechnol. 26, 527-535 (1976).
4. Tomsett, A. D., Hagiwara, T., Miyamoto, A. & Inui, T. Appl. Catal. 26, 391-194 (1984).
5. Weatherbee, G. D. & Bartholomew, C. H. J. Catal. 77, 460-472 (1982).
6. Macdonald, G. J., Ed. The Long-Term Impacts of Increasing Carbon Dioxide Levels, Ballinger Publishing Co., Cambridge, MA, 1982.
7. Tomoyasu, I. & Lunsford, J. H. Nature 314, 721-722 (1985).
8. Otsuka, K., Jinno, K. & Morikawa, A. J. Catal. 100, 353-359 (1986).
9. Weatherbee, G. D. & Bartholomew, C. H. J. Catal. 77, 460-472 (1982).
10. Spinicci, R. & Tofanari, A. Appl. Catal. 41 (1988) 241-252.
11. Lunde, P. J. & Kester, F. L. J. Catal. 30, 423-429 (1973).
12. Gupta, N. M., Kamble, V. S., Rao, K. A. and Iyer, R. M. J. Catal. 60 (1979) 57.
13. Zagli, E. and Falconer, J. L. J. Catal. 69 (1981), 1.
14. Solymosi, F., Erdohelyi, A. and Kocsis, M. J. Chem. Soc., Faraday Trans. I, 77 (1981), 1003.
15. Ferkul, H. E., Stanton, D. J., McCowan, J. D. and Baird, M. C. J. Chem. Soc., Chem. Commun., 1982, 955.
16. Ferkul, H. E., Berlie, J. B., Stanton, D. J., McCowan, J. D. and Baird, M. C. Can. J. Chem., 61 (1983),1306.
17. Gliddon, B. J., Hotchkiss, R. C. and Roberts, R. A. Inst. Chem. Eng. Symp. Ser., 87 (1984), 329; C.A. 102, 64586c.

18. Prairie, M. R., Renken, A., Highfield, J. G., Thampi, K. R., and Gratzel, M. J. Catal. 129, 130-144 (1991).

18.a Vannice, M. A., in "Catalysis, Science and technology" (J. R. Anderson and M. Boudart, Eds.) Vol. 3, Springer verlag, Berlin, 1982.

Shincho, E., Egawa, C., Naito, S. and Tamarta, K., Surf. Sci. 155, 153 (1985).

18.b Henderson, M. A. and Worley, S. D. J. Phys. Chem. 89, 1417 (1985).

Robbins, J. L. J. Catal. 115, 120 (1989).

Yokomizo, G. H., Louis, C. and Bell, A. T. J. Catal. 120, 1 (1989)

19. Solymosi, F., Erdohelyi, A. and Bansagi, T. J. Catal. 68, 371-382 (1981).

20. Ichikawa, S. J. Mol. Catal. 53 (1989) 53-65.

21. Henderson, M. A. and Worley, S. D. J. Phys. Chem., 89 (1985) 1417.

22. Williams, K. J., Boffa, A. B., Salmeron, M., Bell, A.T. and Somorjar, G. A. Cata. Lett. 9 (1991) 415-426.

23. Iizuka, T., Tanaka, Y. and Tanabe, K. J. Catal. 76 (1982) 1.

24. Paushkin, Ya. M., Zhorov, Yu. M. and Gorlov, E. G. Dokl. Akad. Nauk. SSSR, 281 (1985), 1165; C. A. 103, 56715z.

25. Lapidus, A. L. and Savel'ev, M. M. Russ. Chem. Rev. 53 (1984), 535.

26. Weatherbee, G. D. and Bartholomew, C. H. J. Catal. 87 (1984) 352-362; J. Catal. 77 (1982) 460-472; J. Catal. 68 (1981) 67-76.

27. Vance, C. K. and Bartholomew, C. H. Appl. Catal. &, 169-177 (1983).

28. He, M. Y. and White, J. M. J. Mol. Catal. 30 (1985) 415-430.

29. Nozaki, F., Sodesawa, T., Satoh, S. and Kimura, K. J. Catal. 104 (1987) 339-346.

30. Barrault, J., Forquy, C., Menezo, J. C. and Maurel, R. React. Kinet. Catal. Lett., 17 (1981), 373.

31. Pijolat, M. and Perichon, V.. C. R. Seances Acad. Sci., Ser. 2, 295 (1982), 343.

32. Fujimoto, K. and Shikada, T. Appl. Catal. 31, 13-23 (1987).

33. Kuei, C. K. and Lee, M. D. Can. J. Chem. Eng. 69, 347-354 (1991).

34. Fujiwara, M. and Souma, Y. J. Chem. Soc., Chem. Commun., 1992 (10) 767-768.

35. Ramarson, E., Kieffer, R. and Kinnemann, A. Appl. Catal. 4 (1982) 281.

36. Tagawa, T., Pleizier, G. and Amenomiya, Y. Appl. Catal. 18 (1985) 285-293.

37. Denise, B. and Sneeden, R. P. A. Appl. Catal. 28 (1986) 235.

38. Amenomiya, Y. Appl. Catal. 30 (1987) 57-68.

39. Denise, B., Cherifi, O., Bettahar, M. M. and Sneeden, R. P. A. Appl. Catal. 48 (1989) 365.

40. Baussart, H., Delobel, R., Bras, M. L., Maguer, D. L. and Leroy, J. M. Appl. Catal. 14 (1985) 381-389.

41. Chinchen, G. C., Denny, P. J., Parker, D. G., Spencer, M. S. and Whan, D. A. Appl. Catal. 30 (1987) 333-338.

42. Inoue, T., Iizuka, T. and Tanabe, K Bull. Chem. Soc. Jpn. 60 2663-2664 (1987).

43a. Millar, G. J., Rochester, C. H., Howe, C. and Wangh, K. C. Mol. Phys. 1991, 76 (4), 833-849.

43b. Fujita, S., Usui, M., Ohara, E. and Takezawa, N. Cata. Lett. 13 (1992) 349-358.

44. Dubois, J. L., Sayama, K. and Arakawa, H. Chem. Lett. 1992, 1115-1118.

45. Ziessel, R. in "Carbon dioxide as a source of Carbon: biochemical and chemical uses", Aresta, M. and Forti, G. Eds., Reidel Publ., p.113, 1987.

46. Grant, J. L., Goswami, K., Spreer, L. O., Otvos, J. W. and Calvin, M. J. Chem. Soc., Dalton Trans., 2105, 1987.

47. Ishida, H., Terada, T., Tanaka, K. and Tanaka, T. Inorg. Chem., 29, 905, 1990.

48. Craig, C. A., Spreer, L. O., Otvos, J. W. and Calvin M. J. Phys. Chem. 1990, 94, 7957-7960.

49. Kimura, E., Bu, X., Shionoya, M., Wada, S. and Maruyama, S. Inorg. Chem. 31, 4542-4546, 1992.

50. Silavwe, N. D., Goldman, A. S., Ritter, R. and Tyler, D. R. Inorg. Chem. 28, 1231-1242, 1989.

51. Harris, D. G. and Gray, H. B. J. Am. Chem. Soc., 97, 3037, 1975.

52. Belmon, K. A., Vanderpool, R. A., Tsai, J.-C., Kahn, M. A. and nicholas, K. M. J. Am. Chem. Soc., 110, 2004-2005, 1988.

53. Kanemoto, M., Ishihara, K., Wada, Y., Sakata, T., Mori, H. and Yanagida Chem. Lett. 835-836, 1992.

54. Aliwi, S. M. J. Photochem. Photobiol. A: Chem., 67 (1992) 329-336.

55. Willner, I., Maidan, R., Mandler, D, Durr, H., Dorr, G. and Zengerle, K. J. Am. Chem. Soc. 1987, 109, 6080-6086.

56. Inoue, T., Fujishima, A., Konishi, S. and Honda, K. Nature 1979, 277, 637.

57. Kanemoto, M., Shiragami, T., Pac, C. and Yanagida, S. Chem. Lett. 1990, 931.

58. Ulman, M., Aurian-Blajeni, B. and Halmann, M. Isr. J. Chem. 1982, 22, 177.

59. Chandrasekaran, K. and Thomas, J. K. Chem. Phys. Lett. 1983, &, 99.

60. Haimann, M., Katzir, V., Borgarello, E. and Kiwi, J. Sol. Energy Mater. 1984, 10, 85.

61. Yamamura, S., Kojima, H., Iyoda, J. and Kawai, W. J. Electroanal. Chem. 1987, 225, 287; and 1989, 247, 333.

62. Eggins, B. R., Irvine, J. T. S., Murphy, E. P. and Grimshaw, J. J. Chem. Soc., Chem. Commun. 1988, 1123.

63. Dzhabiev, T. S., Tarasov, B. B. and Uskov, A. M. Catal. Today 1992, 13(4)

695-6.

64. Hirano, K., Inoue, K. and Yatsu, T. J. Photochem. Photobiol. A: Chem. 64 (1992) 255-258.

65. Thampi, K. R., kiwi, J. and Gratzel, M. Nature 327 (1987) 506-508.

66. Melsheimer, J., Guo, W., Ziegler, D., Wesemann, M. and Schlogl, R. Catal. Lett. 11 (1991) 157-168.

67. Lichtin, N. N., Vijayakumar, K. M. and Rubio, B. I. J. Catal. 104, 246-251 (1987).

68. Ogura, K., Kawano, M. and Adachi, D. J. Mol. Catal. 72 (1992) 173-179.

69. Ogura, K., Kawano, M., Yano, J. and Sakata, Y. J. Photochem. Photobiol. A: Chem., 66 (1992) 91-97.

70. Chanon, F. and Chanon, M. in "Photocatalysis, fundamentals and applications" Ed. Serpone, N. and Pelizzetti, E., John Wiley & Sons New York, pp. 489.

71. Howe, R. F. 'Tailored Metal Catalysts", Ed. Iwasawa, Y., D. Reidel Publishing Co. Holland, 1988, pp. 141.

72. Bailey D. C. Bailey and Langer, S. H. Chem. Rev. 81, 1981, 110.

73. Howe, R. F. Inorg. Chem. 1976, 15, 486.

74. Brenner, A., Hucul, D. A. Prepr. Div. Petrol. Chem., Am. Chem. Soc. 1977, 22, 1221.

75. Brenner, A., Hucul, D. A. and Hardwick, S. J. Inorg. Chem. 1979, 18, 1478.

76. Howe, R. F. J. Chem. Soc., Faraday trans. 1, 1975, 71, 1689.

77. Howe, R. F., Davidson, D. E., Whan, D. A. J. Chem. Soc., Faraday Trans. 1, 1972, 68, 2266.

78. Brenner, A. and Burwell, R. L. Jr. J. Am. Chem. Soc. 1975, 97, 2565.

79. Brenner, A., Hucul, D. A. J. Catal. 1980, 61, 216.

80. Brenner, A. and Burwel, R. L. Jr. J. Catal. 1978, 52, 353.

81. Olsthoorn, A. A. and Moulijn, J. A. J. Mol. Catal. 1980, 8, 147.

82. Banks, R. L. U. S. Patent 3 463 827, 1969.

83. Geoffrey, G. L. J. Chem. Educ., 60, 861 (1983).

84. a. Almond, M. J. and Downs, A. J. J. Chem. Soc. Dalton Trans., 1988, 809.
b. Almond, M. J. and Hahne, M. J. Chem. Soc. Dalton Trans., 1988, 2255.

85. Germer, T. A. and Ho, W. J. Chem. Phys., 1988, 89, 562.

86. Wadw, Y., nakaoka, C. and Morikawa, A. Chem. Lett. 1988, 25-26.

87. Simon, R. C., Mendoza, E. A. and Gafney, H. D. Inorg. Chem. 1988, 27, 2733-2742.

88. Simon, R. C., Gafney, H. D. and Morse, R. L. Inorg. Chem. 1983, 22, 573-574.

89. Geoffroy, G. L., Wrighton, M. S. Organometallic Photochemistry, Academic: New Youk, 1979, pp 46-49.

90. Perutz, R. N. and Turner, J. J. J. Am. Chem. Soc. 1975, 97, 4791-4800.

91. Graham, M. A., Polikoff, M. and Turner, J. J. J. Chem. Soc. A 1971, 2939.

92. Morse, D. L. private communication, Corning Hlass Works, 1984.

93. Pino, p., Braca, G., Sbrana, G. and Cuccuru, A. Chem. & Ind. 1968, 1732.

94. Kuznetsov, V. L., Bell, A. T., Yermakov, Y. I. J Catal. (1980), 65, 374-379.

95. Theolier, A., Choplin, A., D'Ornelas, L.' Basset, J. M., Zanderighi, G. Sourisseau, C., Polyhedron (1983), 2, 119.

96. Simpson, A. F., Whyman, R. J. Organomet. Chem. (1981), 213, 157.

97. Doi, Y., Yano, K. Inorg. Chim. Acta (1983), 76, L71-3.

98. Dieter, T. and Gafney, H. D. Inorg. Chem. 1988, 27, 1730.

99. Desrosiers, M. F., Wink, D. A., Trantman, R., Friedman, A. E. and Ford, P. C J. Am. Chem. Soc., 108 (1986) 1917-1927.

100. Desrosiers, M. F., Wink, D. A. and Ford, P. C. Inorg, Chem., 24 (1985) 2-3.

101. Malito, J., Markiewicz, S. and Poe, A. Inorg. Chem., 21 (1982) 4335-4337.

102. Johnson, B. F. G. 'Transition Metal Clusters", Johnson, B. F. G., Ed., Wiley: New Youk, 1980, pp.29.

103. Jackson, R. L. and Trusheim, M. R. J. Am. Chem. Soc. 104, 1982, 6590-6596.

104. Mendoza, E. A., Wolkow, E., Sunil, D., Wong, P., Sokolov, J., Rafailovich, M. H., den Boer, M., Gafney, H. D. Langmuir, 7,3046 (1991).

105. Elmer, T. H. J. Am. Ceram. Soc. 1970, 53, 171.

106. Nordberg, M. E. J. Am. Ceram. Soc. 1944, 27, 299.

107. Elmer, T. H., Chapman, I. D. and Norberg, I. F. J. Phys. Chem. 1962, 66, 1517.

108. Gafney, H. D. In Photochemistry on Solid Surfaces, Anpo, M., Matsuura, T., Eds, Elsevier: New York, 1989, p 272.

109. Hair, M. L., Chapman, I. D. J. Am. Ceram. Soc. 1966, 49, 651; Trans. Faraday Soc. 1965, 61, 1507.

110. Snyder, L. R., Ward, J. W. J. Phys. Chem. 1966, 70, 3941.

111. Huber, T. E., Huber, C. A. J. Phys. Chem. 1990, 94, 2502.

112. Damme, H. V. In "Photocatalysis", Serpone, N., Pelizzetti, E. Eds, John Wiley & Sons: New York, 1989, p.176.

113. Susa, K., et.al., "Method for Producing Silica Glass", U. S. Patent 4,317,668, Filed Jan 21, 1981.

114. Doi, Y.; Yano, K. Inorg. Chim. Acta. (1976), 76, L71-3.

115. Calderazzo, F.; L'Eplatlenier, F. Inorg. Chem. (1967), 6,1220-4.

116. Bruce, M. I.; Stone, F. G. A. Angew. Chem. Int. Ed. Engl. (1968), 7, 427-32.

117. Candlin, J. P.; Shortland, A. C. J. Organomet. Chem. (1969), 16, 289-99. 105.

118. Kettle, S. F. A.; etal. Inorg. Chem. (1980), 19, 1961-73.

119. Tyler, D. R.; Levenson, R. A.; Gray, H. B.. J. Am. Chem. Soc. (1978), 100, 7888-93..

120. Bruce, M. I.; Shaw, G.; Stone, F. G. A.. J. Chem. Soc. Dalton (1972), 2094.
121. Calvert, J.; and Pitts. J. "Photochemistry", Wiley, New York, 1966, P. 783.
122. Cant, N. W. ; Little, L. H. Can. J. Chem. 1964, 42, 802-809; 1965, 43, 1252-1254.
123. Low, M. J. D. ; Ramasubramanian, N. J. Phys. Chem. 1966, 9, 2740.
124. Little, L. H. "Infrared Spectra of Adsorbed Species", Academic Press: New York, 1966,p. 174.
125. Wolfgang, S. and Gafney, H. D. J. Phys. Chem. 1983, 87, 5395-5401.
126. Kennelly, T., Gafney, H. D. and Braun, M. J. Am. Chem. Soc. 1985, 107, 4431-4440.
127. Colton, R. and Rix, C. J. Aust. J. Chem. 1969, 22, 305.
128. Schid, G. ; Bose, R. and Wolz, E. Chem. Ber. 1975, 108, 26.
129. Pope, M. T. "Heteropoly and Isopoly Oxometalates", Springer-Verlag, Heidelberg, 1983.
130. Krylov, O. V. "Catalysis by Non-Metals, Rules for Catalyst Selection", Academic Press, New York, 1970.
131. Iler, R. K. "The Chemistry of Silica", Wiley-Interscience, New York, 1979, P. 551.
132. All, K. G. J. Organomet. Chem. 1975, 87, 203.
133. Griffith, W. P. and Wickins, T. D. J. Chem. Soc. A, 1087 (1966)
134. Griffith, W. P. and Lesniak, P. J. B. J. Chem. Soc. A, 1066 (1969)
135. Nyquist, R. A. ; Kagel, R. O. Infrared Spectra of Inorganic Compounds: 3800-45 cm^{-1}, Academic Press, New York, 1971.
136. Ward, J. W. and Habgood, H. W. J. Phys. Chem. 70, 1178, 1966.
137. Rethwisch, D. G. and Dumesic, J. A. Langmuir, 1986, 2, 73-79.

138. a. Lercher, J. A. and Noller, H. J. Catal. 77, 1982, 152-158.

b. Diem, M. Hunter College, CUNY private communication.

139. Che, M. and Tench, A. J. Adv. Catal. 1982, 31, 77.

140. Anpo, M.; Tanahashi, I.; Kubokawa, Y. J. Chem. Soc., Faraday Trans. 1 1982, 78, 2121.

141. Kazansky, V. B.; Pershin, A. N.; Shelimov, B. N. Proc. Int. Congr. Catal., 7th 1980, B-1210.

142. Anpo, M.; Tanahashi, I.; Kubokawa, Y. J. Phys. Chem. 1980, 84, 3440.

143. Anpo, M.; Tanahashi, I.; Kubokawa, Y. J. Phys. Chem. 1982, 86, 1.

144. Anpo, M.; Mihara, K.; Kubokawa, Y. J. Catal 1986, 97,272.

145. Shelimov, B. N.; Elev, I. V.; Kazansky, V. B. J. Catal. 1986, 98, 70.

146. Iwasawa, Y. Adv. Catal. 1987, 35, 187.

147. Shelimov, B. N., Pershin, A. N., Kazansky, V. B. J. Catal. 1980, 64, 426.

148. Kazansky, V. B. Kinet. Katal. 1982, 24, 1338.

149. Ono, T., Anpo, M., Kubokawa, Y. J. Phys. Chem. 1986, 90, 4780.

150. Anpo, M.; Kondo, M.; Coluccia, S.; Louis, C.; Che, M. J. Am. Chem. Soc. 1989,111, 8791.

151. Che, M.; Tench, A. J. Adv. Catal. 1982, 31,77; Ibid. 1983, 32, 1.

152. Anpo, M.; Yamada, Y.; Kubokawa, Y.; Coluccia, A.; Zecchina, A.; Che, M. J. Chem. Soc., Faraday Trans. 1 1988, 84, 751.

153. Anpo, M.; Yamada, Y. Mater. Chem. Phys. 1988, 18, 465.

154. Anpo, M.; Suzuka, T.; Kubokawa, Y. J. Phys. Chem. 1984, 88, 5778.

155. Darsillo, M. S., Gafney, H. D. and Paquette, M. S. Inorg. Chem. 1988, 27, 2815-2819.

156. Hair, M. L. "Infrared Spectroscopy in Surface Chemistry" Marcel Dekker, New York 1967.

157. Sidorov, A N. Zh. fiz. khim. 30, 995, 1956.

158. Iannibello, A., Villa, P. L. and Marengo, S. Gazz. Chim. Ital. 109, 521 (1979).

159. Fan, J. Ph. D. Thesis, CUNY, 1992.

160. Dieter, T. Ph.D. Thesis, CUNY, 1985.

161. Stencel, J. M., Makovsky, L. E., Diehl, J. R. and Sarkus, T. A. J. Raman Spectrosc. 15, 282 (1984).

162. Chan, S. S., Wachs, I. E., Murrell, L. L., Wang, L. and Hall, W. K. J. Phys. Chem. 88, 5831(1984).

163. Horsley, J. A., Wachs, I. E., Brown, J. M., Via, G. H. and Hardcastle, F. D., J. Phys. Chem. 91, 4014(1987).

164. Grunert, W., Shpiro, E. S., Feldhaus, R., Anders, K., Antoshin, G. V. and Minachev, Kh. M. J. Catal. 107, 522(1987).

165. Vermaire, D. C. and van Berge, P. C. J. Catal. 116, 309(1989).

166. Salvati, L., Jr., Makovsky, L. E., Stencel, J. M., Brown, F. R. and Hercules, D. M., J. Phys. Chem. 85, 3700(1981).

167. Murrell, L. L., Grenoble, D. C., Baker, R. T. K., Prestridge, E. B., Fung, S. C., Chianelli, R. R., Cramer, S. P. J. Catal. 79, 203(1983).

168. Yan, Q. and Liu, H. Fenzi Cuihua 1988, 2(2), 87.

169. Reddy, B. M., Rao, K. S. P., Mastikhin, V. M. J. Catal. 113, 556(1988).

170. Sedawa, K. and Hall, W. K. J. Catal. 77, 221(1982).

171. Ogata, E., Kayima, Y. and Ohta, N., J. Catal. 29, 296 (1979).

172. hattori, H., Asada, N. and Tanabe, K. Bull. Chem. Soc. Japan 51, 1704 (1978)

173. Davis, B. H. J. Catal. 55, 158 (1978).

174. Soled, S. L., McVicker, G. B., Murrell, L. L., Sherman, L.G., Dispenziere, N. C., Jr., Hsu, S. I. and Waldman, D., J. Catal. 111, 286 (1988).

175. Anpo, M. and Chiba K., J. Mol. Catal. 1992, 74(1-3) 207-12.

176. Schiavello, M. and Sclafani, A. in "Photoelectrochemistry, photocataltsis and Photoreactors", Schiavello, M. Ed., Reidel Publ., p.503, 1985.

177. Lewis, S. N. and Rosenbluth, L. M. in "Photocatalysis", Serpone, N. and Pelizzetti, E. Eds. John Wiley & Sons, New York, 1989, p. 136.

178. Erdohelyi, A., Pasztor, M., and Solymosi, F., J. Catal. 98, 166(1986).

179. Weatherbee, G. D. and Bartholomew, C. H., J.Catal. 87, 352(1984).

180. Ishihara, T., Fujita, T., Mizuhara, Y. and Takita, Y. Chem. Lett. 2237-2240,1991.

181. Oades, R. D., Morris, S. R. and Moyes, R. B. Cata Today, 10(1991) 379-385.

182. Besson, B., Choplin, A., D'Ornelas, L., Basset, J. M. Chem. Commun. 1982, 842.

183. Nakamoto, K. Infrared and Raman Spectra of Inorganic and Coordination Compounds, 3rd ed., Wiley-Interscience: New York, 1980, p 290.